



Norwegian University of Life Sciences
Faculty of Environmental Sciences
and Natural Resource Management

Philosophiae Doctor (PhD)
Thesis 2022:14

Performance of a photovoltaic-thermal system in a tropical environment of central Ghana

Ytelse av et fotovoltaisk-termisk system
i et tropisk miljø i det sentrale Ghana

Saeed Abdul-Ganiyu

Performance of a photovoltaic-thermal system in a tropical environment of central Ghana

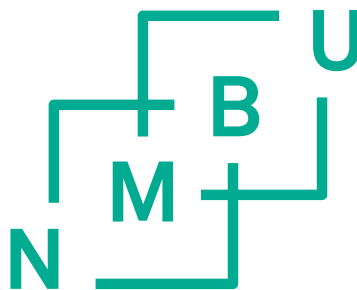
Ytelse av et fotovoltaisk-termisk system i et tropisk miljø i det sentrale Ghana

Philosophiae Doctor (PhD) Thesis

Saeed Abdul-Ganiyu

Norwegian University of Life Sciences
Faculty of Environmental Sciences and Natural Resource Management

Ås (2022)



Supervisors and Evaluation Committee

Supervisors

Professor Muiyiwa Samuel Adaramola (Main Supervisor)
Renewable Energy Group
Faculty of Environmental Sciences and Natural Resource Management
Norwegian University of Life Sciences (NMBU)
P.O. Box 5003 NMBU, NO-1432 Ås, Norway

Professor Seidu Razak (Co-Supervisor)
Department of Ocean Operations and Civil Engineering
Norwegian University of Science and Technology (NTNU)
Ålesund, Norway

Dr. Emmanuel Wendsongre Ramde (Co-Supervisor)
Senior Lecturer
Department of Mechanical Engineering
Kwame Nkrumah University of Science and Technology (KNUST)
Kumasi, Ghana

Dr. David Ato Quansah (Co-Supervisor)
Senior Lecturer
Department of Mechanical Engineering
Kwame Nkrumah University of Science and Technology (KNUST)
Kumasi, Ghana

Evaluation Committee

Professor Olanrewaju Miracle Oyewola
Fiji National University
School of Mechanical Engineering, Fiji national University, Derrick Campus
Suva, Fiji

Associate Professor Andres Olivares
Western Norway University of Applied Sciences
Bjørnsons Gate 45,
5528 Haugesund, Norway

Professor Kristin Linnerud
Faculty of Environmental Sciences and Natural Resource Management,
NMBU, P.O. Box 5003
1432 Ås, Norway

Acknowledgements

All praises and thanks be to the Almighty God for granting me the resilience to endure whatever life threw at me during this study. The PhD journey has been a true life-changing experience for me, and it would not have been possible without the support and guidance of many individuals and institutions.

I am most grateful to my main supervisor, Prof. Muyiwa Samuel Adaramola for the PhD opportunity in Norway. In fact, there came a time when I almost gave up on the PhD due to some personal setbacks which prolonged the time I spent undertaking my field work in Ghana. Without his guidance, constant support and unwavering ability to drive me back on track, this PhD would not have been achievable. Many thanks also go to my second supervisor, Prof. Seidu Razak, for believing in me by introducing me to Prof. Adaramola which contributed to this PhD fellowship at NMBU. I am also ever grateful for the commitment of his personal time and resources to ensure my comfortable stay in Norway. I lack adequate words to express my profound gratitude to Prof. Seidu for without him, this PhD wouldn't have been possible. I will also like to acknowledge the PhD scholarship support by the UPER-CRET (Upgrading Education and Research Capacity in Renewable Energy Technologies) Program, funded by Energy and Petroleum (EnPe) Project of Norwegian Agency for Development Cooperation (NORAD). I will like to use this opportunity to express my sincere gratitude to the management of NORAD-EnPe.

I am ever grateful to Dr. Emmanuel Ramde for providing the needed technical support and resources to ensure I was always comfortable at KNUST during my time in Ghana for data collection. Special thanks also go to Dr. David Atto Quansah for his brotherliness during our time together in Norway and his subsequent invaluable technical support, encouragements and assistance throughout the challenging times of my PhD journey, right from the beginning to the end of the study. Dr. Ramde and Dr. Quansah formed part of my supervisory team and I deem it an honor to have tapped from their knowledge and expertise. I would also like to express my sincere gratitude to the Brew Hammond Energy Centre, KNUST, for their support in Ghana. I also appreciate the support I got from Professor Ahmed Abdul-Rahman (Current Dean of School of Engineering, KNUST), Dr.

Lena Dzifa Mensah (Dept. of Mechanical Engineering, KNUST) and Mr. Robert Kyere (Technician, Solar Lab, KNUST).

My sincere thanks also go to the Faculty of Environmental Sciences and Natural Resource Management (MINA), NMBU. I would like to mention Dr. Denis Kwame Edem Dzebre for his invaluable assistance of varying forms and for the warmth he extended to me during our time together in Norway and for always making me feel so welcomed. Also, to all former colleagues at MINA (Mekdes, Solrun, Yennie, Thomas and the rest) thanks for your warm friendship. I would also like to thank Mr. Kjetil Sandnes and Volue Instrument Technology Ås (formerly Scanmatic Instrument Technology) for their assistance in purchases and organization of materials for the experimental setup for this thesis. I also thank the Ås muslim community for opening their doors to me. To my family in Ålesund (Fatimat and the kids), I am grateful for the warm reception.

To my wife Salamatu who managed our home in my absence and supportive family, especially my brothers Zakaria and Aminu, I say thank you. To my dad Seidu Sakara who didn't live to see the end of this PhD, God be with you. I will like to thank the entire GOP family (special mention of Harun for IT solutions; also, A. Razak (Zakus), Nurudeen, A. Karim and Ahmed for their constant encouragement), and my friends Mr. Samuel Oyewale and Dr. Isaac Sackey (Berlin).

Finally, and most importantly, I wish to once again express my sincere gratitude to the Almighty God for the success of this PhD has not been by my strength, but by His will for my life.

Alhamdulillah

Table of Contents

Supervisors and Evaluation Committee	2
Acknowledgements	3
Abbreviations and definitions.....	6
List of papers	10
Abstract	11
Norsk Sammendrag	13
Synopsis	15
1 Introduction	16
2 Fundamental theory of modules	24
3 Materials and Methods	44
4 Results and discussion.....	60
5 Conclusions.....	66
6 Limitations of work, future studies and engineering direction.	68
References.....	70
7 Articles/Papers.....	77
I Investigation of Solar Photovoltaic-Thermal (PVT) and Solar Photovoltaic (PV) Performance: A Case Study in Ghana.....
II Techno-economic analysis of solar photovoltaic (PV) and solar photovoltaic thermal (PVT) systems using exergy analysis.....
III Study Effect of flow rate on flat-plate water-based Photovoltaic-Thermal (PVT) system performance by analytical technique
8 Appendices

Abbreviations and definitions

English letters

A_m	Effective module surface area (m^2)
A_{th}	Area of thermal collector
A_x	surface x, where x is a positive integer
b	Economic life of the system (years)
C_1	A constant = $2\pi h S_o^2 = 3.74177 \times 10^8 \text{ W } \mu\text{m}^4/\text{m}^2$
C_2	A constant = $h S_o/k = 1.43878 \times 10^4 \text{ } \mu\text{m K}$
C_b	Conductance of the bond between the fin and copper circular pipes
C_t	Total cost (\$)
c_p	Specific heat capacity of water ($\text{kJ}/\text{kg } ^\circ\text{C}$)
d	Characteristic linear dimension in m
d_p	The thickness of the pottant
D	External diameter of the pipes
D_i	Internal diameter of the pipes
E_{BG}	Band-gap energy
$E_{c.el}$	Electrical energy generated by cell, per unit area
$E_{c.th}$	Thermal energy generated by cell, per unit area
$E_{c.th-p}$	Transfer of thermal energy, per unit area, from the cell to the thermal plate
$E_{c.l}$	Solar cell energy losses per unit area
E_{dc}	DC electrical power (W)
E_{g-c}	Energy, per unit area from glass to solar cell
$E_{g-p'}$	Energy per unit area due to insolation incident between the cells to pottant
$E_{g,l-a}$	Net energy per unit area from the glass to ambient
E_n	Electric valve n, where n is an integer
E_{PH}	Photo energy
E_{th}	Useful thermal power gain (W)
Ex_{el}	Electrical exergy in (kWh)
Ex_{th}	Thermal exergy in (kWh)
Ex_{out}	Net exergy output of PVT system in (kWh)
Ex_{pvt-t}	Annual exergy from the system in year t in (kWh)
f	frequency
F	Efficiency factor
F_{12}	View factor of surface 2 from 1
F_c	Collector efficiency factor
FF	Fill factor
F_R	Heat removal factor
G_p	In-plane irradiance in (W/m^2)
h	Plank's constant
h_c	Convection heat transfer coefficient
h_{fi}	Heat-transfer coefficient of the fluid
h_r	Radiation heat transfer coefficient
$h_{c,g-a}$	Convective heat transfer coefficient from glass to ambient.
$h_{r,c-g}$	Radiation heat transfer coefficient from cell to glass
h_w	Wind heat transfer coefficient ($\text{W}/\text{m}^2 \text{ } ^\circ\text{C}$)

I_O	Reverse bias (or dark) saturation current
$I_{bat,t}$	The installed cost (\$) of battery in year t
I_D	Diode or dark current
I_{MPP}	Current at MPP
I_{ph}	Photocurrent
I_{sc}	Short circuit current
I_t	Total investment expenditure in year t
$I_{inv,t}$	The installed cost (\$) of inverter in year t
J	Radiosity
k_C	Thermal conductivity
k	Boltzmann constant (given as 1.602×10^{19} J/V)
k_b	Back insulation conductivity
k_f	Thermal conductivity of the fluid in W/m K
k_g	Cover glass thermal conductivity
k_p	Coefficient of thermal conductivity of the pottant
k_{th}	Absorber thermal conductivity
L	Representative dimension
L_b	Back insulation thickness
L_e	Edge insulation thickness
l_g	Cover glass thickness
L_t	Financial loan cost in year t
l_{th}	Absorber thickness
$LCOE$	Levelized Cost of Energy
$LCOEx$	Levelized Cost of Exergy
\dot{m}	Mean mass flow rate
m_w	Mass flowrate of water
M_t or $O\&M$	Operation and maintenance cost (\$)
N	Number of glass covers
n	Ideality factor ranging from 1(ideal) to 2
N_u	Convection heat transfer coefficient
NPV	Net present value
P	Power
p	Parking factor of the cell
P_b	Total emissive power of blackbody
P_{bx}	Total emissive power from blackbody x, where x is a positive integer
P_e	Real surface emissive power
$P_{b\lambda}$	Monochromatic emissive power
P_r	Prandtl number
P_{MPP}	Maximum power point
PV_{CF}	Present value of the cash flow (\$)
PV_{Ex}	Present value of the exergy (W)
q	Electron charge (1.381×10^{23} J/K)
Q_{12}	Net radiation exchange between surfaces 1 and 2
Q_u	Useful thermal energy
r	Discount rate (%)
r_i	The refraction index of the medium
R	Collector perimeter
R_e	Reynolds number

R_S	Series resistor
R_{SH}	Shunt resistor
S	Speed of light ($S_o \approx 300,000$ km/s in a vacuum)
Sp_t	Total support and incentives in year t (\$)
t	Time in years
T	Absolute temperature
T_1 or T_i	Water inlet temperature in °C
T_2 or T_c	PVT cells back temperature in °C
T_3 or T_o	Water output temperature in °C
T_4 or T_c	PV cells back temperature in °C
T_5	Reservoir water temperature in °C
T_a	Ambient temperature in °C
$T_{a,min}$	Minimum ambient temperature
\dot{T}_c	Mean temperature for cell
\dot{T}_g	Mean temperature for glass
T_p	Absorber plate surface temperature
\dot{T}_p	Average plate temperature
T_{ref}	Reference temperature in °C
Tx_t	Total tax paid in year t (\$)
T_{sky}	Sky temperature
U_b	Back loss coefficient
U_e	Edge loss coefficient.
U_t	Top loss coefficients
U_L	Overall losses coefficient
v	The fluid flow rate
V	Voltage
V_D	Diode voltage
V_{MPP}	Voltage at MPP
V_n	Manual valve n, where n is an integer
V_{oc}	Open circuit voltage
V_T	Thermal voltage
W	Pipe spacing
w	Wind speed in m/s

Greek letters

α	Absorptivity
α_c	absorptance of the solar cell
α_g	cover glass absorptance
β	temperature dependent coefficient of electrical efficiency
ε	Emissivity
ε_c	emissivity for cell
ε_g	emittance of cover glass
ε_{th}	emittance of thermal absorber
ε_{ϑ}	temperature coefficient of parameter ϑ
η_0	efficiency at standard test conditions (STC)
η_{el}	Module electrical efficiency (%)
η_{ex}	Overall exergy efficiency (%)
η_{PVT}	Total efficiency of the PVT (%)

η_{th}	Module's thermal efficiency (%)
ϑ_{T_c}	parameter value at cell temperature T_c
$\vartheta_{T_{ref}}$	parameter value at reference temperature T_{ref}
θ	collector tilt (deg)
τ_g	glass transmittance
λ	wavelength
ρ	reflectivity
ρ_g	reflectivity of the glass
σ	Stefan–Boltzmann constant = $5.6697 \times 10^{-8} \text{ W/m}^2 \text{ K}^4$
τ	transmissivity
τ_g	Transmittance of glass
τ_p	Transmittance of pottant
ω	dynamic viscosity in pascals

Abbreviations

AIST	Japan National Institute of Advanced Industrial Science and Technology
BOS	Balance-of-system
CCT	Control circuit
CIS	Copper Indium Selenium
CdTe	Cadmium telluride
CO ₂	Carbon dioxide
DC or dc	Direct current
EnPe	Energy and Petroleum
FHG-ISE	Fraunhofer Institut für Solare Energiesysteme
IEA	International Energy Agency
IRENA	International Renewable Energy Agency
KNUST	Kwame Nkrumah University of Science and Technology
mc-Si	Mono-crystalline silicon
MINA	Faculty of Environmental Sciences and Natural Resource Management
MPPT	Maximum Power Point
NMBU	Norges miljø- og biovitenskapelige universitet (Norwegian University of Life Sciences)
NORAD	Norwegian Agency for Development Cooperation
NREL	National Renewable Energy Laboratory
Pt 100	Platinum temperature transducer
PV	Photovoltaic
PV_Bat	Photovoltaic Battery
PVT	Photovoltaic-thermal
PVT_Bat	Photovoltaic-thermal battery
RH	Relative humidity
SDG	Sustainable Development Goal
SE4ALL	Sustainable Energy for All
STC	Standard Test Condition (which are defined as Irradiance = 1000 W/m^2 , $T_c = 25 \text{ }^\circ\text{C}$, and air-mass ratio = 1.5)
UPER-CRET	Upgrading Education and Research Capacity in Renewable Energy Technologies
WHO	World Health Organization

List of papers

-
- Paper 1** **Saeed Abdul-Ganiyu**, David A. Quansah, Emmanuel W. Ramde, Razak Seidu and Muyiwa S. Adaramola (2020). Investigation of Solar Photovoltaic-Thermal (PVT) and Solar Photovoltaic (PV) Performance: A Case Study in Ghana. *Energies*, Volume 13 (11), May 2020, 2701; <https://doi.org/10.3390/en13112701>
- Paper 2** **Saeed Abdul-Ganiyu**, David A. Quansah, Emmanuel W. Ramde, Razak Seidu and Muyiwa S. Adaramola (2021). Techno-economic analysis of solar photovoltaic (PV) and solar photovoltaic thermal (PVT) systems using exergy analysis. *Sustainable Energy Technologies and Assessments*, Volume 47, October 2021, 101520; <https://doi.org/10.1016/j.seta.2021.101520>
- Paper 3** **Saeed Abdul-Ganiyu**, David A. Quansah, Emmanuel W. Ramde, Razak Seidu and Muyiwa S. Adaramola. Study Effect of flow rate on flat-plate water-based Photovoltaic-Thermal (PVT) system performance by analytical technique. *Journal of Cleaner Production*, Volume 321, September 2021, 128985; <https://doi.org/10.1016/j.jclepro.2021.128985>
-

Abstract

Access to energy has been heavily linked to socio-economic development. It is therefore not surprising that the energy poverty in sub-Saharan Africa has affected development in the subregion. However, as development increasingly becomes emissions-constrained, the role of renewable technologies takes on added significance and urgency. Thus, in the case of Sub-Saharan Africa, solar energy technologies come in handy in reducing the energy deficit while addressing emissions concerns. One innovative solar technology that combines conventional PV and solar thermal systems into one is the photovoltaic-thermal (PVT) technology. Although the PVT technology is seen to have a lot of potential in providing remote solutions, its performance is heavily linked to the environment where it is deployed. Nonetheless, the PVT technology has not been commercially successful as the conventional systems due to many reasons including lack of information and standards about the technology. Also, the PVT technology requires higher initial capital costs compared to separate solar PV and thermal systems – raising the question of whether it is really worth such investments.

Investment decision on the other hand relies on data regarding expected system performance in the deployed environment. While the PVT technology has been investigated in many places in the world, little can be said about field data on the technology in sub-Saharan Africa. The aim of this thesis is thus to scientifically contribute to bridging the data under-representation from countries in Africa in the area of PVT by assessing the technology in a tropical environment of Ghana.

To that end, an experimental setup comprising a water-based mono-crystalline PVT and a conventional mono-crystalline PV is installed at the Kwame Nkrumah University of Science and Technology in Kumasi and its short to long term performance assessed. The results for the study were communicated in three journal articles (Papers 1, 2 and 3).

Paper 1 assessed the real-life outdoor technical performance of the PVT module against a conventional PV system in a hot humid tropical climate in Ghana. Whereas the highest monthly mean efficiency recorded for the PV was 12.7%, the highest combined measured monthly mean electrical/thermal efficiency of the PVT was 56.1%. Based on their technical performances, it was concluded that the PVT is a worthy prospective alternative

energy source in off-grid situations, especially when both electrical and thermal energies are desired.

Paper 2 investigated the long term technical and economic viability of the PVT module in comparison with the conventional PV over a 25 year-period. It was observed that whereas it required about twice the upfront-cost for the PV-system/m² to setup the PVT-system/m², the battery cost accounted for about 61% and 34% of life cycle cost for PV and PVT systems respectively. Nonetheless, the PVT generally performed better than the PV in stand-alone situations when installed with batteries as back-up. However, the PV system becomes more economically viable than the PVT system when both systems were installed without batteries.

Paper 3 focused on the effect of flowrate on the performance optimization of the PVT system. The optimal flowrate for the PVT was observed to be 0.063 kg/s m². It was concluded that the commercial PVT system did not perform as expected in exergy terms when compared with separately installed conventional PV and thermal systems. The use of exergy at various mass flowrates and irradiances showed that using only combined efficiency, which is widely used approach, is not enough to assess PVT general performance.

In terms of degradation, it was generally concluded that the rate of degradation of output exergy due to ageing was projected to be lower in the commercial PVT module than the conventional PV module. This has been estimated to reach 11.3 % and 12.8 % respectively for the PVT and PV modules in their estimated 25-year economic life, which translates into approximately 6.1 % of total exergy losses for each module over the period. In addition, whereas the output losses of the PVT system increased curvilinearly from 15.4% to 26.7% over its economic life, that of the PV system increased from 16.1% to 31.7%.

Norsk Sammendrag

Tilgang til energi har stor korrelasjon med sosioøkonomisk utvikling. Derfor er det ikke overraskende at energifattigdom i Afrika sør for Sahara har påvirket økonomisk utviklingen i subregionen. Ettersom utviklingen i økende grad blir utslippsbegrenset, får fornybar teknologis rolle større betydning. I Afrika sør for Sahara, kommer solenergiteknologier til nytte for å redusere energiunderskuddet og utslippsproblemer. En innovativ solteknologi kombinerer konvensjonelt PV-system og sol termisk system til fotovoltaisk-termisk teknologi (PVT). Selv om PVT -teknologien har et stort potensial særlig i landlige områder, er ytelsen sterkt knyttet til miljøet der den er installert. PVT-teknologien har ikke vært kommersielt vellykket sammenlignet med de konvensjonelle systemene på grunn av mange årsaker, som mangel på informasjon og standarder til teknologien. PVT -teknologien krever også høyere startkapitalkostnader sammenlignet med separate solcelle -PV- og termiske systemer. Her kan man stille spørsmålet om det virkelig er verdt slike investeringer. Investeringsbeslutning er på den annen side avhengig av data om forventet systemytelse i det miljøet hvor systemet er installert.

Selv om PVT-teknologien har blitt undersøkt mange steder i verden, kan lite sies om feltdata om teknologien i Afrika sør for Sahara. Målet med denne oppgaven er å bidra til å bygge bro over datagapet ved å vurdere ytelsen til en PVT i et tropisk miljø i Ghana. For dette formål er et eksperimentelt oppsett som består av en vannbasert monokrystallinsk PVT og en konvensjonell monokrystallinsk PV installert ved Kwame Nkrumah University of Science and Technology i Kumasi, og dens korte til langsiktige ytelse vurderes. Resultatene for studien ble presenterte i tre tidsskriftartikler (1, 2 og 3).

I Artikkel 1 ble den virkelige utendørs ytelsen til PVT-modulen vurdert opp mot et konvensjonelt PV-system i et varmt fuktig tropisk klima i Ghana. Resultatene viser at den høyeste målte månedlige gjennomsnittlige effektiviteten for PV var 12,7%, mens den høyeste målte månedlige gjennomsnittlige elektriske / termiske effektiviteten til PVT var 56,1%. Det ble konkludert med at PVT er en verdig potensiell alternativ energikilde i områder utenfor strømmettet.

Artikkel 2 undersøkte den langsiktige tekniske og økonomiske levedyktigheten til PVT-modulen i sammenligning med den konvensjonelle PV-en over en 25-års periode. Resultatene viste at mens det krevde omtrent to ganger den opprinnelige kostnaden for å sette opp PV-systemet/m² enn for å sette opp PVT-systemet/m², var batterikostnaden omtrent 61% og 34% av livssyklus-kostnadene for henholdsvis PV- og PVT-systemer. Generelt fungerte PVT systemet bedre enn PV i frittstående situasjoner installert med batterier. PV -systemet blir imidlertid mer økonomisk levedyktig enn PVT -systemet når begge systemene ble installert uten batterier.

Artikkel 3 fokuserte på effekten av vannstrømningshastighet på ytelsesoptimaliseringen av PVT -systemet. Resultatene viste at den optimale strømningshastigheten for PVT var 0,063 kg/s m². Det ble konkludert med at det kommersielle PVT -systemet ikke fungerte som forventet med tanke på energi sammenlignet med separat installerte konvensjonelle PV- og termiske systemer. Bruken av eksergi ved forskjellige massestrømningshastigheter og bestrålinger viste at det ikke er nok å bruke bare kombinert effektivitet, som er mye brukt, for å vurdere dens generelle ytelse.

Når det gjelder nedbrytning, ble det generelt konkludert med at nedbrytningshastigheten for utgående eksergi på grunn av aldring anslås å være lavere i den kommersielle PVT -modulen enn i den konvensjonelle PV-modulen. Dette har blitt estimert til å nå henholdsvis 11,3 % og 12,8 % for PVT- og PV -modulene i deres estimerte økonomiske levetid på 25 år, noe som gir omtrent 6,1 % av de totale eksergitapene for hver modul over perioden. Mens energitapene til PVT -systemet økte krumlinjært fra 15,4% til 26,7% i løpet av dets økonomiske levetid, økte energitapene til PV systemet fra 16.1% til 31.7%.

Synopsis

1 Introduction

1.1 Energy and socio-economic development

Socio-economic development across the globe is linked to the availability of reliable energy. Meanwhile, billions of people worldwide do not have access to electricity, clean cooking and space heating [1] and are trapped extensively in a vicious cycle of poverty. The situation is particularly dire in Africa, which is home to 17% of the world's population but generates only 4% of global power supply [2]. Indeed, efforts to promote electrification are gaining momentum on the continent but are far outpaced by rapid population growth. As of 2019, the electrification rate in sub-Saharan Africa was 47.9% [2] with frequent electricity disruptions and economic losses. The corollary of this is that four out of five people in sub-Saharan Africa rely on the use of environmentally unsustainable energy sources such as fuel wood, mainly for heating water and cooking food resulting in deforestation and pulmonary diseases. Apart from the environmental impacts, these energy sources have been associated with significant health risks. According to World Health Organization (WHO), household air pollution from cooking with traditional solid fuels contributes to between three and four million premature deaths every year, globally [3]; this exceeds deaths due to malaria [4] and tuberculosis [5] combined.

Africa is experiencing a rapid urbanization coupled with increased development of small, medium and large-scale businesses. It is therefore anticipated that the overall demand for energy will continue to expand in Africa, as increasing prosperity in fast-growing urban economies lifts millions of people from poverty [6]. The growing energy demand poses a significant challenge- how to meet Africa' increasing energy demand as it grows and prospers while also reducing carbon emissions.

Carbon emission is projected to grow an average of 0.6 % per year between 2015 and 2040 [7]. Concerns emanating from global warming, Carbon dioxide (CO₂) emissions, depleting fossil fuel reserves have become topical issues in the current global energy scenario [8] [9]. As a result, 195 countries adopted the first-ever universal, legally binding global climate deal in Paris in December 2015 [10] [11]. The agreement sets out a global action plan to put the world on track to reducing the impacts of climate change by limiting

global warming to well below 2°C [10]. The International Energy Agency's (IEA) 450 Scenario suggests that carbon emissions need to fall by around 30% by 2035 to have a good chance of achieving the goals set out in Paris [6]. There is therefore a need to cut down on fossil fuel as sources of energy for cleaner and sustainable sources. Although energy-related CO₂ emissions remained stable in 2019, largely due to economic downturn as a result of the global COVID-19 pandemic, the world is not on track to limit global warming to well below 2°C as stipulated in the Paris Agreement [12].

The global energy poverty challenge has therefore become one in which both socio-economic development and reduction in global greenhouse gas emissions are pursued concurrently [13]. The United Nation's Sustainable Energy for All (SE4ALL) program is an example of many global initiatives that attempt to demonstrate the feasibility of pursuing these multiple goals without controversy. The SE4ALL initiative presents a nexus between energy access and climate change, and environmental sustainability more broadly - to mobilize various stakeholders to achieve universal access to modern energy services, doubling the share of renewable energy in the global energy mix and doubling the rate of improvement in energy efficiency, all by 2030 [13].

1.2 Renewable Energy Trends and Technologies in sub-Saharan Africa

Renewable energy global power share is estimated to increase from 7% in 2015 to nearly 20% by 2035 [6]. The importance of renewable sources to the global energy order is highlighted in the era of the novel global COVID-19 pandemic. The exogenous impact of the pandemic on global economic slowdown and its adverse effect on energy demand had little influence on the growth of renewables in power generation. In 2019, renewables were the only source of electricity to record demand growth over this period, due to low operating costs and preferential access to electricity networks [12]. Nonetheless, the stated reasons may not constitute a global representation of the situation in its entirety.

Expanding renewable energy access in Africa, for instance, will not only reduce poverty and greenhouse gases but will also improve gender equality and sanitation on the continent [14]. Apart from energy provision, renewable technology has the potential to reduce the continents employment deficits. However, a recent IRENA (International Renewable Energy Agency) report shows that less than 2 % of 11 million renewable-

energy jobs created globally is in sub-Saharan Africa [15]. These and many more have hampered industrial expansion on the continent and access to quality life, making it the poorest continent on the globe.

Among the renewable energy technologies that exist today, those based on solar energy has greatest potential in meeting the growing energy needs in Africa since it is an abundant and essentially inexhaustible source of energy accessible [8]. Africa has the richest solar resources in the world, but accounts for less than 1% of global solar PV installed capacity [2] mainly due to lack of favorable renewable energy policies such as those advancing affordability. Solar resources provide the option of decentralized (and off-grid) solutions to remote settlements because they are more reliable and much quicker to deploy. For example, the number of people who gained access to electricity through solar home systems in sub-Saharan Africa increased from two million in 2016 to approximately five million in 2018 [2].

Solar energy is commonly exploited through two main mechanisms, which are heat energy (for solar thermal systems) and light energy (solar photovoltaic systems). A hybrid photovoltaic-thermal (PVT) system combined these two mechanisms together as a single system. The solar PV component generates electricity while the integrated thermal absorber collects useful heat energy from the solar PV, reducing the solar PV cells temperature and thus, enhance their efficiency [16] [17]. Figure 1.1 shows an elaborate classification of PVT.

Hybrid PVT collectors are capable of reaching net (electrical plus thermal) efficiencies of 70% or higher, with electrical efficiencies up to 15–20% and thermal efficiencies in excess of 50%, depending on the conditions [18]. The combination of two technologies in one module also has the potential to reduce the use of materials, the time of installation, and the required space [19].

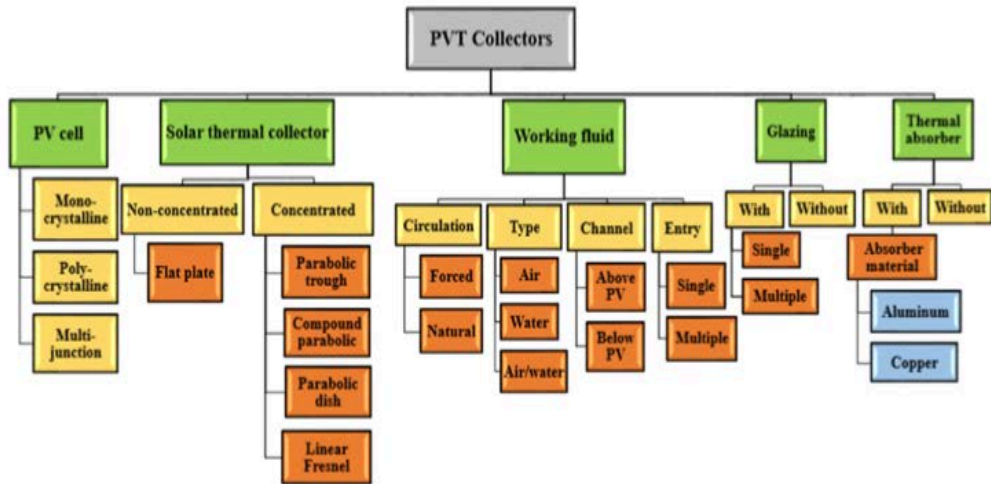


Figure 1.1: Classification of PVT solar collectors [20]

Ghana is in the tropical region of sub-Saharan Africa with relatively high ambient temperature and low wind speeds. Quansah et al. [21] have shown that solar PV systems installed in this region generally have higher module temperatures, which lead to power losses and hence, relative low performance ratios. This raises a concern about how to reduce PV modules temperature and thereby, improve their performance, and also harness the heat energy for potential users in the said environment. The PVT technology serves both purposes and hence the basis to investigate it in comparison with the PV technology in the said environment.

The advantages of the PVT system in generating electricity and simultaneously extracting the heat generated for useful means are suitable for residential applications. However, despite the potential of PVT systems, commercial PVT systems are still not as popular as stand-alone, and separately installed, PV and Thermal systems [22]. However, the deployment of stand-alone solar PVT technology requires higher initial capital costs - compared to separate solar PV and thermal systems - raising the question of whether it is really worth such investments. This could be ascertained scientifically by investigating its overall life cycle performance in the economic environment it is to be deployed. Investment due-diligence requires an understanding of the risk-return profiles to facilitate informed decisions. Therefore, this study will also seek to understand the economic feasibility of the PVT technology in comparison with the conventional PV

system in the economic environment of Ghana.

1.3 Problem Statement

PVT technologies have been studied since 1970s, including variation in designs, working fluids and other performance-influencing factors [17, 23]. The thermal and electric energy outputs depend on many factors, some of which are irradiance, ambient temperature, wind speed, circulating fluid temperature and flowrate [24, 25, 26]. Unlike indoor test conditions, climatic conditions could vary significantly affecting general performance and resilience of designs. For instance, the harsh harmattan weather conditions of sub-Saharan West Africa set it apart from other places in the world.

Two key factors to assess PVT system performance and technical characterization are the climatic conditions [27] and the operation temperature [28]. However, several of the experimental studies to predict the performance of PVTs were carried out in Europe (e.g. Spain [24], Cyprus [25] [29], Netherlands [30], France/Germany [31] and Greece [32]) and many parts of Asia (e.g. Malaysia [33], Taiwan [34], Hongkong [35], and China [36] [37]) with minimal experimental investigation records on the subject in sub-Saharan Africa in open literature. The few studies on PVT technology in Africa in the literature are based on climates of North Africa sub-region [26] [38] [39] and the country of South Africa [39] [40] [41] [42]. In the case of West Africa, studies on solar technology are either separately conducted on solar photovoltaic systems (e.g. [43] [44] [45] [46] [47] [48]) or solar thermal systems [48] [49] [50] [51], with very little evidence of studies on performance of the combined technology (PVT) in the literature. Like Aste et al. [27], Rajoria et al. [8] have also shown that PVT systems performance is directly related to climatic conditions. Thus, a performance assessment in the intended environment of deployment is necessary to make informed decisions on the technology.

In the case of economic performance, comparative techno-economic analyses of energy from flat-plate water PVT and conventional PV systems have been undertaken by a few authors from various locations worldwide. Herrando et al. [52] developed a model to assess the suitability of hybrid PVT systems for the provision of electricity and hot water in a domestic household in the temperate United Kingdom environment. They studied

the influence of varying collector flowrate and the covering factor of the solar collector with PV. They concluded that, with respect to primary energy and decarbonization, the PVT systems offered significantly improved proposition over equivalent conventional PV-only systems, but at a higher cost. In a further study, Herrando and Markides [53] considered the economic aspects based on which invaluable policy-related conclusion were drawn concerning the influence incentives including a proposed Renewable Heat Incentives. In addition to previous conclusions [52], they opined that although domestic heating demands in the UK outweighs electricity consumption by a factor of about 4, the support landscape strongly favoured electricity microgeneration which in turn favours PV only technology. Kalogirou and Tripanagnostopoulos [32] investigated the industrial application of PVT systems, relative to conventional PV systems. They proved the economic viability of the systems by showing that positive life cycle savings are obtained in the case of PVT systems compared with the PV, and the savings increased for higher load temperature applications. In another study [54], Tselepis and Tripanagnostopoulos undertook a cost/benefit analysis of PVT systems, and compared the payback time with separately installed conventional PV and solar thermal under support schemes and conditions in Greece.

The aforementioned comparative economic feasibility studies for the conventional PV and PVT ([52], [53], [32], [54]) were all based on energy analysis. Both electrical and heat are of different thermodynamic energy qualities and hence not comparable. Whereas energy is a conserved quantity based on the first law of thermodynamics, exergy is not conserved and is based on the second law of thermodynamics. Thus, exergy analysis allows qualitative assessment by comparing electrical and thermal energy based on the same standard and thus serves as a better parameter for comparing the two energies. Secondly, different pricing regimes and uneven incentive policies for heat and electrical energy in different economies could affect results for different regions. Thirdly, the study by Kalogirou and Tripanagnostopoulos [32] was skewed towards achieving higher heat energy for industrial application at the expense of electrical energy. Thus, flowrate analysis to achieve optimal overall performance for the PVT was not considered. Such a setup may affect the overall efficiency of the PVT.

Ghana has an all-year and near-uniform solar resource of average daily peak sun hours of 5.1 h [55] (see Appendix A), but like most countries in West Africa, water heating is mostly by either biomass, natural gas or electrical heaters with minimal use of solar options. Notwithstanding, the commercialization of PVT technology has generally not been successful [24] as the separate conventional PV and solar heaters. According to the IEA (Task 60), this is largely due to lack of information about the possibilities and benefits of PVT solutions, and the lack of international standards, which creates less confidence for end users [56]. These and many more have necessitated the need for a regional (or climate) based investigation of the PVT technology.

1.4 Aim and objectives of the thesis

Based on the aforementioned, the overall aim of this thesis is to assess the performance of a PVT in a tropical environment of Ghana. The specific objectives are:

1. To evaluate the technical performance of a flat plate water PVT system in comparison with a conventional system (Paper 1).
2. To assess life time cost effectiveness of flat plate water PVT system using exergy analysis as an economic parameter (Paper 2).
3. To assess the effect of flowrate on the performance optimization of flat plate water PVT system against the conventional PV system (Paper 3).

1.5 Contribution and Significance of Study

It is expected that the results of this study will contribute to the general body of knowledge. The study explores the use of exergy as an economic parameter in assessing the long-term feasibility of the PVT system in comparison with conventional systems. Secondly, this thesis is also expected to contribute to efforts at addressing issues of data under-representation from countries in Africa in the area of PVT technology. Thirdly, this thesis will be beneficial to stakeholders in making informed decision with regards to the options available to them in the use of solar technology. Residential and hospitality industry could significantly benefit hugely from reduced water heating and electricity bills through the use of PVT systems. Lastly, the findings of this study are expected to be directly beneficial to Sustainable Development Goal (SDG) 7, which is affordable and clean energy, and indirectly to other SDGs, such as SDG 3 (good health and well-being), SDG 11 (sustainable cities and communities), and SDG 13 (climate action).

1.6 Organization and structure of the Thesis

The thesis is based on three papers and generally structured into five sections. The first section introduces the topic, the problem statement and also presents the main aim and objectives of the study. The second section presents the fundamental theory underpinning the operation of the PV and PVT modules used for the study. Section three deals with the research methodology which details the experimental setup, analytical models and techniques to process information collected from the setup. Section four presents the main findings following the analysis of data from the experiment aimed at addressing the main objectives of the thesis. The fifth section presents a summary of the major conclusions of the entire study. The final section looks into limitations of the work and recommends practicable engineering directions based on findings as well as perspectives for further research.

2 Fundamental theory of modules

This section explains the theories behind the general solar energy conversions by the PV and PVT modules used in this thesis. It begins with the fundamental theory of photovoltaic cells. The general physics of heat transfers between materials is then addressed. This is followed by theory of operation of water flat plate thermal collectors. Finally, the analytical models for thermal energy transfer across the PVT are presented.

2.1 Fundamental theory of photovoltaic cells

The solar PV cell is a solid-state device which converts sunlight, as a stream of photons, into electrical power. The working principle of solar cells is based on the photovoltaic effect, that is, the generation of a potential difference at the junction of two different materials in response to electromagnetic radiation. For an absorbed photon to cause a photovoltaic effect in a semiconductor, its energy has to be greater than or, at least, equal to the band gap energy (E_{BG}) of the material [57]. The band-gap is therefore the minimum energy required to move an electron from the valence band to the conduction band of a material at a particular temperature. In semiconductors, this energy decreases with temperature. A photon (E_{PH}) energized electron (negative) leaves behind a hole (positive) causing charges separation across the material. Figure 2.1 is an illustration of this phenomenon. Excess energy is converted into heat. Also, the freed electron may give up its absorbed energy in the form of heat and fall back to recombine with a hole in the valence band.

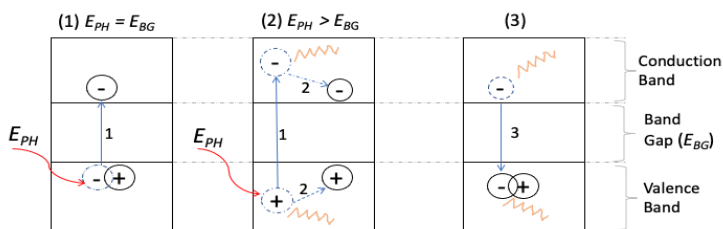


Figure 2.1: Photon absorption in a semi-conductor with band-gap E_{BG} showing the following scenarios: (1) E_{PH} excites an electron into the conduction band leaving behind an electron; (2) For $E_{PH} > E_{BG}$, the excess energy is converted to heat; (3) the excited electron gives up its energy as heat to recombine with a hole. [57]

A solar cell is commonly configured as a positive-negative (p-n) junction made from silicon resources. The positive-negative (p-n) junctions of silicon solar cells are made by diffusing an n-type dopant into one side of a p-type wafer (or vice versa). A simplified

structure of a solar cell showing silicon p-n junction is shown in Figure 3. When light of suitable wavelength is incident on the cell, it causes photovoltaic effect across the junction. Excess absorbed light energy is converted to heat.

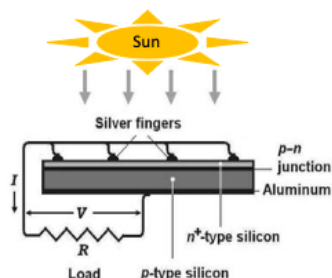


Figure 2.2: Structure of a solar cell showing silicon p-n junction and electrical contacts [58].

Solar cell technologies

Solar cell technology is an evolving one with ongoing research to improve both their performance and cost-effectiveness. This has led to many other solar cell technologies (See Table 2.1 for some examples). The traditional crystalline silicon cells are classified as first- generation cells. These cells may be monocrystalline or polycrystalline silicon with large grain sizes. Although they are more efficient at lower temperatures, they are also expensive to manufacture. They are however the most dominant type of PV cells in the market due to their stable power output over longer periods [59]. Thin-film cells are considered as the second-generation PV cells. They are cheaper than the first-generation cells because they require less silicon material. They however have a smaller share of the market because of their lower efficiency and precarious power output with time [59]. Some examples of thin-film technology cells include Amorphous silicon (a-Si), Cadmium telluride (CdTe) and Copper indium gallium selenide (CIGS). The third-generation cells include a range of alternative cells with the potential to overcome the Shockley-Queisser limit of 31-41% power efficiency for single bandgap solar cells [60]. Some common technologies for third generation cells are tandem cells (or multi-layer) cells, dye-sensitized cells, organic solar cells, perovskite solar cell and nano- crystalline (or quantum dot) solar cell [61]. Notwithstanding, some other indirect technologies - such as parabolic troughs, power towers, dish/engine systems and linear Fresnel reflectors - use concentration techniques to produce hot steam for electricity generation [62].

PV equivalent circuit.

An ideal solar cell behaves like a current source connected in parallel with a diode [63]. The current source generates electrical current, I_{ph} , when exposed to solar energy (photons). However, during darkness the solar cell behaves like a diode and generates current, called the diode or dark current (I_D), when connected to an external large voltage supply. This ideal model is completed with resistors to represent the losses and sometimes with additional diodes that take into account the current generated from the recombination of electrons and holes in the depletion region which dominates at lower forward-bias voltages. Figure 2.3 shows the most common solar cell equivalent circuit [63], comprising a current source, one diode and two resistors. The series resistor, R_S , takes into account losses in cell solder bonds, interconnection, junction boxes, etc., whereas the shunt resistor, R_{SH} , takes into account the current leakage (I_{SH}) through the high conductivity shunts across the p-n junction.

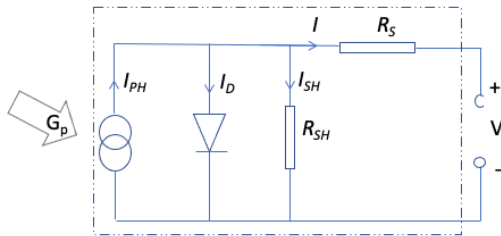


Figure 2.3: An equivalent solar cell circuit

From Kirchoff's current law, the output current I produced by the solar cell is given as:

$$I = I_{ph} - I_D - I_{SH} \quad (2.1)$$

From the Shockley ideal diode equation or the diode law, I_D can be expressed as [60]:

$$I_D = I_o \left[\exp \left(\frac{V_D}{nV_T} \right) - 1 \right], \quad (2.2)$$

where I_o is the reverse bias (or dark) saturation current, V_D is the voltage across the diode, V_T is the thermal voltage, and n is the ideality factor ranging from 1(ideal) to 2. The dark saturation current (I_o) is an extremely important parameter that differentiates one diode from another [64]. I_o is a measure of the recombination of charge pairs in a device. A diode with a larger recombination will have a larger I_o . The thermal voltage can be expressed as:

$$V_T = \frac{kT}{q}, \quad (2.3)$$

where k is the Boltzmann constant (1.602×10^{-19} J/V), T is the absolute temperature of the p-n junction, and q is the electron charge (1.381×10^{-23} J/K). Thus, the characteristic equation, which relates the solar cell parameters to the output current and voltage can be expressed as [65]:

$$I = I_{ph} - I_o \left[\exp\left(\frac{q(V+IR_S)}{nkT}\right) - 1 \right] - \frac{V+IR_S}{R_{SH}}, \quad (2.4)$$

Open circuit voltage

The main parameters that are used to characterize the performance of solar cells are the open circuit voltage V_{oc} , short circuit current I_{sc} , fill factor FF and the maximum power. The conversion efficiency (η) can be determined from these parameters. The extreme current-voltage situations of Equation (2.4) can be used to determine V_{oc} and I_{sc} .

The open-circuit voltage (V_{oc}) is the voltage at which no current flows (i.e., $I = 0$) through the external circuit. It is the maximum voltage that a solar cell can deliver. The V_{oc} corresponds to the forward bias voltage at which the dark current density compensates the photocurrent density. Thus, from Equation (2.4), for $I = 0$, $V_{oc} = V$, $R_{SH} \gg R_S$ and $I_{ph} \gg I_o$:

$$V_{oc} = \frac{kT}{q} \ln\left(\frac{I_{ph}}{I_o} - 1\right) \approx \frac{kT}{q} \ln\frac{I_{ph}}{I_o} \quad (2.5)$$

Short circuit current

The short circuit current, I_{sc} , is the current through the solar cell when the voltage across it is zero (i.e., $V = 0$). Thus, for short circuit condition, Equation (2.4) can be re-written as:

$$I_{sc} = I_{ph} - I_o \left[\exp\left(\frac{qI_{sc}R_S}{nkT}\right) - 1 \right] - \frac{I_{sc}R_S}{R_{SH}}. \quad (2.6)$$

The value of each term in the expression has shown that the second term of the expression is comparatively insignificant [66]. As a result, the second term of the right side of Equation (2.6) can be neglected [65] and the expression can be rewritten as:

$$I_{sc} = \left(\frac{R_{SH}}{R_{SH}+R_S}\right) I_{PH}. \quad (2.7)$$

Equation (2.8) shows that for an ideal solar cell at minimum resistive losses (or ideal situation), the short-circuit current and the photo-generated current are identical. Therefore, I_{sc} is the largest current which may be drawn from the solar cell.

Thus, at $T = 25^\circ\text{C}$, $n = 1$ and $R_{SH} \gg R_S$, the output current (Equation 2.4) and the open circuit voltage (Equation 2.5) can be approximated as:

$$I = I_{ph} - I_o[\exp(38.9V) - 1] \quad (2.8)$$

and

$$V_{oc} = 0.0257 \ln \frac{I_{ph}}{I_o} \quad (2.9)$$

From discussions so far, a plot of current-voltage (I-V) relation shows the extreme current and voltage conditions I_{sc} and V_{oc} respectively. The I-V curve of a PV module (or string) describes its energy conversion capability at the existing conditions of irradiance (light level) and temperature. A typical I-V curve of solar cells' single diode model is shown in Figure 2.4. It also shows the maximum power point (MPP), P_{MPP} . The solar cell should be operated at the maximum power voltage (V_{MPP}) to gain the MPP. The key electrical parameters highlighted in Figure 2.4 are generally provided by the manufacturer of the solar cell (or module).

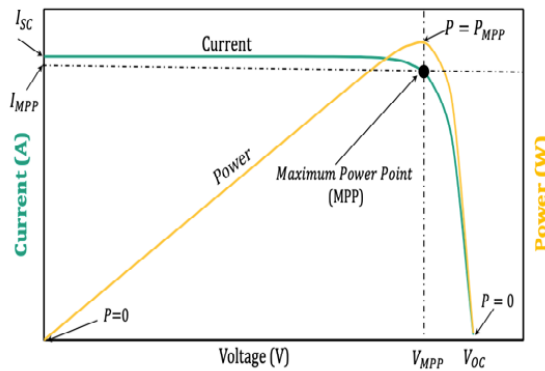


Figure 2.4: A typical I-V curve showing power profile

From the electrical power expression (i.e., $P = IV$), V_{MPP} occurs at the point where $dP/dV = 0$. Modern inverters in PV systems constantly adjust the load, seeking out the maximum operating power point at changing weather conditions.

Fill factor, FF

Although maximum current and voltage conditions for the solar cell are I_{sc} and V_{oc} respectively, Figure 2.4 shows that at both operating points, the power from the solar cell is zero. The fill factor, FF , is defined as the ratio of the maximum power from the solar cell to the product of V_{oc} and I_{sc} so that

$$FF = \frac{P_{MPP}}{V_{OC} \times I_{SC}} = \frac{V_{MPP} \times I_{MPP}}{V_{OC} \times I_{SC}} \quad (2.10)$$

The FF factor depends on the solar cell technologies which influence the shape of the IV curve. Table 2.1 shows V_{oc} , I_{sc} , FF and efficiencies of some selected technologies.

Effect of cell temperature on I-V curve

Environmental conditions, such as temperature or irradiation variations modify the I-V curve [67], and hence, influence the overall performance (energy yield) of solar cells. These variations affect the boundary conditions of the equations and, accordingly, the value of the equivalent circuit parameters. When temperature rises, whereas I_{sc} increases marginally, V_{oc} decreases significantly and the resultant P_{MPP} curve also decreases [63]. Figure 2.5 shows an example of variation of I-V curve of a silicon solar PV module with temperature. These variations are approximately linear with temperature, and most solar panel manufacturers include the rate of variation of the characteristic I-V curve points in the datasheets, either as absolute increase or as percent variation (please see Appendix E for an example of such data sheet). The variations with temperature on current and voltage levels variables, α , (e.g., V_{oc} , I_{sc} and P_{MPP}) can be expressed as [63]:

$$\vartheta_{T_c} = \vartheta_{T_{ref}} \left[1 + \frac{\epsilon_{\vartheta}}{100} (T_c - T_{ref}) \right], \quad (2.11)$$

where ϑ_{T_c} is parameter value at cell temperature T_c , $\vartheta_{T_{ref}}$ is parameter value at reference temperature T_{ref} and ϵ_{ϑ} is the temperature coefficient of ϑ expressed as a percentage change in the variable value with respect to a unit change in temperature ($\epsilon\%/^{\circ}\text{C}$). The temperature coefficient is dependent on the solar cell technology and may differ from one technology to another.

Table 2.1: Selected parameters of different cell technologies tested under the global air mass 1.5 spectrum (1000 W/m²) at 25°C [61]

Generation	Technology	Efficiency (%)	$V_{oc}(V)$	$I_{sc}(mA/cm^2)$	FF (%)	Test Centre (Date)	Description
First	Mono-crystalline silicon (mc-Si)	26.7 ± 0.5	0.738	42.65	84.9	AIST *1 (3/17)	Kaneka n-type rear IBC
	Poly-crystalline silicon (pc-Si)	20.4 ± 0.3	0.665	66.36	77.2	FhG-ISE *2 (10/19)	Hanwha Q cells
Second	Amorphous silicon (a-Si)	10.2 ± 0.3	0.896	16.36	69.8	AIST (7/14)	AIST
	Cadmium telluride (CdTe)	21.0 ± 0.4	0.876	35.25	79.4	Newport (8/14)	First solar
Third	Copper indium gallium selenide (CIGS)	23.4 ± 0.5	0.734	39.58	80.4	AIST (11/18)	Solar Frontier
	Organic thin film	18.2 ± 0.2	0.897	25.72	78.9	NREL *3 (10/20)	SJTU *4 Shanghai
	Dye sensitized	12.3 ± 0.4	1.02	15.17	79.1	Newport (8/19)	EPFL
	Nc-Si (nano crystalline) or quantum dots	11.9 ± 0.3	0.55	29.7	75.0	AIST (2/17)	AIST
	InGaP/GaAs/InGaAs	37.9 ± 1.2	3.065	14.27	86.7	AIST (2/13)	Sharp, two-terminal
Five-junction cell (bonded)	38.8 ± 1.2	4.76	9.56	85.2	NREL (7/13)	Spectrolab, two-terminal	
Perovskite/CIGS	24.2 ± 0.7	1.77	19.24	72.9	FhG-ISE (1/20)	HZB *5, two-terminal	

*1 AIST: Japanese National Institute of Advanced Industrial Science and Technology

*2 FhG-ISE: Fraunhofer Institut für Solare Energiesysteme

*3 NREL: National Renewable Energy Laboratory

*4 SJTU: Shanghai Jiao Tong University

*5 HZB: Helmholtz Zentrum Berlin

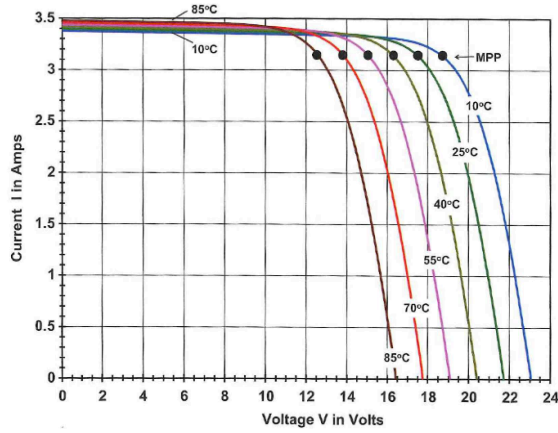


Figure 2.5: An example of variations in IV curves with temperature for a Siemens M55 monocrystalline solar module, at various cell temperatures and 1 kW/m² insolation [68].

Electrical Efficiency

Efficiency of energy systems are generally expressed as output over input energy. Nonetheless, the instantaneous electrical efficiency, η_{el} , of a crystalline solar cell could be expressed as a function of its temperature (T_c) [69]

$$\eta_{el} = \eta_0 [1 - \beta(T_c - 25)], \quad (2.12)$$

where η_0 is the efficiency at standard test condition (STC) (Irradiance = 1000 W/m² and $T_c = 25$ °C), T_c is the solar cell temperature and β is the temperature dependent coefficient of electrical efficiency. As stated in the previous section, β differs with different PV materials used [about 0.0045/K for crystalline silicon, 0.0035/K for copper indium selenide (CIS), 0.0025/K for Cadmium telluride (CdTe) and 0.002/K for amorphous Silicon (a-Si)]. Efficiency of energy systems are generally expressed as output over input energy. Figures 2.5 and 2.6 show that the performance of the solar PV is directly affected by cell temperature.

The photovoltaic efficiency of solar cells is temperature dependent and it generally decreases with the increasing temperature (see Figure 2.6) due to the worse mobility of carriers, diffusion length, as well as lifetime of minority carriers and saturation current. Silicon photovoltaic cells are good absorbers, so their temperature rises significantly

during operation [67]. Thus, to improve the performance of the PV, the cells must be operated at controlled temperatures. One method for achieving that is by extracting the nuisance heat using a thermal absorber on the back of the PV to extract the heat. The most popular PVT technology is the flat plate PVT system.

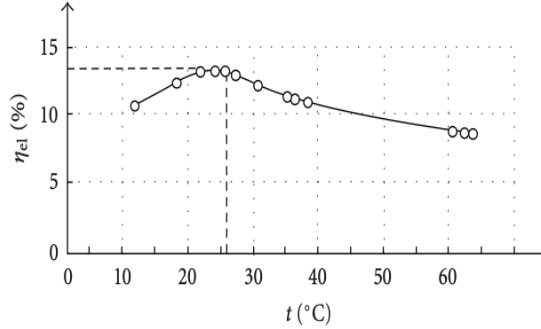


Figure 2.6: Efficiency of a crystalline silicon PV with $\eta_0 = 13.7\%$ as a function of cell temperature [67].

2.2 Fundamental theory of thermal energy transfer

Electromagnetic radiation interaction with surfaces

Heat energy can be transferred either by conduction, convection or radiation. Thermal radiation travels at the speed of light ($S \approx 300,000$ km/s in a vacuum) and is related to the wavelength (λ) and frequency (f) as:

$$S = \lambda f \quad (2.13)$$

When a beam of thermal radiation of wavelength, λ , is incident on a surface, a fraction of it is either reflected, absorbed and or transmitted in phenomena known respectively as reflectivity (ρ), absorptivity (α) and transmissivity (τ). These quantities are related as:

$$\rho + \alpha + \tau = 1 \quad (2.14)$$

A hypothetical blackbody absorbs all impinging thermal radiation such that $\rho = 0$, $\tau = 0$, and $\alpha = 1$. A blackbody is not just a perfect absorber but also characterized by emission of thermal radiation. Max Planck expressed the monochromatic emissive power (rate of energy emission per unit) of a blackbody in terms of temperature and wavelength as [70]

$$P_{b\lambda} = \frac{C_1/r_i^2}{\lambda^5(e^{C_2/\lambda T} - 1)}, \quad (2.15)$$

where $P_{b\lambda}$ is the monochromatic emissive power of a blackbody ($\text{W}/\text{m}^2 \mu\text{m}$), T is absolute temperature of the surface (K), $C_1 = 2\pi h S_0^2 = 3.74177 \times 10^8 \text{ W } \mu\text{m}^4/\text{m}^2$, $C_2 = h S_0/k =$

$1.43878 \times 10^4 \mu\text{m K}$, h is Plank's constant, S_0 is speed of light in a vacuum, k is Boltzmann's constant and r_i is the refraction index of the medium.

The total emissive power, P_b , is related to $P_{b\lambda}$ as

$$P_b = \int_0^{\infty} P_{b\lambda} d\lambda = \sigma T^4 \quad (2.16)$$

Equation (2.16) is the Stefan-Boltzmann law of radiation [71], where σ is the Stefan-Boltzmann constant ($5.6697 \times 10^{-8} \text{ W/m K}^4$). Also, the ratio of the total emissive power, P_b , of a real surface to that of a blackbody, P_e , with both surfaces at the same temperature, is known as emissivity, ε , of the real surface expressed as:

$$\varepsilon = \frac{P_e}{P_b} \quad (2.17)$$

For a real surface, the rate of total radiant energy leaving a surface per unit surface area is called the radiosity (J). The radiant energy leaving the surface includes its original emission and any reflected rays given as [72]:

$$J = \varepsilon P_b + \rho G_T \quad (2.18)$$

where G_T is the irradiation incident on the surface per unit area.

Coefficient of thermal radiation

For two black surfaces separated by non-absorbing medium, the fraction of radiation leaving surface say A_1 that reached surface A_2 is defined as the view factor, F_{12} and is given as [72]

$$Q_{1 \rightarrow 2} = P_{b1} A_1 F_{12} \quad (2.19)$$

The reverse of $Q_{2 \rightarrow 1}$ is also true for (2.19). If both surfaces are emitting, while absorbing all incident radiation from the other surface at the same time, the net radiation exchange between the two black surfaces is given by [72]:

$$Q_{12} = A_1 F_{12} (P_{b1} - P_{b2}) = A_2 F_{21} (P_{b1} - P_{b2}) \quad (2.20)$$

$$(P_{b1} - P_{b2}) = \frac{1}{A_1 F_{12}} Q_{12} = \frac{1}{A_2 F_{21}} Q_{12} \quad (2.21)$$

In an electrical circuit analogy, the term $(P_{b1} - P_{b2})$ is an energy potential difference, Q_{12} represents the flow of the energy, whereas the terms $1/A_2F_{21}$ and $1/A_2F_{21}$ represent the resistances due to the geometric configuration of the two surfaces [70]. If we assumed surface temperatures of T_1 and T_2 for surface A_1 and A_2 respectively, Q_{12} can be written as:

$$Q_{12} = A_1F_{12}\sigma(T_1^4 - T_2^4) = A_2F_{21}\sigma(T_1^4 - T_2^4) \quad (2.22)$$

For the case of opaque gray surfaces; $\tau = 0$, $\varepsilon = \alpha$ and the reflectivity $\rho = 1 - \alpha = 1 - \varepsilon$. From (2.18),

$$J = \varepsilon P_b + (1 - \varepsilon)G_p \quad (2.23)$$

The net radiant energy Q for the gray surface of area A is the difference between incident radiation and radiosity:

$$Q = A(J - G_T) = \frac{A\varepsilon}{1 - \varepsilon}(P_b - J) \quad (2.24)$$

Thus, if (2.34) is compared to an equivalent electric circuit, $(1 - \varepsilon)/A\varepsilon$ is the surface resistance due to the its imperfection as an emitter and absorber of radiation relative to a black surface. However, if we consider two parallel gray surfaces A_1 and A_2 the net radiation exchanges is given as:

$$Q_{12} = A_1F_{12}(J_1 - J_2) = A_2F_{21}(J_1 - J_2) \quad (2.25)$$

Thus, when two gray surfaces exchange radiation, apart from their individual surface resistances, there is also space resistance ($1/A_1F_{12} = 1/A_2F_{21}$) existing between them. Figure 2.7 shows an illustration of resistances between two radiation exchanging surfaces. The net rate of radiation exchange between the two surfaces is given by [72]:

$$Q_{12} = \frac{\sigma(T_1^4 - T_2^4)}{\left[\frac{(1 - \varepsilon_1)}{A_1\varepsilon_1}\right] + \frac{1}{A_1F_{12}} + \left[\frac{(1 - \varepsilon_2)}{A_2\varepsilon_2}\right]} \quad (2.26)$$

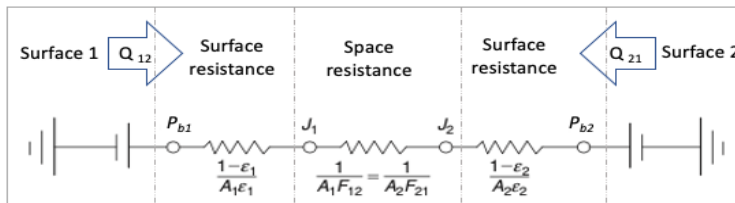


Figure 2.7: An illustration of radiation exchange between two gray surfaces showing equivalent electric network [72].

For two infinite parallel surfaces, $A_1 = A_2 = A$ and $F_{21} = 1$,

$$Q_{12} = \frac{A\sigma(T_1^4 - T_2^4)}{(1/\varepsilon_1) + (1/\varepsilon_2) - 1} \quad (2.27)$$

This can be written as:

$$Q_{12} = Ah_r(T_1 - T_2), \quad (2.28)$$

where

$$h_r = \frac{\sigma(T_1 + T_2)(T_1^2 + T_2^2)}{(1/\varepsilon_1) + (1/\varepsilon_2) - 1} \quad (2.29)$$

For a small convex surface, A_1 , completely enclosed by a very large concave surface, A_2 , $A_1 \ll A_2$ and $F_{12} = 1$:

$$Q_{12} = A_1 \varepsilon_1 \sigma (T_1^4 - T_2^4) \quad (2.30)$$

$$Q_{12} = A_1 h_r (T_1 - T_2), \quad (2.31)$$

where

$$h_r = \varepsilon_1 \sigma (T_1 + T_2)(T_1^2 + T_2^2) \quad (2.32)$$

The variable h_r is the radiation heat transfer coefficient for the different situations.

Coefficient of thermal convection

The convection heat transfer coefficient, h_c , is treated similarly in an equivalent circuit. Thus, if a wall at temperature T_2 is exposed to a cool fluid at temperature T_1 on one side, the convective heat-transfer rate can be given as [71]:

$$Q_c = Ah_c (T_2 - T_1) \quad (2.33)$$

Because of the many factors that affect the convection heat transfer coefficient, calculation of the coefficient is complex. The convective coefficient of heat transfer is calculated by Nusselt number (N_u), defined as the ratio of convection heat transfer to the fluid conduction heat transfer under same conditions. This can be expressed as [71]:

$$N_u = \frac{h_c L}{k_f} = Z R_e^a P_r^b \quad (2.34)$$

Where k_f is the thermal conductivity of the fluid in W/m K, L is representative dimension, R_e is Reynolds number given as $R_e = \dot{m}d/\omega$, P_r is Prandtl number given as $P_r = \omega c_p/k_f$, (Z , a , and b) are constant for the particular type of flow, \dot{m} mean mass flow rate, v is the

fluid flow rate, d characteristic linear dimension in m , ω is the dynamic viscosity in pascals and c_p is the specific heat capacity at constant pressure in $kJ/kg K$.

Thermal conduction

According to the second law of thermodynamics, heat will flow from the hot to the cold in an attempt to equalize the temperature difference, which is quantified in terms of heat flux Q . The heat flux is the rate per unit area at which heat flow in a given direction, which is directly proportional to the temperature difference δT and inversely proportional to the separation in distance δx .

$$\frac{dQ}{dt} = -k_c \frac{dT}{dx} \tag{2.35}$$

It could be seen from Figure 2.8 that the heat flow direction means temperature $T > T + \delta T$. The linear relation has a negative gradient, k_c , called the coefficient of thermal conductivity of the solid material.

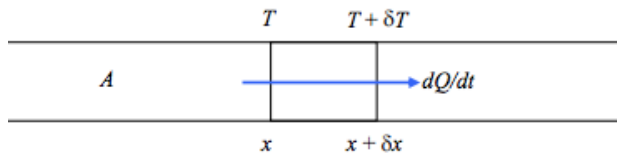


Figure 2.8: An illustration of heat flow through a conductor of cross section area A.

2.3 Fundamental theory of solar thermal collectors

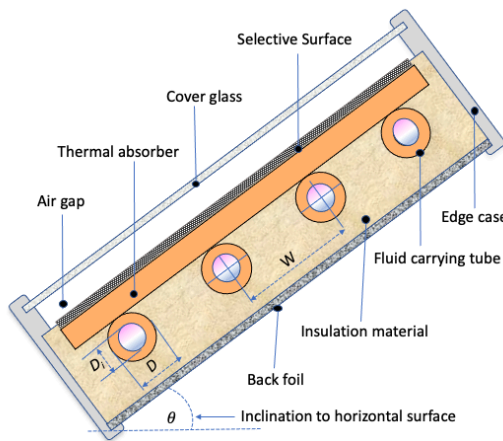


Figure 2.9: An illustration of a simple flat plate water thermal module

Solar thermal collectors convert solar energy directly into thermal energy. They are commonly designed as either flat-plate collectors, evacuated tube collectors, line focus collectors, or point focus/parabolic collectors. The flat-plate collectors may either be glazed (either single or multiple) or unglazed and may be coated with selective surfaces, such as tinnox, and insulated to reduce losses. Some of the common fluid channel design in the absorber include parallel plates, header-riser, serpentine and bionic. The thermal energy transfer medium is predominantly by air, liquids or both. Figure 2.9 shows a simplified water based flat-plate solar collector.

Flat plate water thermal absorber and thermal losses

The general performance of the flat plate solar thermal collector can be evaluated based on the Hottel–Whillier equations [73]. The thermal efficiency of a conventional flat-plate solar collector is the ratio of the useful thermal energy (Q_u) to the overall incident solar radiation (G_p). The maximum ratio of energy reaching the thermal absorber will be the product of the cover glass absorptance (α_g) and transmittance (τ_g). This could be expressed mathematically as:

$$Input = G_p(\alpha\tau)_{gt} \quad (2.36)$$

The total thermal losses are approximated as being proportional to the temperature difference between the absorber plate surface temperature, T_p , and the ambient temperature, T_a and it is expressed as:

$$Losses = U_L(T_p - T_a) \quad (2.37)$$

where U_L is the overall losses coefficient.

The introduction of a fluid as the main heat extraction agent means that a heat removal factor, F_R , must be used to account for the fluid flow rate, collector-to-fluid interface, and inherent properties of the transfer fluid itself. Thus, for a thermal collector of area A_{th} , the useful heat energy, Q_u , can be expressed as [73] :

$$Q_u = A_{th}F_R[G_p(\alpha\tau)_g - U_L(T_i - T_a)], \quad (2.38)$$

Summarily, the Hottel and Whillier-Bliss model (2.38) incorporates a heat removal factor, F_R which compares Q_u to the theoretical energy gain if the entire collector was kept at inlet temperature [74]. Thus F_R can be expressed as a function of fluid parameters as:

$$F_R = \frac{\dot{m}c_p(T_o - T_i)}{A_{th}[G_P(\alpha\tau)_g - U_L(T_i - T_a)]}, \quad (2.39)$$

where T_o outlet temperatures, respectively. The heat removal efficiency factor can also be expressed as follows [73] [70]:

$$F_R = \frac{\dot{m}c_p}{A_{th}U_L} \left[1 - \exp\left(-\frac{A_{th}U_L F_c}{\dot{m}c_p}\right) \right], \quad (2.40)$$

where F_c is the collector efficiency factor expressed as:

$$F_c = \frac{1/U_L}{W \left[\frac{1}{U_L[D+(W-D)F]} + \frac{1}{C_b} + \frac{1}{\pi h_{fi}D_i} \right]}, \quad (2.41)$$

where h_{fi} is the heat-transfer coefficient of the fluid, W is the pipe spacing, C_b is the conductance of the bond between the fin and copper circular pipes, D is the external diameter of the pipes, D_i is the internal diameter of the pipes and F is the fin efficiency factor expressed as [70]:

$$F = \sqrt{\frac{U_L}{k_{th}l_{th} + k_g l_g}}, \quad (2.42)$$

where l_{th} is the absorber thickness, k_{th} is the absorber thermal conductivity, l_g is the cover glass thickness and k_g is the cover glass thermal conductivity. If it is assumed that all losses occur to a common sink temperature T_a , then the overall loss coefficient (U_L) of the collector is the sum of the edge (U_e), top (U_t) and the back (U_b) loss coefficients, expressed as:

$$U_L = U_b + U_e + U_t \quad (2.43)$$

Assuming U_b is limited to heat flow through the back insulation material only, then it can be estimated as:

$$U_b = \frac{k_b}{L_b}, \quad (2.44)$$

where k_b is the insulation conductivity and L_b is the back insulation thickness. For most collectors the evaluation of edge losses is complicated. However, in a well-designed system, the edge loss should be small so that it is not necessary to predict it with great accuracy [70]. The edge losses could be estimated as:

$$U_e = \frac{k_b R l_{th}}{l_e A_{th}}, \quad (2.45)$$

where R is the collector perimeter, l_{th} is the collector thickness and L_e is the edge insulation thickness. Klein [75] has shown that the top losses can also be expressed as:

$$U_t = \left(\frac{N}{\left[\frac{C}{T_p} \frac{(T_{th} - T_a)}{(N+f)} \right]^e + \frac{1}{h_w}} \right)^{-1} + \frac{\sigma(T_{th} + T_a)(T_p^2 + T_a^2)}{\frac{1}{\varepsilon_{th} + 0.00591N h_w} + \frac{2N + f - 1 + 0.133\varepsilon_{th}}{\varepsilon_g} - N}, \quad (2.46)$$

where

N = number of glass covers

$f = (1 + 0.089h_w - 0.1166h_w\varepsilon_{th})(1 + 0.07866N)$

$C = 520(1 - 0.000051\theta^2)$

$e = 0.430(1 - 100/T_{abs})$

θ = collector tilt (deg)

ε_g = emittance of cover glass

ε_{th} = emittance of thermal absorber

h_w = wind heat transfer coefficient ($W/m^2 \text{ } ^\circ C$)

The thermal efficiency of the absorber, η_{th} , could then be determined from (15) as:

$$\eta_{th} = F_R(\alpha\tau)_g - U_L F_R \frac{(T_i - T_a)}{G_p}, \quad (2.47)$$

Equation (2.27) is a linear equation with η_{th} expressed as a function of $(T_i - T_a)/G_T$, ss could be seen from Figure 2.10.

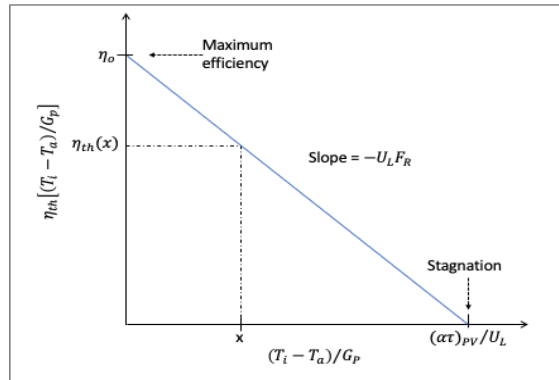


Figure 2.10: A plot of the thermal efficiency curve (2.47).

From Equation (2.38), when input energy becomes equal to energy losses, (i.e., $Q_u = 0$ and $\eta_{th} = 0$ (see Figure 2.10), equilibrium or stagnation temperatures is said to have

occurred. The equilibrium temperatures are substantially higher than ordinary operating temperatures. Once the plate temperature, T_p , can no longer increase, stagnation occurs. It can occur at higher radiation under no flow conditions, or on a cold, windy, clear day where convection and radiation losses are large and the heat loss coefficient, U_L , approaches the magnitude of the energy absorbed. The stagnation temperature could be estimated as:

$$T_p = T_a + \frac{(\alpha\tau)_{gl} G_P}{U_L}, \quad (2.48)$$

At these temperatures the pressure in the collector can be very high and most collector fluids either will have been boiled off or far exceeded their maximum working temperature [70]. Proper design of the collector fluid circuits can alleviate overheating problems. Figure 2.11 shows efficiency curves of some solar collectors and their suitable temperature applications.

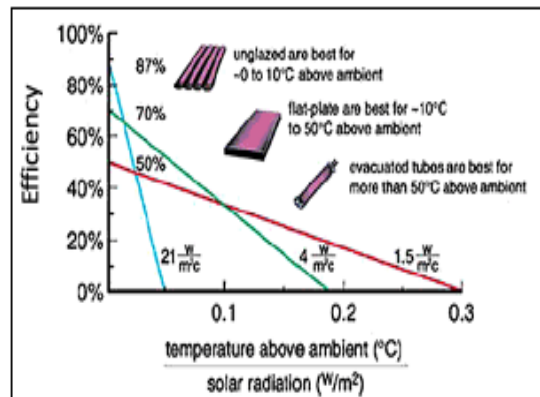


Figure 2.11: Efficiency curves of selected solar collectors showing operation temperatures and suitability [76].

2.4 Analytical model of energy in a PVT system.

The energy transition in the water based flat plate PVT module is summarized in Figure 2.12. This is based on the following assumptions: (1) Insulation in the back and the edges of the module are lossless, (2) There is no heat transfer in the direction of the flow, the energy transferred in the flow direction is by mass transfer, (3) Properties of glass and insulation are independent of temperature (constant), (4) All thermo-physical properties

of the fluid, air gap, and absorber are temperature, and (5) Dust and dirt on the collector are negligible.

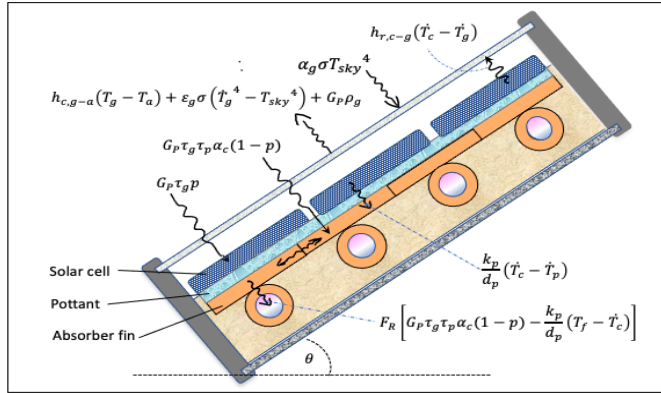


Figure 2.12: Energy transition in a water based flat plate PVT

The solar energy, per unit area, E_{g-c} , reaching the solar cell through the cover glass cover is given by

$$E_{g-c} = G_p \tau_g p \quad (2.49)$$

where τ_g is the transmittance of the glass cover and p is the parking factor of the cell envelope area. Assuming the cover glass is of very low iron content, it means absorption by the glass is negligible. Also, the absorptance of the solar cell, α_c , and τ_g are assumed to be close to unity and hence interreflection of insolation between the cells and the glass surface (s) is neglected. The electrical and thermal energy, per unit area, generated by the solar cell is given respectively as:

$$E_{c.el} = \eta_{el} G_p \tau_g p \quad (2.50)$$

where η_{el} is the cell electrical efficiency. Thus, thermal energy generated by the cell per unit area will be give as:

$$E_{c.th} = \alpha_c E_{g-c} - E_{c.el} - E_{c.l} \quad (2.51)$$

$$E_{c.th} = (\alpha_c - \eta_{el}) G_p \tau_g p - E_{c.l} \quad (2.52)$$

where $E_{c.l}$ is the solar cell energy losses, per unit area, which means that the thermal energy generated by the solar cell is partly lost to the top cover glass by a combination of natural convection and radiation. However, for a PVT, the airgap between the cell and the

cover glass is very thin and therefore losses by convection between cell and glass is assumed to be negligible. Thus $E_{c,l}$ is radiation dominated and is given as:

$$E_{c,l} = h_{r,c-g}(\dot{T}_c - \dot{T}_g) \quad (2.53)$$

where $h_{r,c-g}$ is the radiation heat transfer coefficient from cell to glass expressed as:

$$h_{r,c-g} = \frac{\sigma(\dot{T}_c + \dot{T}_g)(\dot{T}_c^2 + \dot{T}_g^2)}{(1/\varepsilon_c) + (1/\varepsilon_g) - 1} \quad (2.54)$$

where \dot{T}_c , \dot{T}_g , ε_c and ε_g are respectively the mean temperature for cell, mean temperature for glass, emissivity for cell and emissivity for glass. For energy conservation, $E_{c,l}$ is transmitted as part of energy losses by the cover glass to ambient. This is expressed as

$$E_{g,l-a} = h_{c,g-a}(T_g - T_a) + \varepsilon_g \sigma (\dot{T}_g^4 - T_{sky}^4) + G_P \rho_g \quad (2.55)$$

where $E_{g,l-a}$ is net energy per unit area from the glass to ambient, T_{sky} is sky temperature, ρ_g is reflectivity of the glass and $h_{c,g-a}$ is the convective heat transfer coefficient from glass to ambient. Stulz and Wen [77] have shown that

$$h_{c,g-a} = 1.247[(\dot{T}_g - \dot{T}_a) \cos \theta]^{1/3} + 2.658w \quad (2.56)$$

where θ is PVT module's inclination to the horizontal, \dot{T}_a mean ambient temperature and w is wind speed in m/s. Thus, the available thermal energy from the cell per unit area, that is not lost, which is transferred to the thermal plate is given as:

$$E_{c.th} = (\alpha_c - \eta_{el})G_P \tau_g p - h_{r,c-g}(\dot{T}_c - \dot{T}_g) \quad (2.57)$$

If we assume that the pottant between the cell and the thermal plate is infrared radiation opaque, then $E_{c.th-p}$ transfer of energy per unit area from the cell to the thermal plate will be only by conduction. Thus,

$$E_{c.th-p} = \frac{k_p}{d_p}(\dot{T}_c - \dot{T}_p) \quad (2.58)$$

where \dot{T}_p is the average plate temperature, k_p is the thermal conductivity of the pottant and d_p is the thickness of the pottant. This means that \dot{T}_p can be calculated from

$$(\alpha_c - \eta_{el})G_P \tau_g p - h_{r,c-g}(\dot{T}_c - \dot{T}_g) = \frac{k_p}{d_p}(\dot{T}_c - \dot{T}_p) \quad (2.59)$$

Aside $E_{c.th-p}$ there is also energy per unit area, E_{g-p} , due to insolation incident between the cells which is transmitted through the pottant to the thermal absorber which is given as:

$$E_{g-p} = G_p \tau_g \tau_p \alpha_c (1 - p) \quad (2.60)$$

We can now consider heat transfer to fins and subsequently to the tubes along the flow length. From Hottel and Whillier [73], the heat transfer by tubes to the fluid at temperature T_f is given by:

$$Q_{th} = A_{th} F_R \left[G_p \tau_g \tau_p \alpha_c (1 - p) - \frac{k_p}{d_p} (T_f - T_c) \right] \quad (2.61)$$

The losses coefficient in (2.61) - i.e. $U_L = k_p/d_p$ - shows that the absorber losses is only limited to the pottant (i.e. $U_e = U_b = 0$). Thus, F_R for the PVT can be expressed as:

$$F_R = \frac{\dot{m} C_p d_p}{A_{th} k_p} \left[1 - \exp \left(\frac{A_{th} k_p F_c}{\dot{m} C_p d_p} \right) \right], \quad (2.62)$$

where F_c is the collector efficiency factor expressed as:

$$F_c = \frac{d_p/k_p}{W \left[\frac{d_p}{k_p [D + (W-D)F]} + \frac{1}{C_b} + \frac{1}{\pi h_{fi} D_i} \right]}, \quad (2.63)$$

where h_{fi} is the heat-transfer coefficient of the fluid. F is expressed as:

$$F = \sqrt{\frac{k_p/d_p}{k_{th} l_{th} + k_p l_p}}, \quad (2.64)$$

Thus, the thermal efficiency η_{th} of the absorber could be determined from (60).

$$\eta_{th} = F_R \tau_g \tau_p \alpha_c (1 - p) - \frac{k_p}{d_p} F_R \frac{(T_f - T_c)}{G_p}, \quad (2.65)$$

3 Materials and Methods

The methodology used in accomplishing the set objectives for this thesis includes design of experiment, installation of experimental set-up, data measurement and logging over the period of study, analyzing the data with relevant statistical tools. Figure 3.1 conceptualizes the logical relationships between the goal of the thesis, specific objectives, research edge as well as the approach research method. It also clearly shows how the individual research papers contribute to the overall thesis goal.

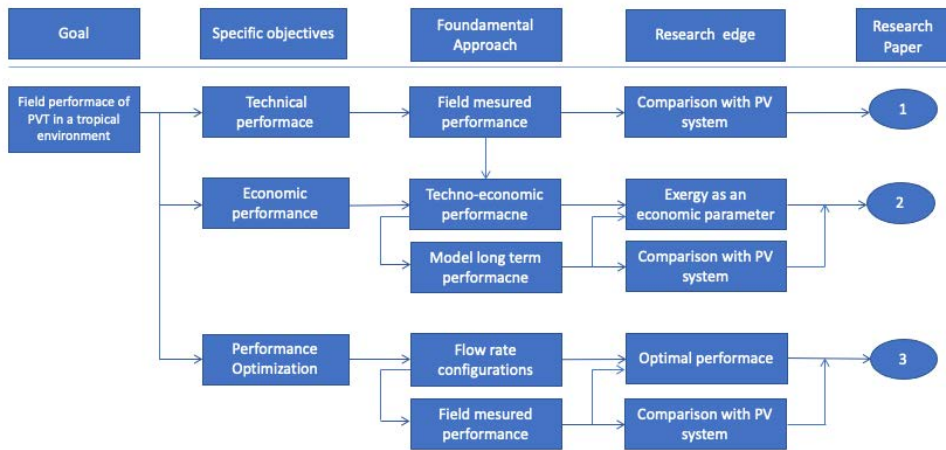


Figure 3.1: Conceptual Framework

3.1 Experimental design and set-up

Experimental design is a method used to organize, conduct, and interpret results of experiments in an efficient way, to obtain useful information through a small number of trials [78]. Proper organization of experiments is a foundation of every thoughtful research. The main goal of any experimental study is to find the relationships between independent variables (factors) and dependent variables (results, outcomes) within the experimental framework. Even though it sounds easy to accomplish, this task can be cumbersome when it is not organized correctly. Inevitably, decisions on an experimental design involve making difficult choices among options because of resource constraints while focusing on the main aim [78].

The experimental set-up for this thesis consists of conventional solar PV installation and hybrid PVT installation, as well as instrumental set-up for measuring ambient weather conditions and other variables. Figure 3.2 shows an elaborate schematic diagram of the experimental setup for this study as could be seen in Papers 1 and 3.

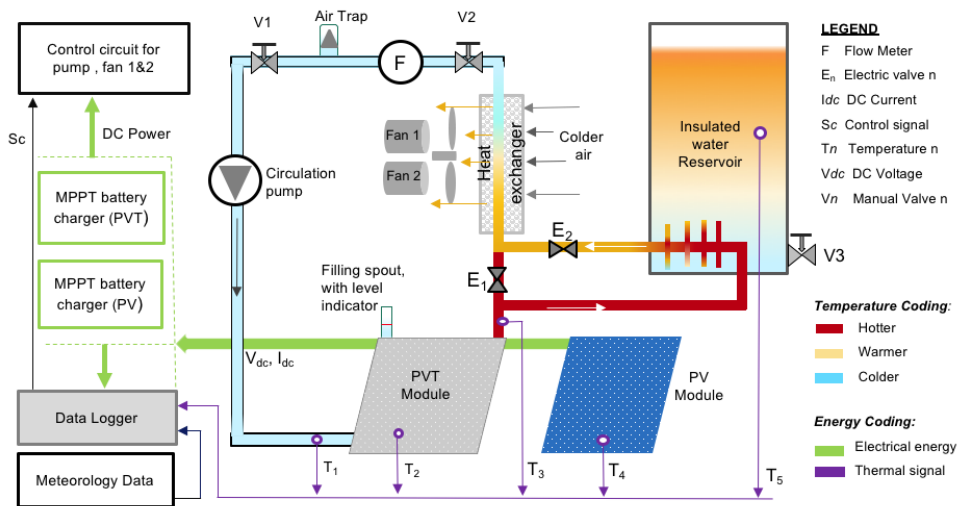


Figure 3.2: The schematic shows the interconnection of components, data measurement points and energy flow of the experimental setup.

The main heat transfer medium (fluid) for the PVT in the setup in Figure 3.2 has been by force-circulation of water. For a closed loop system, the absorber heat transfer fluid is important to the life, design, and operation of the system. Some popular transfer fluids include water, water/glycol mix, synthetic hydrocarbons and silicon. Given the location of the setup with no threats of freezing due to ambient conditions, water has been used in the collector loop because it is readily available, and, it has superior specific heat capacity to any other transfer fluid and it is economically cheaper to access. Water is also odorless and non-toxic in its pure state and therefore easier to handle. Water is also thermally stable and does not degrade with temperature. It therefore requires the use of simple single-walled heat exchangers with little dangers of contamination.

To transfer the thermal energy from the working fluid to the storage tank fluid requires a heat exchanger. The heat exchanger for the setup was made from a 3.6 m length of smooth surfaced cylindrical copper pipe with average external diameter of 0.015 m and

sheet thickness of 0.001 m. Copper pipe has been used because of its good heat conduction property. The copper pipe was coiled into 7 turns with a mean external coil diameter of 0.16 m and a mean pitch of 0.02 m. Figure 3.3 shows a picture of the heat exchanger. The heat exchanger has been placed inside the storage tank closer to its bottom. Heat transfer to stored water has been purely by convection due to gravity. Although the unconventional rule of thumb for sizing is approximately 0.2 m² heat exchanger surface per m² area of flat-plate collectors, this has not been strictly applied in this case because for hybrid collectors the generation of electric power could have a major influence on the thermal performance [72].

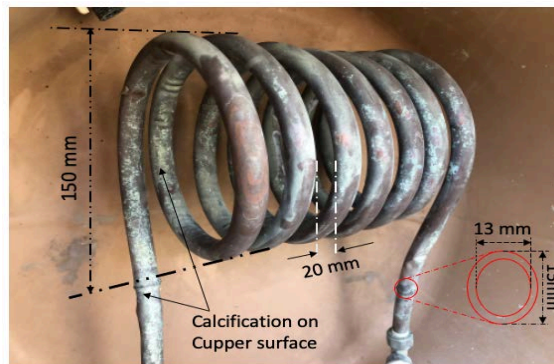


Figure 3.3: Heat exchanger with some dimensions

The main focus of the setup is on the performance of the modules, which is directly related to the fluid inlet temperature for the thermal absorber in the case of the PVT. Lower inlet temperature leads to higher collector efficiency [72] and also lower temperatures for PV cells. Thus, to further reduce the temperature of the returning working water, apart from the conventional heat exchanger in the storage tank, a radiator system has been included in the absorber loop. The radiator is made up of water-to-air heat exchanger with a pair of fans. The sizing of the radiator system was not based on any technical specifications. However, some design details could be found in Appendix F. The radiator system contributes to the performance of the setup in two ways: (1) An important aspect of thermal absorber testing is to keep the specific heat capacity (c_p) and density (ρ) of the fluid used within $\pm 1\%$ over the range of fluid temperatures used during the tests [79]. As could be seen from Figure 3.4, maintaining the inlet temperature between 25-40 °C ensures that ρ and c_p remain with $\pm 1\%$. Thus, radiator system reduces

the chaotic changes in the water inlet temperature - for a test facility in an erratic outdoor environment- and the influence of relatively higher storage water temperatures on the temperature of the returning inlet water. (2) Also, lowering the water inlet temperature relative to ambience reduces thermal losses (see Equation 2.47) and hence improves the efficiency of the setup.

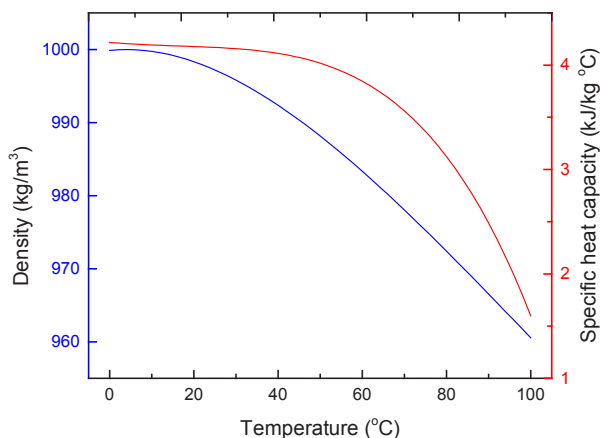


Figure 3.4: A variation of density and specific heat capacity of water with change in temperature at constant pressure of 1bar.

For normal operation of solar collectors, thermal capacitance is provided to alleviate the solar availability and load mismatch and improve the system response to sudden peak loads or loss of solar input. As stated earlier, this also improves the system's efficiency by preventing the heat transfer fluid from quickly reaching high temperatures, which lower the collector efficiency. The water storage tank for the setup is non-pressurized with the heat exchanger installed closer to its base. Figure 3.5 shows some details of the storage tank. The tank used for the study is a cylindrically-shaped 75L plastic thermos vessel with a very tight lid, originally for storing cold and hot substances over short periods for domestic use. This has always been filled to 70L for the study for consistency. The sizing was based on the typically rule of thumb of about 40–80 L per square meter of collector area [72]. To improve its insulation property, an additional 19 mm thick Armaflex sheet has been used to cover its outer curved surface and base. This was then finally covered with a thermal resistance foil to reduce its thermal interaction with the environment (see Appendix G for details). The lid was however not modified. The tank has also been fitted with a manual valve closer to the base to allow for easier emptying of content.



Figure 3.5: Some details of thermal storage vessel showing: (a) the thermos vessel, (b) armaflex insulation, (c) heat exchanger, (d) spout for transducer insertion, (e) non modified lid, (f) thermal resistant foil cover and (g) manual valve

3.1.1 Working principle of the experimental setup

The basic principles of experimental designs are randomization, replication and local control. These principles make a valid test of significance possible. A good experimental setup should obtain relevant information with minimal risk of errors using as minimum resources as possible. As described in Papers 1-3, the operation of a water PVT system involves the working together of many sub-components to achieve desired results. Figure 3.8 shows a flow diagram of sequence of operation of the setup shown in Figure 3.2. As could be seen, the operating conditions depend on whether (irradiance in this case), selected mode of operation (1 or 2) and set variable limits. These are achieved by systematic control circuit with monitoring system (data logger in this case) and well balance load distribution of components to achieve maximum power point (MPPT) operation.

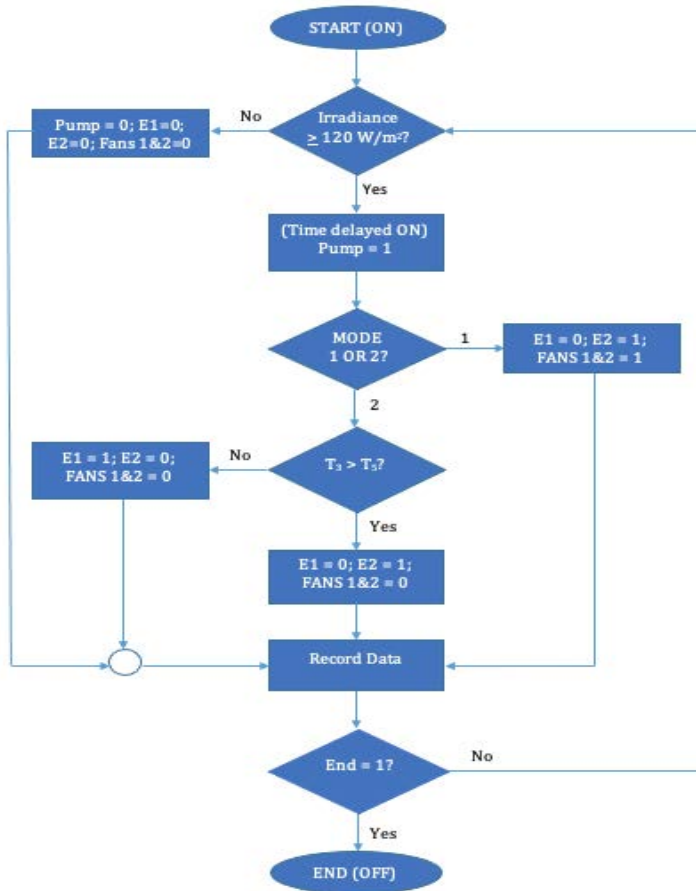


Figure 3.6: Flow diagram of working principle of the experimental setup

3.1.2 Control circuit

One method of reducing human errors in an experimental setup is to automate most of the repetitive activities. This is achieved by using intelligent control systems. As could be seen, Figure 3.7 illustrates a rough design of electrical loads distribution; showing battery chargers, batteries, pump, fans, data logger and the control circuit. This also means that the electrical energy required by the components in the setup is completely generated by the PV and PVT modules, making it an energy independent system. Figure 3.8 also shows fine details of how individual components are interconnected to create an intelligent control circuit (CCT) (Also see Appendices B and C). The CCT includes relays, switches and monitoring system (data logger). It could be seen from the CCT that the setup works

as a stand-alone unit with minimal human interventions. Also, both Figures 3.7 and 3.8 show fuses (i.e., F1-F8) in the circuits for protection against faulty components.

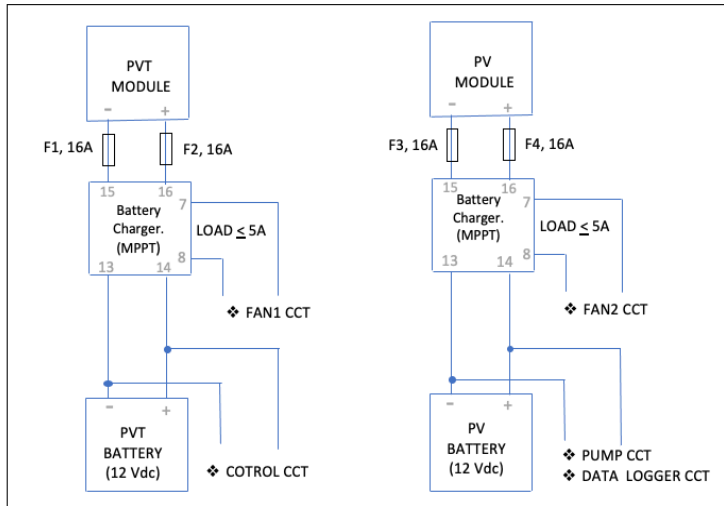


Figure 3.7: Electrical load distribution for PV and PVT sub-systems

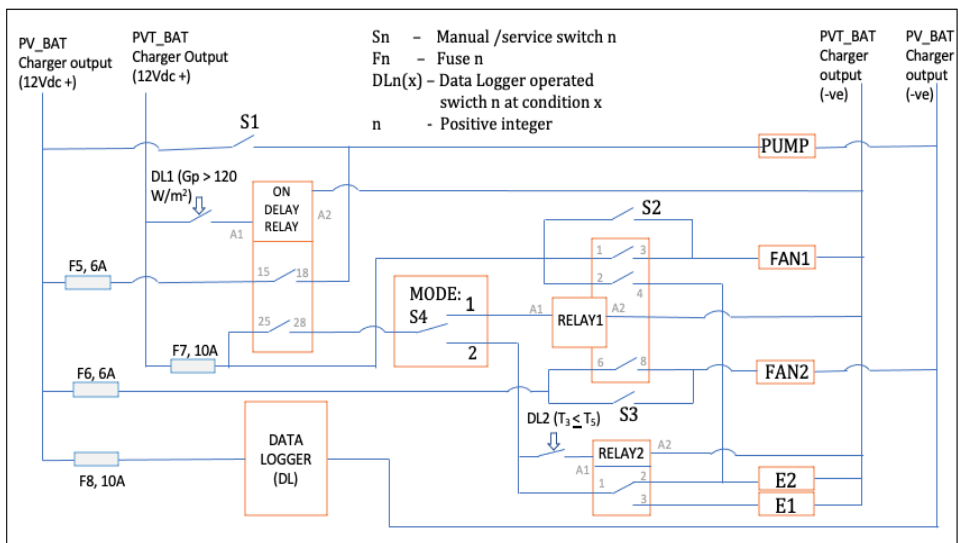


Figure 3.8: Control circuit showing detailed electrical load distribution and interconnections between control relays, switches, fuses and energy sources.

3.1.3 Modes of operation of the PVT sub-system

The PVT sub-system has been designed to operate in two fundamental modes. Figure 3.9(A) shows simplified line diagram of the PVT's closed-loop water circulation circuit in an idle state (pump off). As could be seen from Figure 3.6, this state of operation will occur in any of the modes when G_p (i.e., in-plane irradiance) $< 120 \text{ W/m}^2$.

Operation Mode 1 configuration is biased towards maximizing electrical energy output from the PVT module by cognizant cooling of circulating water in the closed-loop, resulting in relatively lower average cells temperature and hence subsequent improvement in electrical efficiency. In this mode, for experimental reasons, heat transfer to water in reservoir is compromised. Figure 3.9 (B) shows Mode 1 configuration. For an initial condition of $G_p \geq 120 \text{ W/m}^2$, the water is continuously circulated through the water reservoir and water-to-air heat exchanger and returns to the inlet of the PVT module relatively colder. This mode also reduces variations in T_1 to the barest minimum for the outdoor experimental setup. This configuration was used for collecting the primary data for Paper 1.

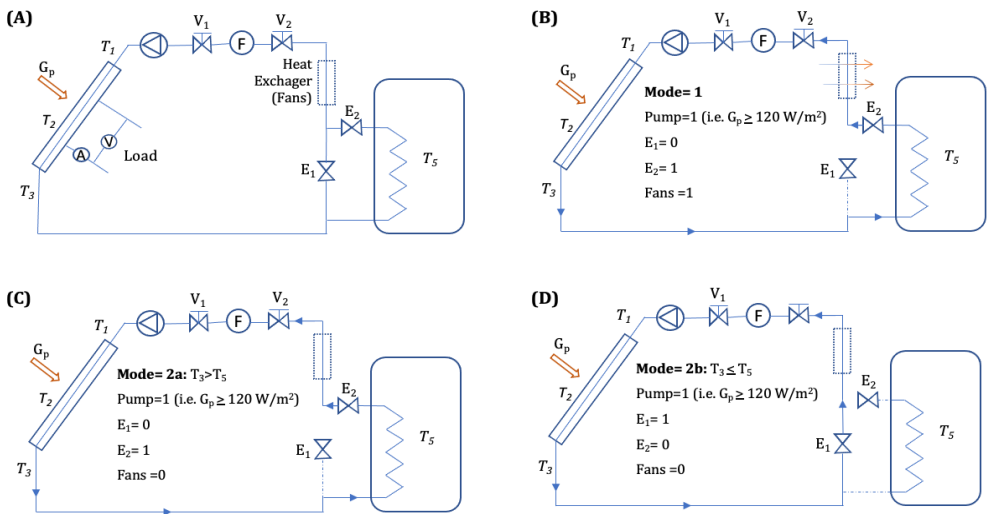


Figure 3.9: (A) Simplified line diagram of the PVT's closed-loop water circulation circuit in an idle state; (B) operational Mode 1 configuration; (C) operational mode 2 configuration when $T_3 > T_5$; (D) operational mode 2 configuration when $T_3 \leq T_5$

Operation Mode 2 explores the heating of stored liquid in a reservoir, a fundamental principle in domestic solar hot water systems. For initial conditions of $G_p \geq 120 \text{ W/m}^2$ and

$T_3 > T_5$, the warmer water from T_3 is continuously circulated through heat exchanger coil in the reservoir till any of the pre-conditions is breached. This configuration is illustrated in Figure 3.9(C). However, as could be seen from Mode 2b configuration shown in Figure 3.9(D), for $G_p \geq 120 \text{ W/m}^2$ and $T_3 \leq T_5$, the exiting water from T_3 is re-circulated through the PVT module until $T_3 > T_5$ when it reverts to configuration Mode 2a. These 2 modes (1 and 2) can be operated together to experiment different scenarios. Both configuration modes 1 and 2 were used in Papers 2 and 3.

3.1.4 Photovoltaic-thermal and Photovoltaic set-up

The experimental set-up for the PVT and PV used in this study was installed on the roof of the Department of Mechanical Engineering laboratory, Kwame Nkrumah University of Science and Technology (KNUST) Kumasi Ghana. The latitude and longitude of the installation are respectively 6.68°N and 1.57°W . Some pictures of the installations are shown in Figure 3.10. The PVT (model: Volther PowerVolt) and PV (model: PV SOL60S-270W) were manufactured and supplied by Solimpeks in Turkey [80]. Table 3.1 also shows some selected information for PV and PVT modules (Also, see Appendix E for technical details).



Figure 3.10: Installation of setup on the roof top of Solar Energy Applications Laboratory at Department of Mechanical Engineering, KNUST Ghana, showing: (A) PV and PVT modules; (B) North facing surface with water circulation and Electric/Data compartments; (C) East facing surface with radiator cooling fans

Table 3.1: Technical specification of PVT and PV collectors.

Parameters	PVT	PV
Manufacturer	Solimpeks, Turkey	Solimpeks, Turkey
Model	Volther PowerVolt	PV SOL60S-270W
Photocell type	mc-Si	mc-Si
Number of cells	72	72
Absorber surface (Thermal)	Copper	-
Module Dimension (mm ³)	1601x828x90	1640x992x45
Aperture Area A_m (m ²)	1.326	1.474
Absorber Area (m ²)	1.194	-
Weight (kg)	24.4	18.3
Nominal electrical power P_{max} (W)	200	270
Thermal Power (W)	630	-
Nominal current I_{mp} (A)	5.43	8.6
Short circuit current I_{sc} (A)	5.67	9.31
Nominal voltage V_{mp} (V)	36.8	31.4
Open circuit voltage V_{oc} (V)	46.43	38.3
Module electrical efficiency (%)	15.08	16.6
Zero loss collector efficiency (%)	47.5	-
Temperature Coefficient of I_{sc} (%/°C)	0.06	0.05
Temperature Coefficient of V_{oc} (%/°C)	-0.34	-0.34
Temperature Coefficient of P_{max} (%/°C)	-0.45	-0.45
Nominal operating cell temperature $NOCT$ (°C)	45±2	45±2

3.1.5 Instrumentations and data collection

A programable Campbell CR300 data logger has been used to record both meteorological and modules' performance data. The measurements are sampled every 10 seconds and then averaged over 15-minute periods, from which hourly, daily, and monthly data are determined. Table 3.2 shows the list of characteristics of the instrumentation used in this study (see Appendix D). Detailed description of instrumentations and data collection can be found in Papers 1 and 3.

Table 3.2: Test Variables and Sensors

Variable	Instrumentation	Measurement accuracy	Resolution
Temperature (°C)	109 Temperature Probe (Pt100)	±0.2 °C (for 0 to 70 °C)	0.01
Irradiance(W/m ²)	Apogee SP-421 pyranometer	±1%	<0.001
Wind speed (m/s)	Decagon DL-2 wind sensor	3%	0.01
Air temperature (°C)	CS215 Temp/RH sensor	±0.4 °C (5 to 40 °C)	0.01
Relative humidity (%)	CS215 Temp/RH sensor	±4% (0 to 100 %) at 25 °C	0.03
Flowrate (L/min)	Mechanical valves set.	Not specified	0.2
Current (A)	Bim205 smart charger w/MPPT	Not specified	0.1
Voltage (V)	Bim205 smart charger w/MPPT	Not specified	0.1

3.2 Climatic conditions at the installation site

The performance of a solar collector is influenced by many interactive weather factors and collector's related parameters. There is however, a very high level of variability and uncertainty in predicting meteorological variables. Nonetheless, PV cell temperature, for instance, is a function of ambient temperature, wind speed and global irradiance [27]. Ghana is a sub-Saharan African country with land mass located within latitude 5 °N - 11 °N and longitude 3 °W - 1 °E [81]. The installation site is in Kumasi, a town in the middle belt rain forest region of Ghana characterized by tropical rainfalls. By the Köppen-Geiger classifications, Kumasi's climate is classified as tropical savanna climate or tropical wet and dry climate of categories *Aw* (for a dry winter) and *As* (for a dry summer). This implies that the average temperature of the coolest month is above 18 °C and precipitation in the driest month is less than 60 mm [82].

In general, Ghana experiences two main climatic seasons namely, the wet and dry seasons. Typically, the wet season in Kumasi starts from April to October. It is normally characterized by cloudy weather conditions, relatively higher mean monthly precipitation, relatively lower mean ambient temperatures, and relatively lower average daily irradiance. The dry season (which predominantly spans November to March) records low-to-no precipitation, higher ambient temperatures, and higher irradiance.

The yearly average daily global insolation and the yearly average daily ambient temperature recorded at the installation site for the year 2019 were 4.05 kWh/m²/day and 27.13 °C respectively, as detailed in Figure 3.11 [83]. However, as could be seen from Figure 3.12, the monthly average wind speed is less than 1.00 m/s, which prospectively indicates that wind speed effects on solar photovoltaic performance could be negligible. However, occasional wind gusts ranging from 3 m/s in February to 11 m/s in October were observed during the period and must be considered in the design of mounting racks for the site.

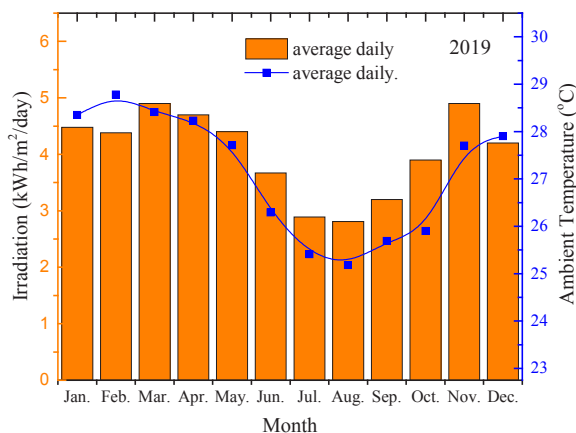


Figure 3.11: Monthly average daily irradiation and monthly average daily ambient temperature at the installation site for the year 2019

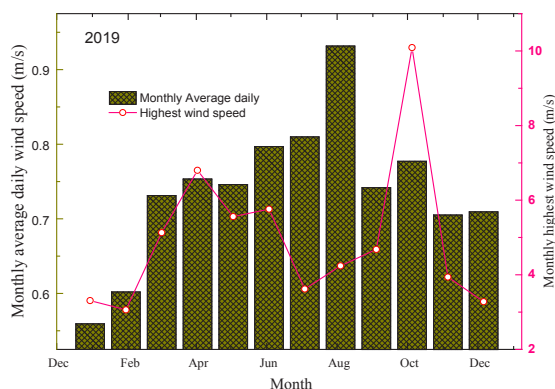


Figure 3.12: Monthly average daily wind speeds at the experimental site

3.3 Data analysis

3.3.1 Energy efficiency and analysis

The overall performance of a convectional PV system is usually examined using selected performance indices, which include energy yield, performance ratio and efficiency. In the case of hybrid PVT system, the overall performance is a combination of both convectional PV (electricity) indices and solar thermal (heat energy) system. The instantaneous electrical efficiency of a crystalline solar cell could be expressed as a function of its temperature (T_c) [69] as:

$$\eta_{el} = \eta_0[1 + \beta(T_c - 25)], \quad (3.1)$$

where η_0 is the efficiency at standard test conditions (STC) (which are defined as Irradiance = 1000 W/m², $T_c = 25$ °C, and air-mass ratio = 1.5), T_c is the solar cell temperature (i.e., T_2 and T_4 for PVT and PV respectively, from Figures 3.2 and 3.9) and β is the temperature dependent coefficient of electrical efficiency. The value of β differs with different PV materials used (about -0.0045/K for crystalline silicon, -0.0035/K for CIS, 0.0025/K for CdTe and -0.002/K for amorphous-Si).

Efficiency of energy systems are generally expressed as ratio of output energy to input energy. The PV module (cell) electrical efficiency (η_{el}) is, therefore, given as:

$$\eta_{el} = \frac{E_{dc}}{A_m * G_p}, \quad (3.2)$$

where E_{dc} is the direct current (DC) power from the module in kW, A_m is the module total surface area (m²) and G_p is the in-plane irradiance (kW/m²). Similarly, the thermal efficiency (η_{th}) is, also, expressed as:

$$\eta_{th} = \frac{E_{th}}{A_m \times G_p}, \quad (3.3)$$

where E_{th} is the useful thermal gains of the system and it is given as:

$$E_{th} = m_w c_p (T_o - T_i), \quad (3.4)$$

where m_w is the water mass flowrate (kg/s), c_p is the specific heat capacity of water (kJ/kg °C) and, T_i and T_o (i.e., T_1 and T_3 respectively, from Figures 3.2 and 3.9) are the inlet and outlet water temperatures respectively, in °C. The total efficiency of the integrated PVT (η_{PVT}) is used to evaluate the overall performance of the system [84]. It can be obtained by combining Equations (3.2) and (3.3) as:

$$\eta_{PVT} = \eta_{th} + \eta_{el} = \frac{E_{dc} + E_{th}}{A_m \times G_p} \quad (3.5)$$

Depending on the available data and desired level of resolution, convectional PV and hybrid PVT systems' efficiencies can be determined on instantaneous, hourly, daily, monthly, and annually bases.

3.3.2 Exergy efficiency and analysis

The exergy analysis is based on the second law of thermodynamics. The overall output exergy (Ex_{out}) from PVT system is expressed as:

$$Ex_{out} = Ex_{th} + Ex_{el}, \quad (3.6)$$

where Ex_{el} is the electrical exergy and Ex_{th} is the thermal exergy. Unlike thermal energy, electrical energy is perfectly convertible, and its exergy content can be taken to be same as the energy content. Thus Ex_{el} and Ex_{th} can be expressed in energy terms in kWh as [85]:

$$Ex_{el} = E_{dc}, \quad (3.7)$$

$$Ex_{th} = E_{th} \left(1 - \frac{T_{ref} + 273}{T_o + 273} \right), \quad (3.8)$$

Equation (3.8) shows that the useful product of a PVT thermal collector is the heat extracted from the absorber plate to the fluid and made available at its outlet temperature, T_o . The Carnot Factor, $[1 - (T_{ref} + 273) / (T_o + 273)]$, shows the reference temperature (T_{ref}) at which the exergy content of the thermal power is zero [24]. T_{ref} is generally assumed to be equal to ambient temperature T_a . This is adopted by numerous authors, such as [24] [86]. However, for an uncontrolled environment, T_a frequently fluctuates periodically. Thermal exergy is affected by such fluctuations as it depends on the value of the reference temperature at the moment when heat is delivered [86]. This therefore introduces thermodynamic contradictions

because the reference temperature is supposed to be constant. Thus, for this paper, the T_{ref} shall correspond to the monthly minimum ambient temperature $T_{a.min}$ recorded in any given month, as recommended by [86]. Therefore,

$$Ex_{th} = E_{th} \left(1 - \frac{T_{a.min} + 273}{T_o + 273} \right), \quad (3.9)$$

Following the same minimum monthly ambient temperature reference point assumption, the overall exergy efficiency of the PVT could be expressed as [87]:

$$\eta_{ex} = \eta_{el} + \eta_{th} \left(1 - \frac{T_{a.min} + 273}{T_o + 273} \right), \quad (3.10)$$

where η_{ex} is the overall exergy efficiency of the hybrid PVT water-heating system.

3.3.3 Economic performance indicators

The economic assessment is made up of costs and benefits of the system. There are many economic performance indicators used by investment professionals, such as levelized cost of energy (LCOE), net present value (NPV) and simple discounted payback period (PP) [88]. The LCOE is a regularly used metric for evaluating the financial and economic viability of energy technologies [89] [90]. In the case of this study, LCOE is evaluated using NPV techniques. LCOE is the price at which energy must be generated from a specific source to break even over the lifetime of the project. In calculating LCOE, all cost factors such as financing, operation costs, maintenance cost, taxes, support, must be considered. The generalized expression for the LCOE over the life span of an energy system is given as [88] [91]:

$$LCOE = \frac{\text{Net Present value of cash flow}}{\text{Present value of energy}}, \quad (3.11)$$

In exergetic terms, the levelized cost of exergy ($LCOEx$) is defined as

$$LCOEx = \frac{\sum_{t=0}^{b-1} PV_{CF}}{\sum_{t=0}^{n-1} PV_{Ex}}, \quad (3.12)$$

$$PV_{CF} = \frac{C_t}{(1+r)^t}, \quad (3.13)$$

$$PV_{Ex} = \frac{Ex_{pvt,t}}{(1+r)^t}, \quad (3.14)$$

where PV_{CF} is the present value of the cash flow, PV_{Ex} is the present value of the exergy, $Ex_{pvt,t}$ is the annual exergy from the system in year t , b is the economic life of the system, r is the discount rate for cash flow and C_t is the total cost in USD (\$) to the setup in year t . Mathematically, C_t is expressed as

$$C_t = I_t + L_t + M_t + Tx_t - Sp_t, \quad (3.15)$$

where I_t is the total investment expenditure, L_t is the financial loan cost, M_t is total operation and maintenance cost, Tx_t is the total tax paid and Sp_t is the total support and incentives, all in the year t .

Table 3.3 shows a summary of economic parameters and prices of balance of system (BOS) devices used in the setup. Although the cost of mounting rack without labour cost is estimated at 10% of the total cost of Module [92] the same is assumed for the PVT system as well. Also, the operation and maintenance (M_t) for both modules were estimated based on studies by Baumgartner [92]. This includes all labour costs as well as provision of security. It should also be noted that systems were acquired without any financial support.

Table 3.3: Economic parameters

Item/Parameter	Size/Rating	Unit Value or cost (\$)	Unit value Reference
PV	270 W	\$ 254	Actual cost
PVT	1.326 m ²	\$ 392.15/m ²	Actual cost
Mounting rack	% of module cost	10 %	[92]
Inverter Cost, $I_{inv,t}$	Paper 2	\$ 300/kW	Actual cost
Battery bank Cost, $I_{bat,t}$	Paper 2	\$ 160/kWh	Actual cost
Water circulation Pump,	10W	\$ 9/W	Actual cost
Control station	Single unit	\$ 50	[93]
O&M cost per year, M_t	% of module cost	5%/annum	Estimated [92]
Storage tank with heat exchanger	100L	\$ 1.5/Liter	Actual cost
Average Electricity tariff for residential users in Ghana	Average	\$ 0.12/kWh	[94]
Discount rate, r (Dec. 2020)	Return on savings	5%	[95]
Financial support package, Sp_t	% of module cost	0%	Actual situation
Exchange rate (02.07.2021)	\$/GH	5.76	[96]

4 Results and discussion

The findings of this study have been presented in **Paper 1**, **Paper 2** and **Paper 3**. **Paper 1** investigated the influence of meteorological conditions on general energy output and performance indicators, including efficiencies, while **Paper 3** assessed the detailed influence of flowrate configurations of heat extraction fluid on PVT performance. **Paper 2** studied the economic feasibilities of the PVT for its projected life span in the installed environment.

4.1 Climatic effects on performance

The electrical energy efficiency of any PV system is directly related to its cells temperature. **Paper1** studied the influence of the climatic factors (irradiance, ambient temperature and wind velocity) on the temperature of the PVT and PV modules. The average daytime temperatures of the PV module were relatively higher than average PVT module temperatures, ranging between 1.3% to 6.9% higher [83]. Table 4.1 details effects of climatic factors on module temperatures.

Table 4.1: A summary of weather data and module temperatures

Month	Ambient Conditions			Average Daily T_{cell}	
	G_p kWh/m ² /d ay	T_a °C	w m/s	PV °C	PVT °C
January	4.49	30.57	0.56	42.26	40.21
February	4.39	30.86	0.60	42.87	40.69
March	4.90	30.94	0.73	44.22	41.19
April	4.72	30.67	0.75	43.60	40.98
May	4.44	29.88	0.75	41.65	39.33
June	3.67	28.08	0.80	37.87	36.38
July	2.90	26.79	0.81	34.69	34.01
August	2.82	26.62	0.93	34.62	34.17
September	3.20	27.31	0.74	37.16	35.97
October	3.94	28.00	0.78	40.08	38.08
November	4.90	29.91	0.71	43.65	40.80
December	4.25	30.10	0.71	42.58	39.74

PV cells temperature are directly linked to their efficiency (Equation 3.1). An advantage of the PVT over the PV is the cooling effect of the working fluid on the cells. Following

that, in the case of the PVT module, **Paper 3** has shown that increasing mass flowrate of the water (m_w) reduced its temperature non-linearly until such a value ($m_w = \sim 0.082$ kg/s in this case) that any further increase did not result in significant changes in T_c for a specific irradiance. For instance, the T_c significantly reduced by almost 11.3% from 60.3 °C to 53.4 °C for m_w variation from 0.025 – 0.067 kg/s at an irradiance of 900 W/m² [97].

4.2 Energy and Exergy Efficiency of modules

Paper 1 assessed the energetic efficiencies of the modules based on their output energies. Rated electrical efficiencies (DC) for PV and PVT are 16.6% and 15.1% respectively, whereas zero loss thermal efficiency of the PVT thermal collector is 48.0 %, as shown in Table 3.1 for STC. However, in reality, there are significant variations in instantaneous efficiencies calculated from input and output energies from modules installed in uncontrolled environments, which are predominantly lower than values measured at STC. For example, **Paper 1** has shown that the annual average daily electrical efficiencies for the PV and PVT modules were 12.1 % and 10.8 %, whereas the average efficiency of the thermal collector was 36.3 % [83].

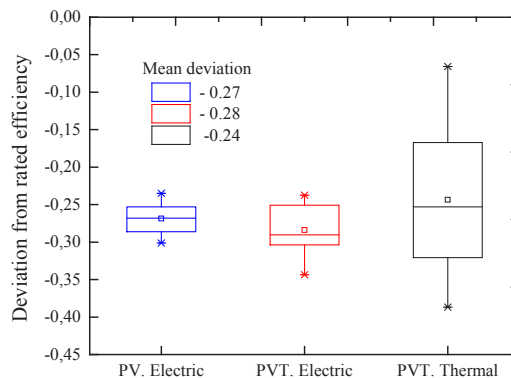


Figure 4.1: Range of deviation of instantaneous energy efficiencies from rated efficiencies at STC

Figure 4.1 shows the range of deviations of instantaneous efficiencies of modules, installed in uncontrolled environment, from rated efficiencies. It could be seen that the mean deviations of the electrical efficiencies for the PV and PVT modules are -26.9 % and -28.3% respectively, whereas the thermal efficiency of the PVT system deviated by -24.3%. This means that although the instantaneous thermal efficiencies for the PVT had wider range variation of 29.4% to 44.8% (**Paper 1** [83]) it recorded the lowest mean

deviation from its rated efficiency. Also, the PVT's instantaneous electrical efficiencies recorded the highest mean deviation from rated efficiency, which is not very different from what was recorded from the PV module. This however means that, the cooling of the PVT cells did not translate directly into efficiency improvement, as compared to the PV cells.

It has also been shown in **Paper 3** that, in exergy terms, the commercial PVT only began to perform better than the conventional PV at higher irradiance (i.e., $\sim 790 \text{ W/m}^2$ in this case) as could be seen from Figure 4.2. However, whereas the PVT seemed to show a relatively stable exergy efficiency with increase in G_p , the PV suffered a decrease in exergy efficiency due to the debilitating effect of higher T_c in the absence of any active cooling. This observation about stability of the PVT exergy efficiency is only true at a specific mass flowrate ($m_w = 0.033 \text{ kg/s}$).

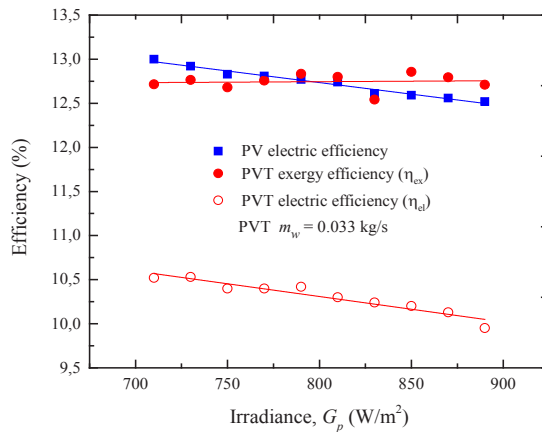


Figure 4.2: Exergy comparison between the conventional PV and the commercial PVT at manufacture's recommended mass flowrate of 0.033 kg/s

4.3 Long term energy and exergy performance

For the purpose of this analysis, the water circulation through the thermal system of the commercial PVT has been set at manufactures recommended mass flowrate of 0.033 kg/s (2 L/min). The estimated gross annual average outputs from the PVT module for the 25-year economic period are 170.85 kWh/m^2 and 519.69 kWh/m^2 and 377.15 kWh/m^2 for electrical energy (E_{dc}), thermal energy (E_{th}) and total exergy (Ex_{out}) respectively. In the case of the PV module, gross annual average electrical energy output is estimated at $192.58 \text{ kWh/m}^2/\text{annum}$ for the period, which is the same as its exergy (see Equation 3.7).

Paper 2 presented analytical models in a comparative energy and exergy study over a 25-year lifetime of the PVT and PV subsystems. Both subsystems have been modeled with TRNSYS for their economic life-cycle projections based on field measured data. The degradation rate of PVT module and PV module outputs were predicted based on manufacturer warranty information for the modules and measured data, including exergy performance. As could be seen from Figure 4.3, the PV module and PVT module output exergies are estimated to degenerate by 12.8 % and 11.3 % respectively at the end of the 25-year period of continuous exposure. This translates to approximately 6.1% of total exergy lost for each module over the period of study.

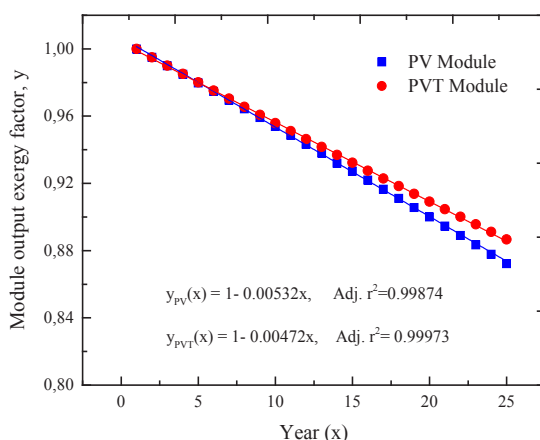


Figure 4.3: Projected exergy output from PV and PVT modules over life span.

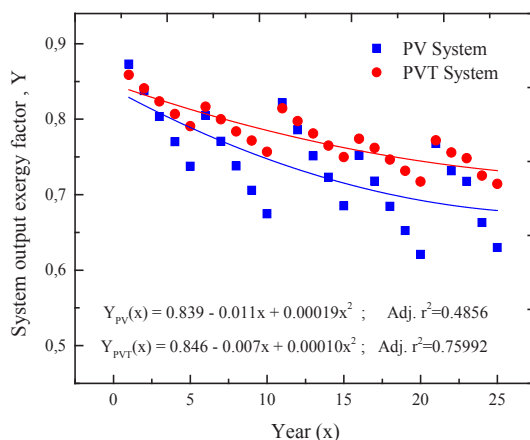


Figure 4.4: Effect of system losses on net exergy output over the years of study.

However, in reality, BOS components contribute to losses in energy transition from modules to load. Figure 4.4 shows that for the period of study, the average net exergy output from the commercial PVT system degenerates curvilinearly from approximately 84.6% to 73.3%, as against 83.9% to 68.3% for the PV system. Thus, the exergy degeneration rate of the commercial PVT is lower than recorded for the conventional PV. The non-linear variation of average percentage of available exergy could be attributed to occasional replacements of BOS devices, as they reached their end of useful life within the study period.

4.4 Economic performance

The economic evaluation of the PV and PVT systems are based on a reference scenario described in **Paper 2** with battery storage capacity in full use ($\beta_t = 1$) at default input parameters ($G_p = 4.5 \text{ kWh/m}^2/\text{day}$, $r = 0.05$, $O\&M = 5\%$ of module cost, and $Sp_t = 0$) for the 25-year project lifecycle. **Paper 2** also introduces levelized cost of exergy ($LCOEx$) as an economic parameter for fairer economic comparison between the commercial PVT and conventional PV.

One main barrier or concern for the use of renewable energy technology is their high investment cost, with a chunk of it required upfront. For the reference scenario, the net present value of life cycle cashflow (PV_{CF}) per unit area for the PV and PVT sub-systems were respectively \$ 1083/m² and \$ 1665/m². Thus, as expected, the running cost of the commercial PVT system has been generally higher than the conventional PV system. Upfront cost amounted to 58.5% and 68.6% of the net PV_{CF} for the PV and PVT systems respectively. Thus, it requires approximately 80% more upfront cost for setting up the conventional PV-system/m² to setup the commercial PVT-system/m² [98].

The cost of exergy produced from the PVT system (\$ 0.33/kWh) is however generally cheaper than that from the PV system (0.45/kWh) but more expensive than residential tariffs for grid power in Ghana (i.e., \$ 0.06-0.16/kWh, depending on the units of electricity consumed per month [94]). However, for a scenario where the modules are freely acquired through support policies like the National Rooftop Solar Programme [99] and installed without any batteries, the PV system has achieved grid parity in all regions (\$

0.06 - 0.13/kWh) in Ghana, whereas the *LCOEx* for PVT (\$ 0.09 – 0.19 kWh) has compared favorably with tariffs in regions with daily peak sun hours > 3.65 h.

4.5 In comparison with conventional PV systems

Unlike PVTs, conventional PVs are already one of the leading products in the global renewable energy charge. For the commercial PVT to compete well with the conventional systems, the cooling effect on the cells should translate into both electrical energy and thermal energy gains. This calls for alternative design and improvement of the commercial systems. The most common thermal absorber in PVT technology is the tube and sheet design [24] [83] [30]. However, some alternative absorber designs in literature with encouraging performance include spiral flow absorber [33], aluminium-alloy flat box with rectangular channel absorber [35], and serpentine channel absorber [100]. The use of nanofluid technology for heat transfer has also been reported to improve both thermal and electrical energy performance of the PVT [101].

5 Conclusions

The primary aim of this research was to make an original scientific contribution to the subject of real-life performance of a commercial PVT in an uncontrolled environment in West-Africa, by studying a system installed in a Ghanaian environment in comparison with a conventional PV system. Like any solar system, climatic conditions are key to the performance of the PVT collectors. However, although some studies on operational performance of solar PV modules in Ghana can be found in the open literature (e.g. [46] [21] [102]), this experimental study has been the first known attempt to assess a commercial PVT module's real-life performance in the West Africa sub-region. Moreover, for the first time, this research has attempted a comparative study between the two technologies (PV and PVT) in Ghana.

In relation to the research objectives, the major conclusions of the study are presented below:

- The average daytime temperatures of the PVT cells were relatively lower than average PV cells, ranging between 1.3% to 6.9% lower. However, the relatively colder PVT cells did not translate directly into electric efficiency improvement, as compared to conventional PV cells. This means that, in terms of electrical energy production, although the commercial PVT operated at lower cell temperatures, its electrical efficiency remained lower than that of the conventional PV at all times.
- In exergy efficiency terms the commercial PVT, operated at manufacturer's recommended mass flowrate, performs better than the conventional PV only when irradiance is beyond a specific higher value ($\sim 790 \text{ W/m}^2$ in this case). Whereas the PVT's exergy efficiency remains constant with increasing irradiance, the PV's exergy efficiency reduces linearly from higher to lower values, in comparison with the PVT's.
- In terms of technical performance, the gross annual average exergy outputs in their life-cycles are 192.58 kWh/m^2 and 377.15 kWh/m^2 respectively measured from the PV and PVT systems.
- The rate of degradation of output exergy due to ageing was projected to be lower in the commercial PVT module than the conventional PV module. This has been

estimated to reach 11.3 % and 12.8 % respectively for the PVT and PV modules in their estimated 25year economic life, which translates into approximately 6.1 % of total exergy losses for each module over the period. Also, whereas the output losses of the PVT system increased curvilinearly from 15.4% to 26.7% over its economic life, that of the PV system increased from 16.1% to 31.7%.

- For complete standalone systems (configured with battery and inverter), the net present value of life cycle cashflow (PV_{CF}) per unit area for the PV and PVT systems are estimated at \$ 1083 and \$ 1665. Upfront costs amounted to 58.5% and 68.6% of PV_{CF} for setting up the PV and PVT systems respectively. The study estimated the upfront cost to be approximately twice what was required in setting up the conventional PV system to setup the same surface area of the commercial PVT system.
- The study introduced the use of levelized cost of exergy ($LCOEx$) as an economic parameter, instead of energy, for a fairer cost comparison of net energy from PV and PVT systems. The cost of exergy produced from the PVT system is averagely 36.4% cheaper than from the PV system, but more expensive than residential tariffs for grid power in Ghana. However, when installed without batteries, the PV's exergy becomes cheaper.

6 Limitations of work, future studies and engineering direction.

Following the conclusions above, it is possible to state that the current thesis has successfully assessed the field performance of a commercial PVT in the context of the listed objectives. While the methods adopted in this thesis accounted for significant sources of uncertainties, some issues could be recommended as subjects for further investigation and to potentially minimize uncertainties in the assessments:

- The results highlight the importance of climatic conditions. The reliability of climate impact assessments depends on the quality and duration of the weather data. However, climatic related impact assessments were based on measured weather data over a single year. Since weather changes are very unpredictable, such short-term data may not be enough to draw accurate conclusions. Further studies on impact assessment should be based on long term weather data collected at installation site.
- Also, the prediction of long-term performance of the PVT and PV modules were based on analytical models and a TRNSYS model based on the same short-term measured data. Since this study is the first of its kind in such an environment, with unique weather conditions like harmattan, there is no evidence in literature to ascertain the veracity of the models in the long term. Thus, further research based on long term observations is necessary to validate or correct existing models and to accurately predict long term performance.
- The study was also based on only mono-crystalline silicon technology for both PV and PVT modules. This was because of non-availability of commercial PVT products on the Ghanaian market. The only available source in Europe ready to export to Ghana had only crystalline silicon modules in stock. While the results may have been based on modules from one technology and manufacturer, yet it provides stronger reference for comparison with other products across other geo-climatic zones. However, future works could expand scope to include other PV and PVT technologies from different manufactures and technologies.
- Extreme test conditions are rare to achieve in real life situations. Well-equipped simulation solar labs with measuring instrument and weather conditioning

possibilities should be established for future works to generate data in support of solar industry in Ghana. With that in place, the PVT's behavior in such extremities could be assessed in the future.

- A lifecycle assessment is a comprehensive tool for quantifying the lifetime environmental impacts of energy systems. However, the study focused on the productive life of the modules without considering environmental impacts. Future studies into lifecycle assessment of the PVT and PV modules will evaluate adverse impacts from cradle-to-grave; starting from inputs (raw materials & energy) and production outflows (emissions, waste & product), transportation, use, decommissioning and management as waste.
- The study was premised on the reported high temperatures of PVs installed in that environment. The PVT was therefore investigated as an alternative technology, without considering stand-alone thermal systems. A future study could assess the performance PVT against both PV's and solar thermal systems in that environment

For the commercial PVT to compete well with the conventional systems, the cooling effect on the cells should translate into both electrical energy and thermal energy gains. Its electrical efficiency was generally lower than that of the conventional PV system. Different assembling techniques and materials could be used to improve the PVT electrical efficiency. Also, cheaper, and more efficient batteries with longer charge/discharge lifecycles could significantly improve both techno and economic performance of stand-alone PV/PVT systems. This observation is, however, based on mc-Si technology and specific commercial manufacturer's design, may not be generalized for all other PV/PVT technologies.

References

- [1] "WHO," 21 May 2019. [Online]. Available: <https://www.who.int/news/item/21-05-2019-more-people-have-access-to-electricity-than-ever-before-but-world-is-falling-short-of-sustainable-energy-goals>. [Accessed 3 February 2021].
- [2] "SDG7: Data and Projections," [Online]. Available: <https://www.iea.org/reports/sdg7-data-and-projections/access-to-electricity>. [Accessed 22 March 2021].
- [3] "WHO: Household air pollution and health," 8 May 2018. [Online]. Available: <https://www.who.int/en/news-room/fact-sheets/detail/household-air-pollution-and-health>. [Accessed 10 February 2021].
- [4] "WHO Malaria," 30 November 2020. [Online]. Available: <https://www.who.int/en/news-room/fact-sheets/detail/malaria>. [Accessed 30 November 2021].
- [5] "WHO Tuberculosis," 14 October 2020. [Online]. Available: <https://www.who.int/en/news-room/fact-sheets/detail/tuberculosis>. [Accessed 10 February 2021].
- [6] "BP Energy Outlook," 2017. [Online]. Available: <https://www.bp.com/content/dam/bp/business-sites/en/global/corporate/pdfs/energy-economics/energy-outlook/bp-energy-outlook-2017.pdf>. [Accessed 20 January 2021].
- [7] "International Energy Outlook 2017," 14 September 2017. [Online]. Available: [https://www.eia.gov/outlooks/ieo/pdf/0484\(2017\).pdf](https://www.eia.gov/outlooks/ieo/pdf/0484(2017).pdf). [Accessed 25 11 2020].
- [8] C. Rajoria, S. Agrawal and G. Tiwari, "Overall thermal energy and exergy analysis of hybrid photovoltaic thermal array," *Solar Energy*, vol. 86, pp. 1531-1538, 2012.
- [9] F. Ghani, M. Duke and C. J.K., "Estimation of photovoltaic conversion efficiency of a building integrated photovoltaic/thermal (BIPV/T) collector array using an artificial neural network," *Solar Energy*, vol. 86, pp. 3378-3387, 2012.
- [10] "Paris Agreement," UN, 2015. [Online]. Available: https://unfccc.int/sites/default/files/english_paris_agreement.pdf. [Accessed 6 January 2021].
- [11] "UN Treaty Collection," UN, 12 December 2015. [Online]. Available: https://treaties.un.org/pages/ViewDetails.aspx?src=TREATY&mtdsg_no=XXVII-7-d&chapter=27&clang=_en. [Accessed 6 January 2021].
- [12] "REN21," June 2020. [Online]. Available: https://www.ren21.net/wp-content/uploads/2019/05/gsr_2020_full_report_en.pdf. [Accessed 14 12 2020].
- [13] "Sustainable Energy for All," [Online]. Available: http://www.se4all.org/sites/default/files/l/2013/09/SG_Sustainable_Energy_for_All_vision_final_clean.pdf. [Accessed 3 February 2021].
- [14] M. Kibati and V. G. Desroches, "Power For All," 16 November 2018. [Online]. Available: <https://www.powerforall.org/insights/africa/electrifying-africas-labor-market>. [Accessed 9 February 2021].
- [15] "IRENA," 2020. [Online]. Available: <https://www.irena.org/publications/2019/Jun/Renewable-Energy-and-Jobs-Annual-Review-2019>. [Accessed 10 February 2021].

- [16] S. Baljit, C. H.Y and S. K, "Review of building integrated applications of photovoltaic and solar thermal systems," *Journal of Cleaner Production*, vol. 137, pp. 677-689, 2016.
- [17] H. Zondag, "Flat-plate PV-Thermal collectors and systems: A review," *Ren. and Sust. Energy Reviews*, vol. 12, no. 4, pp. 891-959, 2008.
- [18] I. Gurracino, C. Markides, A. Mellor and N. Ekins-Daukes, "Dynamic coupled thermal and electrical modelling of sheet and tube hybrid photovoltaic/ thermal (PVT) collectors," *Appl. Therm. Eng.*, vol. 101, pp. 778-795, 2016.
- [19] C. Good, "Environmental impact assessment of hybrid photovoltaic-thermal (PV/T) Systems – A review.," *Renewable and sustainable energy reviews*, vol. 55, pp. 234-239, 2016.
- [20] H. Amal, E. H. Hicham, L. Thiery, R. Mohamad and K. Mahmoud, "Review on photovoltaic/thermal hybrid solar collectors: Classifications, T applications and new systems," *Solar Energy*, vol. 207, pp. 1321-1347, 2020.
- [21] D. A. Quansah, M. S. Adaramola and G. K. Appiah, "Performance analysis of different grid-connected solar photovoltaic (PV) system technologies with combined capacity of 20 kW located in humid tropical climate," *International Journal of Hydrogen Energy*, vol. 42 , pp. 4626 - 4635, 2017.
- [22] M. Fuentes, M. Vivar, J. de la Cassa and J. Aguilera, "An experimental comparison between commercial hybrid PV-T and simple PV systems intended for BIPV," *Renewable and Sustainable Energy Reviews*, vol. 93, pp. 110-120, 2018.
- [23] T. Chow, "A review on photovoltaic/thermal hybrid solar technology," *Applied Energy*, vol. 87, pp. 365-379, 2010.
- [24] M. Fuentes, M. Vivar, J. de la Casa and J. Aguilera, "An experimental comparison between commercial hybrid PV-T and simple PV systems intended for BIPV," *Renewable and Sustainable Energy Reviews*, vol. 93, pp. 110-120, 2018.
- [25] C. de Keizer, M. de Jong, T. Mendes, M. Katiyar, W. Folkerts, C. Rindt and H. Zondag, "Evaluating the thermal and electrical performance of several uncovered PVT collectors with a field test," *Energy Procedia*, vol. 91, pp. 20-26, 2016.
- [26] O. Rejeb, H. Dhaou and A. Jemni, "A numerical investigation of a photovoltaic thermal (PV/T) collector," *Renew. Energy*, vol. 77, pp. 43-50, 2015.
- [27] N. Aste, C. del Pero and F. Leonforte, "Water flat plate PV-thermal collectors: A review," *Solar Energy*, vol. 102, pp. 98-115, 2014.
- [28] M. Lämmle, A. Olivia, M. Hermann, K. Kramer and W. Kramer, "PVT collector technologies in solar thermal systems. A systematic assessment of electrical and thermal yields with the novel characteristic temperature approach," *Solar Energy*, vol. 155, pp. 867-879, 2017.
- [29] A. S. Kalogirou, "Use of TRNSYS for modelling and simulation of a hybrid pv-thermal solar system for Cyprus," *Renewable Energy*, vol. 23, no. 2, pp. 247-260, 2001.
- [30] I. Guarracino, J. Freeman, A. Ramos, A. S. Kalogirou, J. N. Ekins-Daukes and N. C. Markides, "Systematic testing of hybrid PV-thermal (PVT) solar collectors in steady-state and dynamic outdoor conditions," *Applied Energy*, vol. 240, pp. 1014-1030, 2019.
- [31] P. Dupeyrat, C. Ménézo, M. Rommel and H. Henning, "Efficient single glazed flat plate photovoltaic-thermal hybrid collector for domestic hot water system," *Sol. Energy*, vol. 85, pp. 1457-1468, 2011.

- [32] S. Kalogirou and Y. Tripanagnostopoulos, "Industrial application of PV/T solar energy systems," *Applied Thermal Engineering*, vol. 27, p. 1259–1270, 2007.
- [33] A. Fudholi, S. Kamaruzzaman, H. M. Yazdi, H. M. Ruslan, A. Ibrahim and A. H. Kazem, "Performance analysis of photovoltaic thermal (PVT) water collectors," *Energy Conversion and Management*, vol. 78, pp. 641-651, 2014.
- [34] B. Huang, T. Lin, W. Hung and F. Sun, "Performance evaluation of solar photovoltaic/thermal systems," *Sol. Energy*, vol. 70, pp. 443-448, 2001.
- [35] T. Chow, J. Ji and W. He, "Photovoltaic-Thermal Collector System for Domestic Application," *J. Sol. Energy Eng.*, vol. 129, no. 2, pp. 205-209, 2007.
- [36] W. He, T. Chow, J. Ji, J. Lu, G. Pei and L. Chan, "Hybrid photovoltaic and thermal solar-collector designed for natural circulation of water," *Appl. Energy*, vol. 83, pp. 199-210, 2006.
- [37] J. Ji, J. Han, T. Chow, H. Yi, J. Lu, W. He and W. Sun, "Effect of fluid flow and packing factor on energy performace of a wall-mounted hybrid photovoltaic/water-heating collector system.," *Energy Build*, vol. 38, pp. 1380-1387, 2006.
- [38] M. Hazami, A. Ali Riahi, F. Mehdaoui, O. Omeima Nouicer and A. Farhat, "Energetic and exergetic performances analysis of a PV/T (photovoltaic thermal) solar system tested and simulated under Tunisian (North Africa) climatic conditions," *Energy 2016*, vol. 10715, pp. 78-94, 2016.
- [39] M. Abdulkadir and S. Muhammad, "Design and construction of a thermosiphonic solar photovoltaic: Thermal water heating system for sustainable development in temperate regions of Africa.," *J. Altern. Energy Sources Technol*, vol. 8, pp. 1-8, 2017.
- [40] J. Siecker, K. Kusakan and B. Numbi, "Optimal switching control of PV/T systems with energy storage using forced water circulation: Case of South Africa," *J. Energy Storage*, vol. 20, pp. 264-278, 2018.
- [41] A. Oyieke and F. Inambao, "Performance characterisation of a hybrid flat-plate vacuum insulated photovoltaic/thermal solar power module in subtropical climate," *Int. J. Photoenergy*, no. 2, pp. 1-15, 2016.
- [42] O. Apuko and Inambao, "Simulation and performance evaluation of a vacuum insulated hybrid solar photovoltaic/thermal power module for domestic applications in South Africa," *TMC Acad. J.*, no. 9, pp. 1-19, 2015.
- [43] W. Sawadogo, B. Abiodun and E. Okogbue, "Impacts of global warming on photovoltaic power generation over West Africa," *Renew. Energy*, vol. 151, pp. 263-277, 2020.
- [44] S. Meunier, M. Heinrich, L. Quéval, J. Cherni, L. Vido, A. Darga, P. Dessante, B. Multon, P. Kitanidis and C. Marchand, "A validated model of a photovoltaic water pumping system for o-grid rural communities," *Appl. Energy*, vol. 241, pp. 580-591, 2019.
- [45] D. Akinyele, O. Babatunde, C. Monyei, L. Olatomiwa, A. Okediji, D. Ighravwe, O. Abiodun, M. Onasanya and K. Temikotan, "Possibility of solar thermal power generation technologies in Nigeria: Challenges and policy directions.," *Renew. Energy Focus*, vol. 29, pp. 24-41, 2019.
- [46] F. Nyarko, G. Takyi, E. Amalu and M. Adaramola, "Generating temperature cycle profile from in-situ climatic condition for accurate prediction of thermo-mechanical degradation of c-Si photovoltaic module," *Eng. Sci. Technology Int. J.*, vol. 22, pp. 502-514, 2019.

- [47] D. Quansah and M. Adaramola, "Assessment of early degradation and performance loss in five co-located solar photovoltaic module technologies installed in Ghana using performance ratio time-series regression.," *Renew. Energy*, vol. 131, pp. 900-910, 2019.
- [48] A. Yushchenko, A. de Bono, B. Chatenoux, M. Patel and M. Ray, "GIS-based assessment of photovoltaic (PV) and concentrated solar power (CSP) generation potential in West Africa," *Renew. Sustain. Energy Rev.*, no. 81, pp. 2088-2103, 2018.
- [49] M. Simo-Tagne, M. Ndukwu, A. Zoulalian, L. Bennamoun, F. Kifani-Sahban and Y. Rogaume, "Numerical analysis and validation of a natural convection mix-mode solar dryer for drying red chilli under variable conditions," *Renew. Energy*, vol. 151, pp. 659-673, 2020.
- [50] O. Ogunmodimu and Okoroigwe, "E.C. Solar thermal electricity in Nigeria: Prospects and challenges," *Energy Policy*, vol. 128, pp. 440-448, 2019.
- [51] Y. Seshie, K. N'Tsoukpoe, P. Neveu, Y. Coulibaly and Y. Azoumah, "Small scale concentrating solar plants for rural electrification.," *Renew. Sustain. Energy Rev.*, vol. 90, pp. 195-209, 2018.
- [52] M. Herrando, N. C. Markides and K. Hellgardt, "A UK-based assessment of hybrid PV and solar-thermal systems for domestic heating and power: System performance," *Applied Energy*, vol. 122, pp. 288-309, 2014.
- [53] M. Herrando and C. N. Markides, "Hybrid PV and solar-thermal systems for domestic heat and power provision in the UK: Techno-economic considerations," vol. 161, pp. 512-532, 2016.
- [54] S. Tselepis and Y. Tripanagnostopoulos, "Economic analysis of hybrid photovoltaic/thermal solar systems and comparison with standard PV modules," in *Proceedings of the International Conference On PV in Europe*, 2001.
- [55] [Online]. Available: [http://energycom.gov.gh/files/Solar%20Data%20-%20final\(1\).pdf](http://energycom.gov.gh/files/Solar%20Data%20-%20final(1).pdf). [Accessed 10 November 2020].
- [56] "SHC TASK 60," Task 60, February 2019. [Online]. Available: <https://task60.iea-shc.org/highlights>. [Accessed 20 September 2020].
- [57] S. Arno, J. Klaus, I. Olindo, V. S. René and M. Zeman, *Solar Energy: The physics and engineering of photovoltaic conversion technologies and systems*, Cambridge: UIT Cambridge Ltd, 2016.
- [58] J. C. C., *Physics of Solar Energy*, USA: John Wiley & Sons, Inc, 2011.
- [59] A. B. Waheed, "A review on solar cells from Si-single crystals to porous materials and quantum dots," *J. of Adv. Research*, vol. 6, no. 2, pp. 123-132, 2015.
- [60] W. Shockley, "The Theory of p-n Junctions in Semiconductors and p-n Junction Transistors.," *Bell Syst. Tech.*, vol. 28, pp. 435-489, 1949.
- [61] G. Martin, D. Ewan, H.-E. Jochen, Y. Masahiro, K. Nikos and H. Xiaojing, "Solar cell efficiency tables (version 57)," *Progress in Photovoltaics*, 2020.
- [62] B. H. Mohammed, D. Ali, C. M. Keitumetse, A. Lana and A. Niaz, "Solar energy—A look into power generation, challenges, and a solar-powered future," *Int. Journ. of Energy research*, 2018.
- [63] J. Cubas, S. Pindado and C. d. Manuel, "Explicit Expressions for Solar Panel Equivalent Circuit Parameters Based on Analytical Formulation and the Lambert W-Function," *Energies*, vol. 7, pp. 4098-4115, 2014.

- [64] A. Cuevas, "The Recombination Parameter J_0 ," *Energy Procedia*, vol. 55, pp. 53-62, 2014.
- [65] K. Kennerud, "Analysis of Performance Degradation in CdS Solar Cells," *IEEE Trans. Aerosp. Electron. Syst.*, Vols. AES-5, pp. 912-917, 1969.
- [66] C. Javier, P. Santiago and V. Marta, "On the analytical approach for modeling photovoltaic systems behavior," *Journal of Power Sources*, vol. 247, pp. 467-474, 2014.
- [67] R. Ewa, "Performance Analysis of a Photovoltaic-Thermal Integrated System," *Int. Journal of Photoenergy*, vol. 2009, 2009.
- [68] "Everything about solar energy," 4 August 2015. [Online]. Available: <http://energyprofessionalsymposium.com/?p=9811>. [Accessed 6 January 2022].
- [69] D. Evans, "Simplified method for predicting PV array output," *Solar Energy*, vol. 27, pp. 555-560, 1981.
- [70] J. Duffie and W. Beckman, *Solar engineering of thermal processes*. 2nd ed., New York: John Wiley and Sons, Inc., 1991.
- [71] M. Kutz, *Heat transfer Calculations*, McGraw-Hill Companies, 2004.
- [72] A. K. Soteris, *Solar Energy Engineering Processes and Systems (2nd Edition)*, Elsevier, 2014.
- [73] H. Hottel and A. Whiller, "Evaluation of flat-plate solar collector performance, In: The conference on the Use of Solar Energy," *The Scientific Basis*, vol. 2, no. 1, pp. 74-104, 1958.
- [74] A. James, D. Zahir, S. Sinisa and M. Lascelle, "Performance testing of thermal and photovoltaic thermal solar collectors," *Energy Science & Engineering*, vol. 3, no. 4, pp. 310-326, 2015.
- [75] S. Klein, "Calculation of Flat-Plate Loss Coefficients," *Solar Energy*, vol. 17, no. 79, 1975.
- [76] W. Andy, "Whole building design guide," 11 November 2016. [Online]. Available: <https://www.wbdg.org/resources/solar-water-heating>. [Accessed 20 Jan 2022].
- [77] J. Stulz and L. Wen, "Thermal Performance Testing and Analysis of Photovoltaic Modules in Natural Sunlight," 1977.
- [78] D. Jelena, b. Svetlana and D. Zorica, "Experimental design application and interpretation in pharmaceutical technology," *Computer-Aided Application in Pharmaceutical Technology*, pp. 31-56, 2013.
- [79] "International standard ISO /FDIS 9806," 2013. [Online]. Available: www.iso.org. [Accessed 2021].
- [80] "Solimpeks solar energy corpl," [Online]. Available: <https://solimpeks.com>. [Accessed 20 January 2022].
- [81] "World Atlas," 9 November 2020. [Online]. Available: <https://www.worldatlas.com/maps/ghana>. [Accessed 10 February 2021].
- [82] M. Peel, Finlayson and M. T.A., "Updated world map of the Koppen-Geiger climate classification," *Hydrology and Earth System Sciences Discussions*, pp. 439-473, 2007.
- [83] S. Abdul-Ganiyu, A. D. Quansah, W. E. Ramde, R. Seidu and A. S. Muiyiwa, "Investigation of Solar Photovoltaic-Thermal (PVT) and Solar Photovoltaic (PV) Performance: A Case Study in Ghana," *energies*, 2020.

- [84] E. Radziemska, "Performance Analysis of a Photovoltaic-Thermal Integrated System," *International Journal of Photoenergy*, vol. 2009, 2009.
- [85] M. Bosanac, B. Sørensen, I. Katic, H. Sørensen, B. Nielsen and J. Badran, "Photovoltaic/Thermal Solar Collectors and Their Potential in Denmark," 21 May 2003. [Online]. Available: <https://www.yumpu.com/en/document/read/4467325/photovoltaic-thermal-solar-collectors-and-their-potential-in-denmark>. [Accessed 8 June 2020].
- [86] M. Pons, "On the Reference State for Exergy when Ambient Temperature Fluctuates*," *Int. J of Thermodynamics*, vol. 12, no. 3, pp. 113-121, 2009.
- [87] A. Tiwari and M. Sodha, "Performance evaluation of solar PV/T system: an experimental validation," *Sol Energy*, vol. 80, no. 7, pp. 751-759, 2006.
- [88] Y. Gu, X. Zhang, J. A. Myhren, M. Han, X. Chen and Y. Yuan, "Techno-economic analysis of a solar photovoltaic/thermal (PV/T) concentrator for building application in Sweden using Monte Carlo method," *Energy Conversion and Management*, vol. 165, pp. 8-24, 2018.
- [89] A. D. Quansah, A. S. Muiyiwa, E. A. Isaac and K. E. Anto, "An Assessment of Grid-Charged Inverter-Battery Systems for Domestic Applications in Ghana," *Journal of Solar Energy*, 2016.
- [90] D. A. Quansah and M. S. Adaramola, "Economic assessment of a-Si and CIS thin film solar PV technologies in Ghana," *Sustainable Energy Technologies and Assessments*, vol. 18, p. 164–174, 2016.
- [91] C. B. Riggs, R. Biedenharn, C. Dougher, V. Y. Ji, Q. Xu, V. Romanin, S. D. Codd, M. J. Zahler and D. M. Escarra, "Techno-economic analysis of hybrid PV/T systems for process heat using electricity to subsidize the cost of heat," *Applied Energy*, vol. 208, pp. 1370-1378, 2017.
- [92] F. Baumgartner, "Photovoltaic (PV) balance of system components: Basic, performance.," *The Performance of Photovoltaic (PV) Systems Modelling, Measurement and Assessment*, pp. 135-181, 2017.
- [93] "SOLIMPEKS," [Online]. Available: <https://www.solimpeks.com/volther-powervolt-en>. [Accessed 9 February 2021].
- [94] "PURC," 16 December 2021. [Online]. Available: <https://www.purc.com.gh/attachment/642643-20210225110236.pdf>. [Accessed 18 July 2021].
- [95] "Saving Interest Rates," Standard Chartered Bank, [Online]. Available: <https://www.sc.com/gh/save/savings-plus/>. [Accessed 26 July 2021].
- [96] "BOG," 2020. [Online]. Available: <https://www.bog.gov.gh/>. [Accessed 17 July 2021].
- [97] S. Abdul-Ganiyu, A. D. Quansah, W. E. Ramde, R. Seidu and A. S. Muiyiwa, "Flow-rate analysis of a commercial flat-plate water-based PVT system," *Journal of Cleaner Production*, vol. 321, no. JCLP 128985, 2021.
- [98] S. Abdul-Ganiyu, A. D. Quansah, W. E. Ramde, R. Seidu and A. S. Muiyiwa, "Techno-economic analysis of solar photovoltaic (PV) and solar photovoltaic thermal (PVT) systems using exergy analysis," *Sustainable Energy Technologies and Assessments*, vol. 47, no. 101520, October 2021.
- [99] K. F. Appiah, "The National Rooftop Solar Programme," 9 August 2016. [Online]. Available: <http://energycom.gov.gh/files/ROOFTOP%20SOLAR%20PROG->





Presentation%20@%202nd%20Ghana%20Renewable%20Energy%20Fair1.pdf.
[Accessed 10 June 2020].

- [100] J. Allan, Z. Dehouche, S. Stankovic and L. Mauricette, "Performance testing of thermal and photovoltaic thermal solar collectors," *Energy Science & Engineering*, vol. 3, no. 4, pp. 310-326, 2015.
- [101] H. Fayaz, R. Nasrin, N. Rahim and M. Hasanuzzaman, "Energy and exergy analysis of the PVT system: Effect of nanofluid flow rate," *Solar Energy*, vol. 169, pp. 217-230, 2018.
- [102] K. G. Adanu, "Performance of a 268 Wp stand-alone PV system test facility," in *Proceedings of 1994 IEEE 1st World Conference on Photovoltaic Energy Conversion - WCPEC (A Joint Conference of PVSC, PVSEC and PSEC)*, Hawaii, 1994b.

Paper I

Article

Investigation of Solar Photovoltaic-Thermal (PVT) and Solar Photovoltaic (PV) Performance: A Case Study in Ghana

Saeed Abdul-Ganiyu ¹, David A Quansah ^{2,3} , Emmanuel W Ramde ^{2,3} , Razak Seidu ⁴ 
and Muyiwa S. Adaramola ^{1,*} 

- ¹ Faculty of Environmental Sciences and Natural Resources Management, Norwegian University of Life Science, Høgskoleveien 12, 1433 Ås, Norway; abdul-ganiyu.saeed@nmbu.no
 - ² Department of Mechanical Engineering, Kwame Nkrumah University of Science and Technology (KNUST), Kumasi AK-448-6464, Ghana; daquansah.coe@knust.edu.gh (D.A.Q.); eramde@gmail.com (E.W.R.)
 - ³ The Brew-Hammond Energy Centre, Kwame Nkrumah University of Science and Technology (KNUST), Kumasi AK-448-6464, Ghana
 - ⁴ Department of Ocean Operations and Civil Engineering, Norwegian University of Science and Technology, 6025 Ålesund, Norway; rased@ntnu.no
- * Correspondence: muyiwa.adaramola@nmbu.no; Tel.: +47-976-90-282

Received: 31 March 2020; Accepted: 19 May 2020; Published: 28 May 2020



Abstract: The main objective of this paper is to experimentally assess the real-life outdoor performance of a photovoltaic-thermal (PVT) module against a conventional photovoltaic (PV) system in a hot humid tropical climate in Ghana. An experimental setup comprising a water-based mono-crystalline silicon PVT and an ordinary mono-crystalline silicon PV was installed on a rooftop at the Kwame Nkrumah University of Science and Technology in Kumasi and results evaluated for the entire year of 2019. It was observed that the annual total output energy of PV module was 194.79 kWh/m² whereas that of the PVT for electrical and thermal outputs were 149.92 kWh/m² and 1087.79 kWh/m², respectively. The yearly average daily electrical energy yield for the PV and PVT were 3.21 kWh/kW_p/day and 2.72 kWh/kW_p/day, respectively. The annual performance ratios for the PV and PVT (based on electrical energy output only) were 79.2% and 51.6%, respectively, whilst their capacity factors were, respectively, 13.4% and 11.3%. Whereas the highest monthly mean efficiency recorded for the PV was 12.7%, the highest combined measured monthly mean electrical/thermal efficiency of the PVT was 56.1%. It is also concluded that the PVT is a worthy prospective alternative energy source in off-grid situations.

Keywords: photovoltaic-thermal; solar PV; efficiency; energy yield

1. Introduction

Solar energy is commonly collected as heat and electricity through thermal and photovoltaic (PV) technologies, respectively. A hybrid photovoltaic-thermal (PVT) integrates a solar thermal absorber and a PV into one unit. Whereas the PV cells generate electricity, the integrated thermal system absorbs residual heat energy from the cells and thus reduces their temperature in the process and also enhances their performance [1–3]. The two most cost-effective working fluids are water and air, with water type found to be more efficient [4]. Hybrid PVT collectors can reach net (electrical plus thermal) efficiencies of 70% or higher, with electrical efficiencies up to 15–20% and thermal efficiencies exceeding 50%, depending on the conditions [5]. The PVT technologies have the potential to reduce the use of materials, installation time, and the required space [6]. The advantage of PVTs in generating both electricity and thermal energy simultaneously makes them handy for domestic applications. However, despite

the immense potential, commercial PVT systems are still not as popular as stand-alone, and separately installed, PV and thermal systems [7,8].

PVT technologies have been studied since 1970s, including variation in designs, working fluids and other performance-influencing factors [2,3]. The thermal and electric energy outputs depend on many factors, some of which are irradiance, ambient temperature, wind speed, circulating fluid temperature and flowrate [7,9,10]. It is therefore important that more experimental data from different environmental conditions are collected to enrich available data to cover the different places in the world. The precise projection of solar collector behavior is key for ensuring proper design and reduction in underperformance or system failure; while improved models of PVT systems are required for optimization of the design and operating parameters in order to achieve higher electrical and thermal energy yields and increased energy savings [8].

Unlike indoor test conditions, climatic conditions could vary significantly affecting general performance and resilience of designs. For instance, the harsh harmattan weather conditions of sub-Saharan West Africa sets it apart from other places in the world. Although the efficiency of PVT collectors are affected by meteorological conditions, several of the studies to predict the performance of PVTs were carried out in Europe [7–9,11] and many parts of Asia [12–17], with minimal experimental investigation records on the subject in sub-Saharan Africa in the open literature. Nevertheless, Rejeb et al. numerically investigated a photovoltaic/thermal sheet and tube collector for the semi-arid climatic with hot summer and mild winter in North Africa [10]; but again, their data correspond to simulations, not experimental work.

Africa is home to 17% of the world's population, but, generates 4% of global power supply. As of 2018, the electrification rate in sub-Saharan Africa was 45% with frequent electricity disruptions and economic losses. This and many more have hampered industrial expansion on the continent. Meanwhile, the continent has the richest solar resources in the world, but accounts for less than 1% of global solar PV installed capacity [18]. Solar resources provide the option of decentralized (and off-grid) solutions to remote settlements. The number of people who gained access to electricity through solar home systems in sub-Saharan Africa increased from two million in 2016 to approximately five million in 2018 [18]. This shows that, with the right policies, solar could become one of the top resources in overcoming the energy deficits on the continent. Thus, more research into solar technologies, like PVT, on the continent is needed for informed decision-making by stakeholders.

The few studies on PVT technology in Africa in the literature were based on climates of North Africa sub-region [10,19,20] and the country of South Africa [20–23]. In the case of West Africa, studies on solar technology were either separately conducted on solar photovoltaic systems [24–36] or solar thermal systems [36–39], with very little evidence of studies on performance of the combined technology (PVT) in the literature. The objective of this experimental study is therefore to assess the real-life performance of a water-based commercial PVT module against a PV system installed in a dynamic environment of Kumasi Ghana (in West Africa). The results from this study will provide valuable information about the viability of water PVT as an alternative source of energy for provision of warm water and electricity in (especially off-grid locations) Ghana. Furthermore, experimental data collected and presented in this study will serve as input and validation parameters for modelling and simulation of PVT systems. To the authors, this is the first study of a commercialized PVT in the dynamic tropical weather conditions of West Africa.

2. Materials and Methods

2.1. Experimental Set-up

The experimental set-up for the study was installed on the roof of the Department of Mechanical Engineering laboratory (6.68° N, 1.57° W), Kwame Nkrumah University of Science and Technology (KNUST), Kumasi-Ghana. The set-up consisted of a conventional solar PV and hybrid PVT installations (Figure 1). For ease of comparison and commercial availability, both modules were made up of

mono-crystalline Silicon (mc-Si) PV technology. The selected specifications for the modules are shown in Table 1.

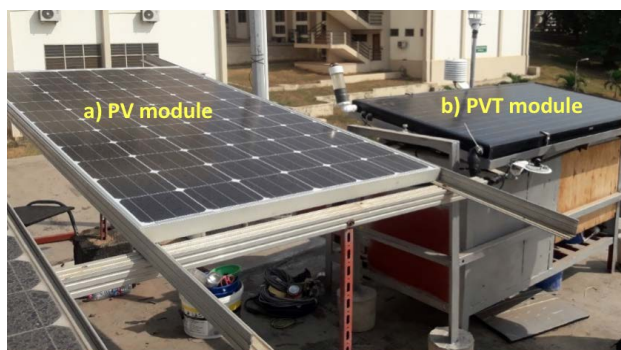


Figure 1. (a) Conventional solar photovoltaic (PV) installation; (b) hybrid photovoltaic-thermal (PVT) installation.

Table 1. Technical specification of PVT and PV collectors.

Parameters	PVT	PV
Dimension (mm ³)	1601 × 828 × 90	1640 × 992 × 45
Aperture area (m ²)	1.326	1.474
Absorber area (m ²)	1.194	-
Weight (kg)	24.4	18.3
Nominal electrical power (W)	200	270
Thermal power (W)	630	-
Nominal current I_{mp} (A)	5.43	8.6
Short circuit current I_{sc} (A)	5.67	9.31
Nominal voltage V_{mp} (V)	37.89	31.4
Open circuit voltage V_{oc} (V)	45.26	38.3
Module electrical efficiency (%)	15.08	16.6
Zero loss collector efficiency (%)	0.48	-
Temperature coefficient of I_{sc} (%/°C)	0.06	0.05
Temperature coefficient of V_{oc} (%/°C)	-0.34	-0.34
Temperature coefficient of P_{max} (%/°C)	-0.45	-0.45
Nominal operating cell temperature $NOCT$ (°C)	45 ± 2	45 ± 2
Absorber Surface (PV)	mc-Si	mc-Si
Absorber surface (T)	Copper	-

Special care was taken to ensure the PV and PVT modules were sourced from the same manufacturer for similarities in peripheral material composition and assembling techniques. The 200 W rated commercial PVT module had a layer of 72 mc-Si PV cells with a flat copper plate thermal system securely attached on its back. A thin adhesive layer, made up of ethylene-vinyl acetate (EVA) layer and the tedlar layer, was used to fix the PV module on to the thermal absorber plate. This compound adhesive layer also acted as a shock absorber to further strengthen the PV module. The heat conducted by the copper thermal plate from the PV cells was transferred by fluid (water in this case) flowing through 14 evenly distributed parallel copper pipes attached to the absorber plate and running from inlet to outlet manifolds. The thermal absorber was then covered with an insulator material and then finally with an aluminum foil to complete the thermal insulation on its back.

Both unshaded PVT and PV modules were oriented towards the south and inclined at a fixed angle of 8°. Tilt angle allowed natural cleaning of the modules during rainfalls, which reduced soiling by dust settlement on the installations, and ensured optimum capture of the solar irradiation for the location. In addition, the modules were manually cleaned on regular basis to reduce the effects

of soiling. As shown in Figure 2, beneath the mounting frame for the PVT installations were two separated compartments for housing the main electrical/logging circuitry and water circulation system.



Figure 2. Photovoltaic-thermal (PVT) showing: (a) south facing surface and cooling fans for radiator (left); (b) north facing face with water circulation compartment and electrical/logging circuitry compartment (right).

2.2. Schematic of the Experimental Setup and Water Circulation

Figure 3 shows a schematic diagram of the experimental setup. The main heat transfer medium for the PVT was by force-circulated water in a closed-loop system. A flow jet direct current (DC) pump, with regulated input power, circulated the water at solar irradiance above 150 W/m^2 when the thermal absorber temperature was greater than its inlet water temperature. The solar irradiance was measured with a pyranometer mounted in-plane on the PVT module. Manual valves V1 and V2 were used to regulate the flow rate and monitored with a mechanical spring flow meter F (see Figure 3). The relatively warm water from the PVT went through a copper-coiled heat exchanger submerged in 70 L of water contained in an insulated tank. For the purpose of the experiment, the circulating water returning into the PVT inlet was further cooled with a water-to-air heat exchanger. This also reduced the problem of potential heat recirculation from the water tank back to the PVT, making it a better stand-alone system.

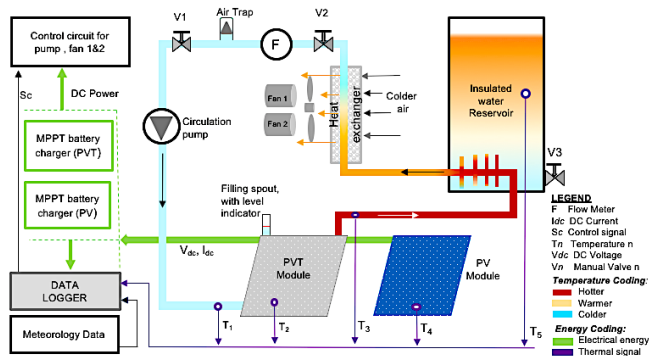


Figure 3. Schematic of the experimental setup.

2.3. Instrumentations, System Control and Data Collection

A programmable data logger (CR300, Campbell Scientific, Logan, UT, USA) was used to record both meteorological and the modules' performance data. The measurements were sampled every 10s and then averaged over 15-min periods, from which hourly, daily and monthly data were determined. The meteorological measurements were the global solar irradiance in plane-of-array (W/m^2), ambient wind velocity (m/s), ambient relative humidity (%) and ambient air temperature ($^{\circ}\text{C}$). The electrical

energy yields from the PVT and PV modules were measured by two dedicated maximum power point tracking (MPPT) battery chargers (BIM 205 Version 1.0, MicroStep-MIS, Bratislava, Slovak Republic). Batteries, radiator fans, data logger and circulation pump were powered from the battery charger, serving as external loads to the modules. Logged data from the battery chargers included output currents (A) and voltages (V) from modules.

Apart from ambient temperature, all other temperatures were separately measured with calibrated temperature sensors (PT100, Campbell Scientific, Logan, Utah, USA). As shown in Figure 3, measured temperatures included the PVT inlet water temperature (T_1), PVT module back temperature (T_2), PVT outlet water temperature (T_3), PV module back temperature (T_4) and water storage tank temperature (T_5). In addition to recording data, the logger was programmed to control the functionalities of the mechanical components in the PVT setup based on real-time in-plane global irradiation. Active water circulation through the PVT was kept at a constant flowrate per desired set value. Table 2 shows the list and basic characteristics of the instrumentation used in this study.

Table 2. Test Variables and Sensors.

Variable	Instrumentation	Measurement Accuracy	Resolution
Flow Gauge (L/min)	Mechanical spring flow meter	not available	0.2
Temperature (°C)	109 Temperature Probe (PT100)	± 0.2 °C (for 0–70 °C)	0.01
Solar irradiance(W/m ²)	Apogee SP-421 pyranometer	$\pm 1\%$	<0.001
Wind speed (m/s)	Decagon DL-2 wind sensor	3%	0.01
Air temperature (°C)	CS215 Temp/RH sensor	± 0.4 °C (5–40 °C)	0.01
Relative humidity (%)	CS215 Temp/RH sensor	$\pm 4\%$ (0–100%) at 25 °C	0.03
Flow rate (L/min)	Mechanical valves set.	Not specified	0.2
Current (A)	Bim205 smart charger w/MPPT	Not specified	0.1
Voltage (V)	Bim205 smart charger w/MPPT	Not specified	0.1

2.4. Data Analysis

2.4.1. Module Temperature

The peak or rated power of a PV module is determined under standard test conditions (STC), which are solar irradiance of 1 kW/m², module temperature of 25 °C and air-mass ratio (AM) of 1.5 (AM = 1.5). However, in real life outdoor situations, the ambient conditions are different from these STC, and hence, the PV module power output will differ from the rated power. The cell temperature T_{cell} (°C) at any ambient temperature T_{amb} (°C) is given as:

$$\frac{T_{cell} - T_{amb}}{NOCT - T_{amb,NOCT}} = \frac{G_p}{G_{p,NOCT}} \times \frac{U_{L,NOCT}}{U_L} \left[1 - \frac{\eta_{cell}}{(\tau\alpha)} \right], \quad (1)$$

where $NOCT$ is the nominal operating cell temperature (°C), G_p is the in-plane global irradiance (W/m²), η_{cell} is cell efficiency (%), $(\tau\alpha)$ is the effective transmittance-absorptance, U_L is the loss coefficient (W/m² °C) and Z_{NOCT} means parameter Z at $NOCT$. The loss coefficient can further be expressed as:

$$U_L = 5.7 + 3.8\omega, \quad (2)$$

where ω is wind speed (m/s). Additionally, at $NOCT$, $T_{amb,NOCT}$ is 20 °C, $G_{p,NOCT}$ is 800 W/m² and ω is 1 m/s, at no load operation (i.e., $\eta_{cell} = 0$). Equation (1) can therefore be simplified as:

$$T_{cell} = T_{amb} + \left[\left(\frac{9.5}{5.7 + 3.8\omega} \right) \times \left(\frac{NOCT - 20}{800} \right) \times G_p \right], \quad (3)$$

Thus the effect of solar irradiance, ambient temperature and wind speed on solar PV module can be quantified by their impact on the module temperature as given in Equation (3).

2.4.2. PV Performance Indices—Energy Yield, Performance Ratio and Efficiency

The performance of a PV system is usually examined using a number of selected performance indices, including energy yield, performance ratio and efficiency. The energy yield is defined as output normalized by the PV system's rated capacity. It specifies how many hours in a day the PV system must operate at its rated power in order to produce the same amount of energy as was measured [40,41]. It is given as:

$$Y_A = \frac{E_{av.d}}{P_{rated}} \quad (4)$$

where Y_A is the array yield in kWh/kW_p/day, $E_{av.d}$ is the average daily module DC energy output (kWh/day) and P_{rated} is the rated kilowatt peak electrical power (kW_p) of the PV module at STC.

The performance ratio (PR) measures the overall effect of losses on the rated output of the system and indicates how close its performance is to the ideal performance during real life operation. The PR is useful for the comparison of modules that receive different amounts of irradiation, especially due to geographical location and or PV inclination. It is given as [40,41]:

$$PR = \frac{E_{av.d}}{P_{rated} \times S_h} \quad (5)$$

where S_h (h/day) is the plane-of-array average daily peak sun-hours, which is the same as the reference yield, Y_R . The reference yield is the ratio of the total in-plane solar radiation to the array reference irradiance, H_R (usually taken as 1 kW/m²). It is a measure of the theoretical energy available at a specific location over a specified time period [41] given as:

$$Y_R = \frac{G_p}{H_R} \quad (6)$$

The PV module efficiency is given as:

$$\eta_{pv} = \frac{100 \times E_{dc}}{A_m \times G_p} \% \quad (7)$$

where A_m is the module total surface area (m²) and G_p is the in-plane solar irradiance (kW/m²). E_{dc} is the DC power from the module in kW. Depending on the available data and desire level of resolution, the efficiencies can be determined on instantaneous, hourly, daily, monthly and annual bases [41].

2.4.3. PVT Performance Indices—Heat Gained, Thermal Energy Yield and Efficiency

The overall performance of a PVT system is a combination of both PV (electricity) and its thermal (heat energy) components. The thermal gain of the system is given as:

$$E_{th} = M_w c_p \Delta T \quad (8)$$

where M_w is the water mass flow rate (kg/s), c_p is the specific heat of water (kJ/kg °C) and ΔT (°C) is the temperature difference, expressed as:

$$\Delta T = T_3 - T_1 \quad (9)$$

where T_1 and T_3 are the inlet and outlet water temperature, respectively (see Figure 3).

The mass flow rate M_w can also be expressed in volumetric terms as:

$$M_w = V_w \cdot \rho(T), \quad (10)$$

where V_w is the volumetric flow rate in m^3/s and $\rho(T)$ is the density of water (kg/m^3) at temperature T . Both c_p and $\rho(T)$ were assumed to be constant ($c_p = 4.18 \text{ J}/\text{kg} \text{ }^\circ\text{C}$, $\rho(T) = 1000 \text{ kg}/\text{m}^3$) throughout the analysis presented in the study.

The thermal efficiency of the PVT is given as:

$$\eta_{th} = \frac{100 \times E_{th}}{A_m \times G_p} \% \quad (11)$$

Combining Equations (7) and (11), the overall efficiency of a PVT system is given as:

$$\eta_{PVT} = \frac{100 \times E_{dc}}{A_m \times G_p} + \frac{100 \times E_{th}}{A_m \times G_p} = \frac{100}{A_m \times G_p} (E_{dc} + E_{th}) \% \quad (12)$$

2.4.4. Clearness Index

The clearness index is the fraction of the solar radiation reaching the top of the atmosphere that makes it through the atmosphere to reach the Earth's surface. It is normally calculated as a ratio of the monthly averaged daily global solar radiation on horizontal surface (H_{av}) to the monthly averaged daily extraterrestrial solar radiation ($H_{o,av}$) at a given site.

The monthly daily average clearness index (K_T):

$$K_T = \frac{H_{av}}{H_{o,av}} \quad (13)$$

The extraterrestrial irradiance H_o can be determined using the mathematical expression:

$$H_o = \frac{24}{\pi} G_{sc} \left(1 + 0.033 \cos\left(\frac{360n}{365}\right) \right) \times \left(\cos L \cos \delta \sin H_{SR} + \frac{\pi}{180} H_{SR} \sin L \sin \delta \right) \quad (14)$$

where n is the day of the year, L is the latitude of the site, δ is the declination angle of the sun, G_{sc} is the extraterrestrial solar constant $1.37 \text{ kW}/\text{m}^2$ and H_{SR} is the sunrise hour given as:

$$H_{SR} = \cos^{-1}[-\tan(L) \tan(\delta)] \quad (15)$$

$H_{o,av}$ can then be calculated as:

$$H_{o,av} = \frac{\sum_{r=1}^R H_o}{R} \quad (16)$$

where R is the number of days in the month. For this study, monthly daily average clearness indexes were generated for the site using HOMER Pro energy simulation software (Version 3.13.6, Homer Energy, Boulder, CO, USA) [42] which employs existing global data sources and libraries in its predictions.

3. Results and Discussion

3.1. Ambient Conditions

The performance of a solar collector is influenced by a number of interactive factors including, weather conditions. There is however, a very high level of variability and uncertainty in predicting meteorological variables. Nonetheless, PV cell temperature, for instance, is a function of ambient temperature, wind speed and global irradiance (Equation (3)).

3.1.1. Ambient Temperature (T_{amb})

Figure 4 shows the monthly variation of measured ambient temperature. It can be observed from Figure 4 that the highest ambient temperature of $37.90 \text{ }^\circ\text{C}$ was recorded in the month of March, whereas the minimum of $19.81 \text{ }^\circ\text{C}$ occurred in October. However, the highest and minimum monthly average daily ambient temperatures of $28.78 \text{ }^\circ\text{C}$ and $25.18 \text{ }^\circ\text{C}$ were recorded in February and August,

respectively. The average ambient temperature is dependent on the time or season of the year. Ghana has two main climatic seasons namely, the wet and dry seasons. Typically, the wet season in Kumasi starts from April to October. It is normally characterized by cloudy weather conditions, relatively higher mean monthly precipitation and relatively lower mean monthly ambient temperatures. The dry season (which predominantly spans November to March) records low-to-no precipitation and higher ambient temperatures.

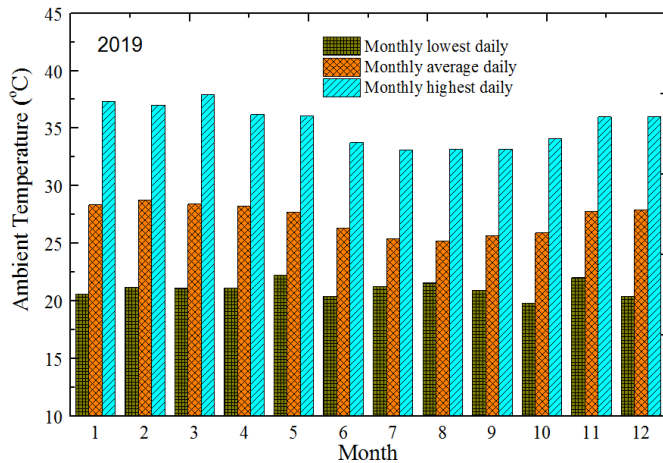


Figure 4. Monthly variation of ambient temperature in 2019.

3.1.2. Solar Irradiation (G_p)

Figure 5 shows the monthly in-plane global solar insolation and monthly average clearness index values in 2019. It was observed that the highest monthly average daily insolation was recorded in the months of March, April and November with clearness index values of 0.53, 0.51 and 0.55, respectively. The lowest monthly average daily irradiances were in July and August (with clearness index values of 0.42 and 0.43, respectively) due to dense cloudy sky conditions. Although the general sky conditions for January and December were not cloudy, they signified the harmattan season when lots of dust and smoke prevailed in the atmosphere and led to high levels of solar attenuation. Annual lowest and highest daily insolation of 0.91 kWh/m²/day and 6.10 kWh/m²/day were observed in the months of June and March, respectively. Furthermore, the annual average daily solar energy for the site was 4.05 kWh/m²/day.

3.1.3. Wind Speed (w)

Figure 6 shows the monthly average and maximum wind speed within the vicinity of the installation. For the period of the study, the monthly average wind speed was less than 1.00 m/s, which prospectively indicated that wind speed effects on solar photovoltaic performance could be negligible. However, observed maximum monthly wind speeds ranged from 3 m/s in February to 11 m/s in October.

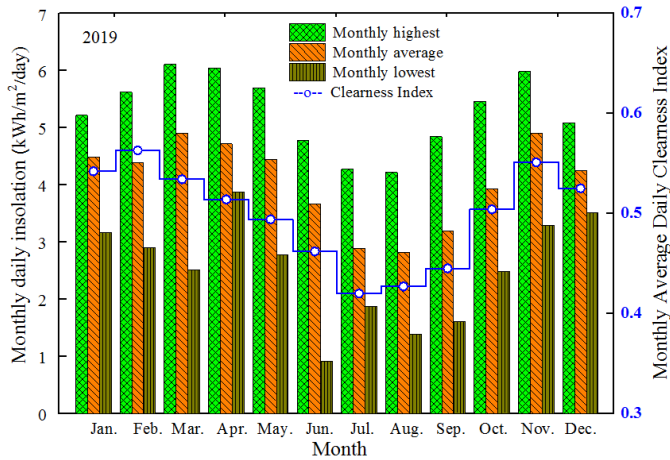


Figure 5. Measured monthly in-plane solar irradiation with clearness index from Homer SW.

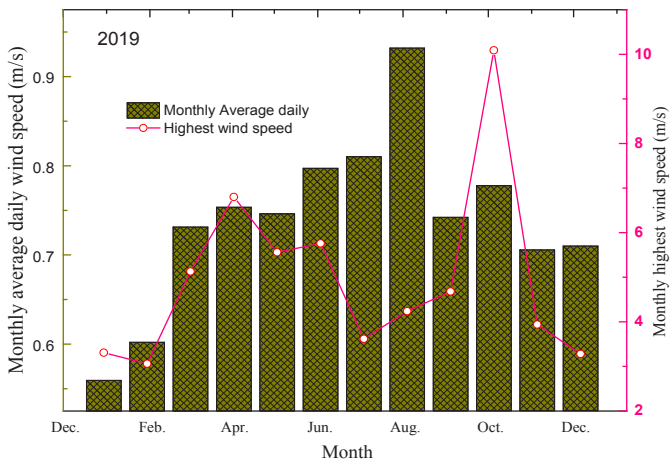


Figure 6. Monthly average daily wind speeds at the experimental site.

3.2. Module Temperature (T_{cell})

The variations in PV and PVT module temperatures at daytime are shown in Figure 7. The recorded average PV module temperatures at daytime were relatively higher than average PVT module temperatures, ranging from 1.3% higher in the month of August to 6.9% higher in March. This could translate into a relatively higher net energy yield per rated wattage for PVT module, due to the lower cell temperature and higher heat recoveries.

Figure 7b,c show the contrasting effects of solar irradiance fluxes on the modules temperatures. Cloudy and unstable weather conditions, smoke and dust in the atmosphere intermittently attenuated incidental solar irradiation resulting in fluctuations and generally lowered ambient temperatures with telling effects on solar module temperature. Nonetheless, the highest recorded operating cell temperatures for the modules for the period under study were 70.6 °C and 60.5 °C for PV module and PVT module, respectively, recorded on the 17 October 2019 (Figure 7c). The high module temperatures were consistent with an earlier study in the same environment [30] where similar

observations were made for different PV technologies. Table 3 presents the summary installations' site ambient conditions and PV and PVT module temperatures.

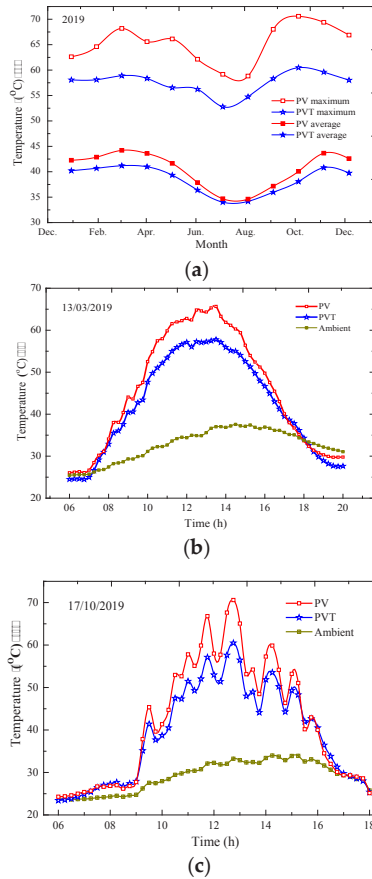


Figure 7. PVT and PV modules temperature profiles at daytime showing variations in: (a) monthly average daily temperatures for 2019; (b) daily temperature variation on a stable sunny day; (c) daily temperature variations on an unstable sunny day.

Table 3. A summary of weather data and module temperatures.

Month	Ambient Conditions			Average Daily T_{cell}	
	H_p , kWh/m ² /day	T_{amb} °C	V m/s	PV °C	PVT °C
January	4.49	30.57	0.56	42.26	40.21
February	4.39	30.86	0.60	42.87	40.69
March	4.90	30.94	0.73	44.22	41.19
April	4.72	30.67	0.75	43.60	40.98
May	4.44	29.88	0.75	41.65	39.33
June	3.67	28.08	0.80	37.87	36.38
July	2.90	26.79	0.81	34.69	34.01
August	2.82	26.62	0.93	34.62	34.17
September	3.20	27.31	0.74	37.16	35.97
October	3.94	28.00	0.78	40.08	38.08
November	4.90	29.91	0.71	43.65	40.80
December	4.25	30.10	0.71	42.58	39.74

3.3. Performance

3.3.1. Electrical Energy Outputs for both PV and PVT

The electrical energy outputs from both PVT and PV were measured at maximum power point (MPP). Both the PV and the PVT outputs followed the same trend as in-plane solar radiation (Figures 5 and 8a). As shown in Figure 8a, in comparison with the other months, the DC outputs from both PV and PVT modules were generally low in the months of June to September. For the PV, the monthly average daily electrical energy outputs varied from 0.39 kWh/m²/day in August to 0.62 kWh/m²/day in April and November. In the case of the PVT however, it varied from 0.29 kWh/m²/day in August to 0.54 kWh/m²/day in April. Unlike the PV, the PVT performance dependency factors go beyond environmental factors to include PV parking factor, type and flow rate of the thermal fluid, type and design of thermal absorber [7,10,11] etc. which were not covered in the scope of this work.

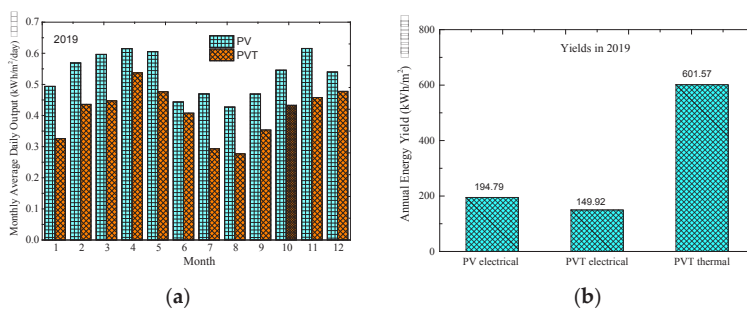


Figure 8. The energy outputs of the PV and PVT showing: (a) monthly average daily electrical energy outputs; (b) net annual energy yields.

The annual total electrical energy measurements, per unit area, assessed from PV and PVT modules were 194.79 kWh/m² and 149.92 kWh/m², respectively (Figure 8b). In addition to the electrical energy, the PVT also provided an added incentive of 601.57 kWh/m² of heat energy over the same period.

3.3.2. Efficiency

The efficiency was based on only DC power output, since the installations were not connected to inverters. It was calculated for every 15 min (data resolution) for daily sun-hour periods (with filtered irradiance ≥ 150 W/m²) and then averaged monthly. Nameplate rated efficiencies (DC) for PV and PVT are 16.60% and 15.08%, respectively (see Table 1). From the results, the monthly averaged electrical efficiency for PV varied from 11.6% to 12.7% over the data collection period, indicating a deviation range of 23.1% to 30.1%, relative to rated efficiency. In the case of the PVT, the electrical efficiency varied from 9.9% to 11.5%, representing a deviation of 28% to 38% from STC rating. In addition to that, the thermal efficiency for the PVT had a wider variation of 29.44% to 44.84%. This represented a deviation of 5.6% to 38% from its zero-loss collector efficiency of 47.5% (see Table 1). This could be attributed to the slow thermal response (time constant of up to 8 min [8]) of the PVT's thermal absorber (copper sheet with pipes in this case) to erratic spectral changes, typical of the study environment [30,43]. It can also be deduced from Table 4 that the average thermal efficiency of the commercial PVT was predominantly lower than those reported in most studies in the literature. This could be attributed to many factors, including poor contact between absorber and PV. A similar observation was made about a commercial water PVT by Guarracino et al. [8] in another study. Notwithstanding this observation, the highest recorded monthly mean net efficiency was 56.14%.

Table 4. Comparison of present study with other water based PVT efficiencies.

Reference	η_{PV} (%)	η_{TH} (%)	η_{PVT} (%)
Fuentes et al. [7]	16.1–19.1	50–70.4	66.1–89.5
Fudholi et al. [12]	11.9–12.4	41.1–48	53.6–66.8
Fudholi et al. [12]	12.2–12.7	46.4–54.6	58.6–66.8
Zhang et al. [13]	9.5	50.0	59.5
Huang et al. [14]	9.0	38.0	47.0
Chow et al. [15]	11.0	51.0	62.0
He et al. [16]	9.8	40.0	49.87
Ji et al. [17]	10.15	45.0	55.15
Present study	9.9–11.5	29.44–44.84	39.34–56.34

3.3.3. Reference Yield

Figure 9 shows that the highest and lowest monthly average daily reference yields were realized in the months of November (4.90 kWh/kW/day) and August (2.81 kWh/kW/day), respectively. The reference yield represents the number of peak sun hours. It is a function of the location, orientation and inclination of the solar PV array. As a result, the monthly daily average reference yield followed the same trend as the irradiance recorded in-plane as shown in Figure 9. The observed low reference yields in the months of July to September could be attributed to low in-plane solar irradiation.

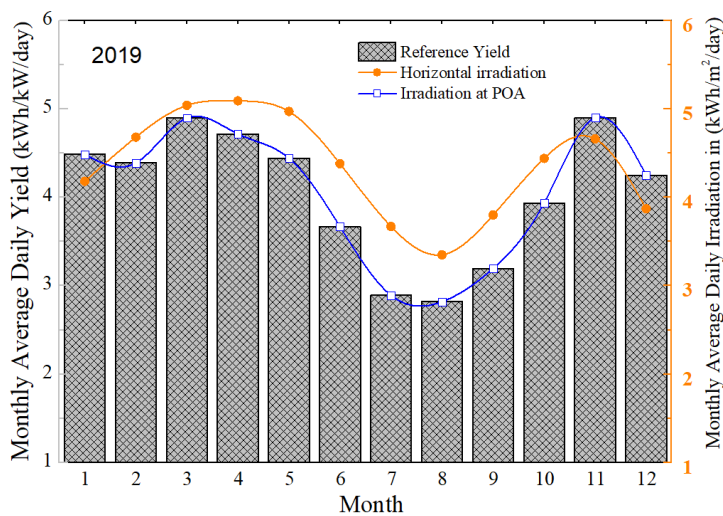


Figure 9. Reference yield compared to monthly average in-plane and horizontal daily irradiation data extracted from RETScreen Expert Viewer Software (Version 6.0.7.55, CanmetENERGY, Varennes, QC, Canada) [44].

3.3.4. Array or Module Yield

The monthly average daily electrical energy yields for the PV and PVT are presented in Figure 10. The energy yield of the PV varied from a low of 2.5 kWh/kW_p/day in the month of August to a high of 3.85 kWh/kW_p/day in the months of April and November. In the case of the PVT, its electrical energy yield varied from a low of 1.83 kWh/kW_p/day in the same month of August to a high of 3.56 kWh/kW_p/day in April. As indicated earlier, the observed lower reference yields in the months of July to September were due to low in-plane solar irradiation. However, during the same period, the PV yields increased compared to the reference yield due to lower ambient temperatures on average translating into lower module temperatures (Figure 7a) and improved performance. The yearly daily

average electrical energy yields for the period of the study were observed to be 3.21 kWh/kW_p/day for the PV module and 2.72 kWh/kW_p/day for the PVT module. The variation in monthly energy yield was similar to a pattern in an earlier study [30] in the same environment on assorted model technologies.

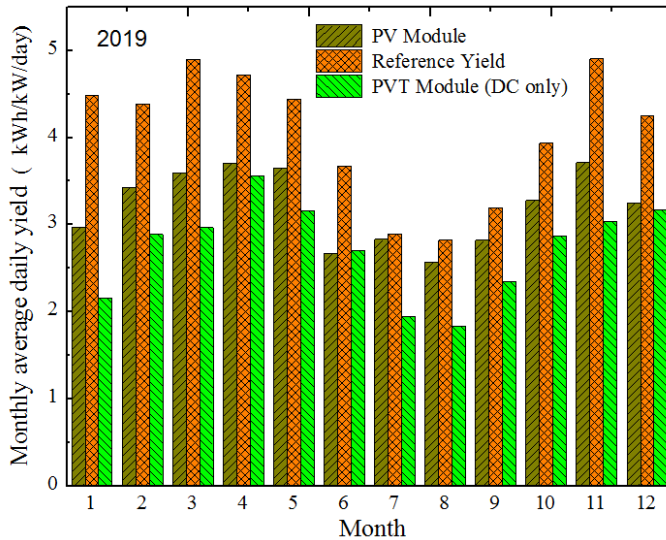


Figure 10. Array yield for PV and PVT modules compared with reference yield.

3.3.5. Performance Ratio (PR)

As indicated earlier PR shows the overall effect of losses on PV ratings. For this study, the PRs for the PV and PVT were 79.2% and 51.6% respectively. These values were not very different from what were reported in other studies as shown in Table 5. The value of the PR is an important way of identifying problems emanating from system component failures and a good guide for improving system performance.

Table 5. Performance parameter for mc-Si modules in the literature.

Location	PR (%)	Reference
Dublin, Ireland	81.50	[40]
Kumasi, Ghana	67.90	[30]
Algeria	80.70	[45]
Ballymena, Ireland	60–62	[46]
Castile and Leon, Spain	69.80	[47]
Malaysia	59.90–79.14	[48]
Sardinia, Italy	83.20–87.3	[49]
Gujarat, India	57.10–93.14	[50]
Malaysia	77.85	[51]
Kumasi, Ghana	79.18	Present study
Kumasi, Ghana (PVT) ¹	51.60	Present study

¹ This is only in reference to the electrical component of the PVT.

3.3.6. Capacity Factor (CF)

The annual capacity factors (CF) of 13.35% and 11.30% were recorded for the PV and PVT, respectively. The CFs show the average of fraction of time in a year when the PV system is available to

generate energy at its rated power output. Thus, the PV and PVT systems considered in this study can be said to have generated their rated electrical power only in about 48 days and 41 days, respectively.

3.4. Comparison between PV and PVT Installations

Table 6 presents the summary of key electrical parameters for PV and PVT installations. Yearly average daily array yields of 3.21 kWh/kW_p/day for the PV module, as against 2.72 kWh/kW_p/day for the PVT module, seemed to suggest the PV module outperformed the PVT in electrical energy production. This was consistent with earlier studies [7]. The electrical energy yield from the PV in this study was on average 25.55% higher than what was generated from the PVT. However, with the additional incentive of thermal energy harvest, the PVT provided a better utilization of solar energy resources than the ordinary PV. Due to the continuous extraction of heat from the modules, the PVT module generally operated at lower module temperatures than the PV module. This was however contradicted by Fuentes et al. [7] who attributed lower electrical performance of PVT to higher module temperatures compared to the PV module. Despite this, the thermal gains of the PVT made it better than PV in terms of total energy output per unit area. The monthly mean efficiency variations of the PVT module in this study also showed that, based on both electrical and thermal energy outputs, its overall efficiency could reach 56.34%, which is significantly higher than the maximum monthly mean value of 12.7% for the PV module. This meant that, in terms of physical installation and space, the PVT gave a better energy output per unit area than the PV. Hence, for better space utilization per energy output, the PVT was a better alternative than the PV. For off-grid rural settlements, the PVT could come in handy in the provision of both electricity and heating. Additionally, this could be very useful in clinics, schools, and for camping.

Table 6. A summary of PV and PVT (electrical properties) performance.

Parameter	PV	PVT
Rated Power of PV (W _p)	270	200
Annual energy output of PV (kWh/year)	315.73	198.19
Annual average daily energy output of PV (Wh/day)	865.02	542.97
Yearly total irradiance (kW/m ²)	14,766.66	14,766.66
Yearly average daily irradiance (kWh/m ² /day)	4.05	4.05
Daily Reference Yield (kWh/kW/day)	4.05	4.05
Daily Module Yield (kWh/kW _p /day)	3.20	2.09
Performance Ratio (%)	79.18	51.60
Annual Capacity factor (%)	13.34	11.30
Efficiency (averaged) (%)	12.14	10.80

4. Conclusions

In this paper, a comparative performance valuation was conducted on water-based PVT and PV modules made of mc-Si cell technology in a dynamic environment for 2019.

- The highest recorded instantaneous module temperatures were 70.6 °C and 60.5 °C for the PV module and PVT module, respectively, recorded in October. On the average, the PV module temperature remained relatively higher than that of PVT by 1.3% to 6.9%.
- The annual total energy output for the PV module was 194.79 kWh/m² while that of the PVT for electrical and thermal outputs was 149.92 kWh/m² and 1087.79 kWh/m², respectively.
- The annual daily mean electrical energy yield for the PV and PVT were 3.21 kWh/kW_p/day and 2.72 kWh/kW_p/day, respectively.
- The annual performance ratios based on only electrical energy for the PV and PVT were 79.2% and 51.6%, respectively, whereas their capacity factors were, respectively, 13.35% and 11.3%.

- The monthly average electrical efficiency values for PV and PVT were 11.6–12.7% and 9.9–11.5% respectively. The thermal efficiency of the PVT had a wider variation from 29.44% to 44.84%. There is however the need to improve the thermal efficiency of commercial PVTs.

This study has shown that the flat plate water PVT application is feasible in environments with similar weather conditions to that of Kumasi. It could also be concluded that, based on the general performance of the two technologies, the PV is a better choice for very large-scale grid-connected systems, where the interest is mostly in electrical energy production. However, for domestic applications and small scale grid systems with provision for thermal energy use, the PVT is a better option. The study could not however cover the exergy analysis, economic evaluations and life cycle assessment of the current PVT/PV setup. These should be carried out so that the actual cost of PVT setup, the net cost of produced energy and their environmental impact could be determined. This information could be useful to stakeholders in Ghana in making informed decisions in energy systems.

Author Contributions: Conceptualization, S.A.-G., and M.S.A.; methodology, S.A.-G.; formal analysis, S.A.-G.; resources, R.S. and M.S.A.; data curation, S.A.-G.; writing—original draft preparation, S.A.-G.; writing—review and editing, D.A.Q., E.W.R., R.S., M.S.A.; supervision, D.A.Q., E.W.R., R.S., M.S.A.; project administration, R.S. and M.S.A.; funding acquisition, R.S. and M.S.A. All authors have read and agreed to the published version of the manuscript.

Acknowledgments: We are grateful to the Norwegian aid agency, Norad, for funding this work through the UPERCRETs project, aimed at building capacity in the area of research through the collaboration between KNUST in Ghana and NMBU in Norway.

Conflicts of Interest: The authors declare no conflict of interest.

References

1. Baljit, S.S.S.; Chan, H.Y.; Sopian, K. Review of building integrated applications of photovoltaic and solar thermal systems. *J. Clean. Prod.* **2016**, *137*, 677–689. [[CrossRef](#)]
2. Zondag, H. Flat-plate PV-Thermal collectors and systems: A review. *Renew. Sustain. Energy Rev.* **2008**, *12*, 891–959. [[CrossRef](#)]
3. Chow, T.T. A review on photovoltaic/thermal hybrid solar technology. *Appl. Energy* **2010**, *87*, 365–379. [[CrossRef](#)]
4. Aste, N.; del Pero, C.; Leonforte, F. Water flat plate PV/thermal collectors: A review. *Sol. Energy* **2014**, *102*, 98–115. [[CrossRef](#)]
5. Guarracino, I.; Markides, C.N.; Mellor, A.; Ekins-Daukes, N.J. Dynamic coupled thermal and electrical modelling of sheet and tube hybrid photovoltaic/thermal (PVT) collectors. *Appl. Therm. Eng.* **2016**, *101*, 778–795. [[CrossRef](#)]
6. Good, C. Environmental impact assessment of hybrid photovoltaic-thermal (PV/T) Systems—A review. *Renew. Sustain. Energy Rev.* **2016**, *55*, 234–239. [[CrossRef](#)]
7. Fuentes, M.; Vivar, M.; de la Casa, J.; Aguilera, J. An experimental comparison between commercial hybrid PV-T and simple PV systems intended for BIPV. *Renew. Sustain. Energy Rev.* **2018**, *93*, 110–120. [[CrossRef](#)]
8. Guarracino, I.; Freeman, J.; Ramos, A.; Kalogirou, S.A.; Ekins-Daukes, N.J.; Markides, C.N. Systematic testing of hybrid PV-thermal (PVT) solar collectors in steady state and dynamic outdoor conditions. *Appl. Energy* **2019**, *240*, 1014–1030. [[CrossRef](#)]
9. de Keizer, C.; de Jong, M.; Mendes, T.; Katiyar, M.; Folkerts, W.; Rindt, C.; Zondag, H. Evaluating the thermal and electrical performance of several uncovered PVT collectors with a field test. *Energy Procedia* **2016**, *91*, 20–26. [[CrossRef](#)]
10. Rejeb, O.; Dhaou, H.; Jemni, A. A numerical investigation of a photovoltaic thermal (PV/T) collector. *Renew. Energy* **2015**, *77*, 43–50. [[CrossRef](#)]
11. Dupeyrat, P.; Ménézo, C.; Rommel, M.; Henning, H.M. Efficient single glazed flat plate photovoltaic-thermal hybrid collector for domestic hot water system. *Sol. Energy* **2011**, *85*, 1457–1468. [[CrossRef](#)]
12. Fudholi, A.; Sopian, K.; Yazdi, M.H.; Ruslan, M.H.; Ibrahim, A.; Kazem, H.A. Performance analysis of photovoltaic thermal (PVT) water collectors. *Energy Convers. Manag.* **2014**, *78*, 641–651. [[CrossRef](#)]

13. Zhang, X.; Zhao, X.; Smith, S.; Xu, J.; Yu, X. Review of R&D progress and practical application of the solar photovoltaic/thermal (PV/T) technologies. *Renew. Sustain. Energy Rev.* **2012**, *16*, 599–617.
14. Huang, B.J.; Lin, T.H.; Hung, W.C.; Sun, F.S. Performance evaluation of solar photovoltaic/thermal systems. *Sol. Energy* **2001**, *70*, 443–448. [[CrossRef](#)]
15. Chow, T.T.; Ji, J.; He, W. Photovoltaic–thermal collector system for domestic application. *J. Sol. Energy Eng.* **2007**, *129*, 205–209. [[CrossRef](#)]
16. He, W.; Chow, T.T.; Ji, J.; Lu, J.P.; Pei, G.; Chan, L.S. Hybrid photovoltaic and thermal solar-collector designed for natural circulation of water. *Appl. Energy* **2006**, *83*, 199–210. [[CrossRef](#)]
17. Ji, J.; Lu, J.P.; Chow, T.T.; He, W.; Pei, G. A sensitivity study of a hybrid photovoltaic/thermal water-heating system with natural circulation. *Appl. Energy* **2007**, *84*, 222–237. [[CrossRef](#)]
18. IEA-Africa Energy Outlook 2019-World Energy Outlook Special Report. Available online: <https://www.ncran.gc.ca/maps-tools-publications/tools/data-analysis-software-modelling/retscreen/7465> (accessed on 22 April 2020).
19. Hazami, M.; Ali Riahi, A.; Mehdaoui, F.; Omeima Nouicer, O.; Farhat, A. Energetic and exergetic performances analysis of a PV/T (photovoltaic thermal) solar system tested and simulated under to Tunisian (North Africa) climatic conditions. *Energy* **2016**, *10715*, 78–94. [[CrossRef](#)]
20. Abdulkadir, M.; Muhammad, S.B. Design and construction of a thermosiphonic solar photovoltaic: Thermal water heating system for sustainable development in temperate regions of Africa. *J. Altern. Energy Sources Technol.* **2017**, *8*, 1–8.
21. Siecker, J.; Kusakan, K.; Numbi, B.P. Optimal switching control of PV/T systems with energy storage using forced water circulation: Case of South Africa. *J. Energy Storage* **2018**, *20*, 264–278. [[CrossRef](#)]
22. Oyiyeke, A.Y.A.; Inambao, F.L. Performance characterisation of a hybrid flat-plate vacuum insulated photovoltaic/thermal solar power module in subtropical climate. *Int. J. Photoenergy* **2016**, *2*, 1–15. [[CrossRef](#)]
23. Apuko, O.A.Y.; Inambao, F.L. Simulation and performance evaluation of a vacuum insulated hybrid solar photovoltaic/thermal power module for domestic applications in South Africa. *TMC Acad. J.* **2015**, *9*, 1–19.
24. Sawadogo, W.; Abiodun, B.J.; Okogbue, E.C. Impacts of global warming on photovoltaic power generation over West Africa. *Renew. Energy* **2020**, *151*, 263–277. [[CrossRef](#)]
25. Meunier, S.; Heinrich, M.; Quéval, L.; Cherni, J.A.; Vido, L.; Darga, A.; Dessante, P.; Multon, B.; Kitanidis, P.K.; Marchand, C. A validated model of a photovoltaic water pumping system for off-grid rural communities. *Appl. Energy* **2019**, *241*, 580–591. [[CrossRef](#)]
26. Akinyele, D.; Babatunde, O.; Monyei, C.; Olatomiwa, L.; Okediji, A.; Ighravwe, D.; Abiodun, O.; Onasanya, M.; Temikotan, K. Possibility of solar thermal power generation technologies in Nigeria: Challenges and policy directions. *Renew. Energy Focus* **2019**, *29*, 24–41. [[CrossRef](#)]
27. Nyarko, F.K.A.; Takyi, G.; Amalu, E.H.; Adaramola, M.S. Generating temperature cycle profile from in-situ climatic condition for accurate prediction of thermo-mechanical degradation of c-Si photovoltaic module. *Eng. Sci. Technol. Int. J.* **2019**, *22*, 502–514. [[CrossRef](#)]
28. Quansah, D.A.; Adaramola, M.S. Assessment of early degradation and performance loss in five co-located solar photovoltaic module technologies installed in Ghana using performance ratio time-series regression. *Renew. Energy* **2019**, *131*, 900–910. [[CrossRef](#)]
29. Quansah, D.A.; Adaramola, M.S. Ageing and degradation in solar photovoltaic modules installed in northern Ghana. *Sol. Energy* **2018**, *173*, 834–847. [[CrossRef](#)]
30. Quansah, D.A.; Muiyiwa, S.A.; Appiah, G.K.; Edwin, I.A. Performance analysis of different grid-connected solar photovoltaic (PV) system technologies with combined capacity of 20 kW located in humid tropical climate. *Int. J. Hydrog. Energy* **2017**, *42*, 4626–4635. [[CrossRef](#)]
31. Enongene, K.E.; Abanda, F.H.; Otene, I.J.J.; Obi, S.I.; Okafor, C. The potential of solar photovoltaic systems for residential homes in Lagos city of Nigeria. *J. Environ. Manag.* **2019**, *24415*, 247–256. [[CrossRef](#)]
32. Caton, P. Design of rural photovoltaic water pumping systems and the potential of manual array tracking for a West-African village. *Sol. Energy Vol.* **2014**, *103*, 288–302. [[CrossRef](#)]
33. Ndiaye, A.; Kébé, C.M.F.; Charki, A.; Ndiaye, P.A.; Sambou, V.; Kobi, A. Degradation evaluation of crystalline-silicon photovoltaic modules after a few operation years in a tropical environment. *Sol. Energy Vol.* **2014**, *103*, 70–77. [[CrossRef](#)]

34. Tossa, A.K.; Soro, Y.M.; Azoumah, Y.; Yamegueu, D. A new approach to estimate the performance and energy productivity of photovoltaic modules in real operating conditions. *Sol. Energy Vol.* **2014**, *110*, 543–560. [CrossRef]
35. Dajuma, A.; Yahaya, S.; Touré, S.; Diedhiou, A.; Adamou, R.; Konaré, A.; Sido, M.; Golba, M. Sensitivity of solar photovoltaic panel efficiency to weather and dust over West Africa: Comparative experimental study between Niamey (Niger) and Abidjan (Côte d’Ivoire). *Comput. Water Energy Environ. Eng.* **2016**, *5*, 123–147. [CrossRef]
36. Yushchenko, A.; de Bono, A.; Chatenoux, B.; Patel, M.K.; Ray, M. GIS-based assessment of photovoltaic (PV) and concentrated solar power (CSP) generation potential in West Africa. *Renew. Sustain. Energy Rev.* **2018**, *81*, 2088–2103. [CrossRef]
37. Simo-Tagne, M.; Ndukwu, M.C.; Zoulalian, A.; Bennamoun, L.; Kifani-Sahban, F.; Rogaume, Y. Numerical analysis and validation of a natural convection mix-mode solar dryer for drying red chilli under variable conditions. *Renew. Energy* **2020**, *151*, 659–673. [CrossRef]
38. Ogunmodimu, O.; Okoroigwe, E.C. Solar thermal electricity in Nigeria: Prospects and challenges. *Energy Policy* **2019**, *128*, 440–448. [CrossRef]
39. Seshie, Y.M.; N’Tsoukpoe, K.E.; Neveu, P.; Coulibaly, Y.; Azoumah, Y.K. Small scale concentrating solar plants for rural electrification. *Renew. Sustain. Energy Rev.* **2018**, *90*, 195–209. [CrossRef]
40. Ayompe, L.M.; Duffy, A.; McCormack, S.J.; Conlon, M. Measured performance of a 1.72 kW rooftop grid connected photovoltaic system in Ireland. *Energy Convers. Manag.* **2011**, *52*, 816–825. [CrossRef]
41. Adaramola, M.S.; Vågnes, E.E.T. Preliminary assessment of a small-scale rooftop PV-grid tied in Norwegian climatic conditions. *Energy Convers. Manag.* **2015**, *90*, 458–465. [CrossRef]
42. Homer Pro Microgrid Analysis Tool-Version 3.13.6. Available online: www.homerenergy.com (accessed on 10 February 2020).
43. Soubdhan, T.; Emilion, R.; Calif, R. Classification of daily solar radiation distributions using a mixture of Drichlet distributions. *Sol. Energy* **2009**, *83*, 1056–1063. [CrossRef]
44. RETScreen Expert- Version 6.0.7.55. Available online: <https://www.ncran.gc.ca/maps-tools-publications/tools/data-analysis-software-modelling/retscreen/7465> (accessed on 13 February 2020).
45. Benatallah, A.; Mostefaou, R.; Bradja, K. Performance of photovoltaic solar system in Algeria. *Desalination* **2007**, *209*, 39–42. [CrossRef]
46. Mondol, J.D.; Yohanis, Y.; Smyth, M.; Norton, B. Long term performance analysis of a grid connected photovoltaic system in Northern Ireland. *Energy Convers. Manag.* **2006**, *47*, 2925–2947. [CrossRef]
47. Miguel, A.D.; Bilbao, J.; Cazorro, J.R.S.; Martin, C. Performance analysis of a grid-connected PV system in a rural site in the northwest of Spain. In Proceedings of the World Renewable Energy Congress VII (WREC 2002), Cologne, Germany, 29 June–5 July 2002; Available online: https://www.researchgate.net/profile/Argimiro_De_Miguel/publication/258221437_Performance_analysis_of_a_grid-connected_PV_system_in_a_rural_site_in_the_Northwest_of_Spain/links/598987884585156058588c9b/Performance-analysis-of-a-grid-connected-PV-system-in-a-rural-site-in-the-Northwest-of-Spain.pdf (accessed on 13 February 2020).
48. Humada, A.M.; Hojabri, M.; Hamada, H.M.; Samsuri, F.B.; Ahmed, M.N. Performance evaluation of two PV technologies (c-Si and CIS) for building integrated photovoltaic based on tropical climate condition: A case study in Malaysia. *Energy Build.* **2016**, *119*, 233–241. [CrossRef]
49. Ghiani, E.; Pilo, F.; Cossu, S. Evaluation of photovoltaic installations performances in Sardinia. *Energy Convers. Manag.* **2013**, *76*, 1134–1142. [CrossRef]
50. Tripathia, B.; Yadav, P.; Rathod, S.; Kumar, M. Performance analysis and comparison of two silicon material based photovoltaic technologies under actual climatic conditions in Western India. *Energy Convers. Manag.* **2014**, *80*, 97–102. [CrossRef]
51. Tan, P.H.; Gan, C.K.; Baharin, K.A. Techno-economic analysis of rooftop PV system in UTeM Malaysia. In Proceedings of the IEEE Xplore 2014, 3rd IET International Conference on Clean Energy and Technology (CEAT), Kuching, Malaysia, 24–26 November 2014.



Paper II



Original article

Techno-economic analysis of solar photovoltaic (PV) and solar photovoltaic thermal (PVT) systems using exergy analysis

Saeed Abdul-Ganiyu^a, David A. Quansah^{b,c}, Emmanuel W. Ramde^{b,c}, Razak Seidu^d, Muyiwa S. Adaramola^{a,*}

^a Faculty of Environmental Sciences and Natural Resources Management, Norwegian University of Life Science, As, Norway

^b Department of Mechanical Engineering, Kwame Nkrumah University of Science and Technology (KNUST), Kumasi, Ghana

^c The Brew-Hammond Energy Centre, Kwame Nkrumah University of Science and Technology (KNUST), Kumasi, Ghana

^d Department of Ocean Operations and Civil Engineering, Norwegian University of Science and Technology, Alesund, Norway

ARTICLE INFO

Keywords:

Exergy
Levelized cost of exergy
Present value
Grid tariff

ABSTRACT

This paper assesses the technical and economic viability of a hybrid water-based mono-crystalline silicon (mc-Si) photovoltaic-thermal (PVT) module in comparison with a conventional mc-Si photovoltaic (PV) module installed in Ghana. Analytical models are developed to analyze the technical and economic performance of the systems over a 25-year period. The study shows that although the PVT system is more expensive to setup, it generally performs better than the conventional PV system when both systems are installed with batteries. The estimated average yearly total exergy to load from PV and PVT sub-systems are respectively 159.42 kWh/m² and 330.15 kWh/m². The levelized cost of exergy (LCOEx) from the PV and PVT basic systems are US\$ 0.45/kWh and US\$ 0.33/kWh respectively for average peak sun hours (S_h) of 4.6 h (installation site). Varying S_h from 4.6 h to 6.5 h (northmost regions of Ghana) reduces the LCOEx for the PV and PVT systems by approximately 18% and 11% respectively. The PV system however becomes more economically viable than the PVT system when both systems are installed without batteries.

Introduction

Solar energy is one of the leading potential resources in solving the energy deficit in sub-Saharan Africa, yet the entire continent accounts for less than 1% of global solar PV installed capacity [1]. The all-year-round availability and near-uniform distribution of solar energy in the sub-region provides the flexibility of energy decentralization, thus making it very practicable in remote locations. Like other renewable energy (RE) technologies, a primary hurdle in solar energy technologies is their high initial cost compared to conventional fossil energy resources [1] thus making the technology inaccessible to many in the sub-region. One way to overcome this hurdle is for policy makers to develop and implement support schemes to overcome the high upfront cost associated with solar energy technologies [2–4]. Such policies will require a well-researched geographically specific assessment covering techno-economic evaluations of RE technologies.

Economic development globally is linked to the availability of reliable energy. About 16.8% of households did not have access to

electricity in Ghana as of 2019 [5]. In 2015, the country suffered energy supply deficits which resulted in power rationing [6] that led to job losses, low economic productivity and expensive, but unsustainable, power supply alternatives. Although the country has rich solar potential, unfortunately, less than 1% of its national grid's installed capacity comes from solar installations [6]. The solar potential of the country could have been exploited to attain its universal access rate by 2020 target [5].

A solar technology that has received a lot of attention in recent years is hybrid photovoltaic thermal (PVT) systems. The PVT technologies combine the functions of a conventional photovoltaic (PV) system and a solar thermal system into one module making them more efficient than the conventional systems. However, the PVT systems are more expensive than conventional PV modules due to the integrated thermal unit and thus necessitates a cost/benefit analysis to assess the limits of their practicality [7].

Comparative techno-economic analyses of energy from flat-plate water PVT and conventional PV systems have been undertaken by a few authors from various locations worldwide. Herrando and Markides

* Corresponding author.

E-mail addresses: abdul-ganiyu.saeed@nmbu.no (S. Abdul-Ganiyu), daqansah.coe@knust.edu.gh (D.A. Quansah), eramde@gmail.com (E.W. Ramde), rased@ntnu.no (R. Seidu), muyiwa.adaramola@nmbu.no (M.S. Adaramola).

<https://doi.org/10.1016/j.seta.2021.101520>

Received 19 November 2020; Received in revised form 10 July 2021; Accepted 2 August 2021

2213-1388/© 2021 The Author(s). Published by Elsevier Ltd. This is an open access article under the CC BY license (<http://creativecommons.org/licenses/by/4.0/>).

Nomenclature	
A_{dc}	Effective module surface area (m^2) for the PVT
A_{pv}	is the effective PV module surface area
A_{th}	thermal absorber surface area (m^2)
C_t	Total cost
DM	Design margin
DOD	Depth of discharge (%)
C_{bat}	battery capacity
C_{inv}	Inverter capacity
D_{aut}	Days of autonomy
d_{bat}	Annual derating factors of battery round-trip efficiency
dg	module degradation (%/year)
d_{inv}	Annual derating factor of inverter-charging system efficiency
D_t	The number of days in year t
$E_{ac..t}$	Net annual electrical energy available to the load
$E_{dc..t}$	Net DC electrical energy (kWh/year) after wiring losses in year t
$E_{dc..50b_t}$	Simulated DC electrical energy output directly from component Type50b.
$E_{dc..t.sim}$	Simulated DC electrical energy output in (KWh/year) in year t
$E_{pmp..t}$	Power consumption by pump in year t ,
$E_{pvt..t}$	Net energy from the PVT module (kWh/year) in year t
$E_{th..t}$	Annual thermal energy (kWh/year) in year
$E_{th..t.sim}$	Simulated thermal energy output in (KWh/year) in year t
$Ex_{pv..t}$	Net exergy to load from PV system in year t
$Ex_{pvt..t}$	Net exergy to load from PVT system in year t
G_t	Yearly average daily solar energy in the year t ($kWh/m^2/day$)
$I_{bat..t}$	The installed cost (\$) of battery in year t
I_t	Total investment expenditure in year t
$I_{inv..t}$	The installed cost (\$) of inverter in year t
k	Heat energy transfer losses factor (%)
$LCOE$	Levelized Cost of Energy
$LCOEx$	Levelized Cost of Exergy
L_t	Financial loan cost in year t
M_t	Operation and maintenance cost
n	Economic life of the system
$P_{pv..rated}$	Module rated electrical capacity at STC in kW
PV_{CF}	Present value of the cash flow
PV_{Ex}	Present value of the exergy
r	Discount rate
Tx_t	total tax paid in year t
S_h	Peak sun hours
Sp_t	total support and incentives in year t
T_o	Water output temperature
T_a	Ambient temperature
$U_{bat..t}$	Unit cost of battery in year t
$U_{inv..t}$	Unit cost of inverter in year t
Greek letters	
β_t	The % of battery involvement in energy conversion
$\eta_{bat..t}$	Battery efficiencies (%) in year t
$\eta_{cv..t}$	Energy conversion efficiency in year t
η_{dc}	Module electrical efficiency (%)
$\eta_{dc..50b_t}$	Energy conversion efficiency of Type50b (%)
η_{th}	Module thermal efficiency (%)
$\eta_{inv..t}$	Inverter efficiencies (%) in year t
ρ	Annual % increase in pump power consumption
Abbreviations	
AC or ac	Alternating current
AGM	Absorbed glass mat.
BOS	Balance-of-system
DC or dc	Direct current
E	Energy
ECOWAS	Economic Community of West African States
ECREE	Centre for Renewable Energy and Energy Efficiency
Ex	Exergy
FIT	Feed-in Tariffs
mc-Si	Mono-crystalline silicon
PURC	Public Utilities Regulatory Commission
PV	Photovoltaic
PVT	Photovoltaic-thermal
RE	Renewable energy
SE4ALL	Sustainable Energy for All
SREP	Scaling-up Renewable Energy Program
STC	Standard Test Condition
TEA	Techno-economic Analysis
UNDP	United Nation Development Program

[8] undertook a techno-economic analysis to assess hybrid PVT systems for distribution of electricity and hot-water provision in a typical house in London, UK. They concluded that, with respect to primary energy and decarbonization, the PVT systems offered significantly improved proposition over equivalent conventional PV-only systems, but at a higher cost. Kalogirou and Tripanagnostopoulos [9] investigated the industrial application of PVT systems, relative to conventional PV systems. They proved the economic viability of the systems by showing that positive life cycle savings are obtained in the case of PVT systems compared with the PV, and the savings increased for higher load temperature applications. In another study, [7] they undertook a cost/benefit analysis of PVT systems, and compared the payback time with separately installed conventional PV and solar thermal under support schemes and conditions in Greece. Kalogirou [10] used TRNSYS software to model and simulate a hybrid PVT system in Cyprus and investigated the life cycle savings and the pay-back time of the system.

The commercialization of PVT technology has generally not been successful [11] as the separate conventional PV and solar heaters, largely due to lack of information about the possibilities and benefits of PVT solutions, and the lack of international standards, which creates less confidence for the final PVT customer [12]. Although there have been

techno-economic studies on PV systems in West Africa in open literature [13,14], similar studies on PVT systems were all based on locations outside the sub-region like Greece [7,9], United Kingdom [8] and Cyprus [10]. However, the general practicability and economic feasibility of both PV and PVT technologies are functions of the geographical location where the technology is deployed, basically due to different weather conditions (e.g. Harmattan in West Africa) and economic environments. Firstly, this paper helps to address the regional based research gap on the techno-economic performance of the flat-plate water-based PVT technology in different environments. In particular, the study examines the economic feasibility of a PVT system in a Ghanaian climate condition. The choice of location is expected to significantly affect the results, due to differences in environmental conditions, economic parameters and government policies (including support systems in place), incentives etc. Secondly, all the cited studies on comparative economic analysis between conventional PV and PVT systems- e.g. studies by Tselepis and Tripanagnostopoulos [7], Herrando and Markides [8], Kalogirou and Tripanagnostopoulos [9] and Kalogirou [10] - were based on energy parameters (levelized cost of energy). This paper however explores the use of levelized cost of exergy ($LCOEx$) as an economic parameter in comparing the two technologies. The use of exergy in this paper allows a

fair quantification and costing of thermal and electrical energies in a single parameter.

Methodology

Energy cost and renewable energy (RE) policies in Ghana

About two-thirds of Ghana's electricity supply (grid power) is from thermal sources which use fossil fuels [6] and weighs heavily on tariffs determination. This also means that the cost of producing energy is affected by exchange rate since fuel is traded in foreign currency on the world market. The cost of electricity (tariff) in Ghana for residential consumers is categorized by total monthly electricity consumption, as shown in Table 1. In addition to the energy cost are charges for street-light, national levies and monthly service charges [15]. The tariffs are reviewed quarterly by the Public Utilities Regulatory Commission (PURC), an institution mandated by law in Ghana to do so.

Although RE technologies are seen as alternative power sources to the grid, they are still relatively more expensive (to set up in Ghana) than the traditional energy technologies and cannot compete with them without supporting policies [16]. There is therefore the need to establish technology-specific reliable framework and long-term policy objectives on the growth of RE in Ghana. Political factors that influence RE growth include public policies, institutional variables and energy security [17]. Some of the most common public policy measures to encourage renewables include subsidies, quota policies, direct investment, research and development, feed-in tariffs (FiT), green certificate, etc.

There have been some efforts by policy makers in the promotion of RE technology in Ghana. The country's version of Sustainable Energy for All (SE4ALL) Action Plan was developed and launched in May 2013 with technical support from United Nation Development Programme (UNDP), Ghana [19]. Following a decision by SE4ALL stakeholders in Africa to refocus Action Plan documents into Action Agendas in December 2013, the ECOWAS Centre for Renewable Energy and Energy Efficiency (ECREEE) provided technical assistance to Ghana to reformulate its Action Plan into an Action Agenda. The government launched a \$ 230 million Scaling-up Renewable Energy program (SREP) investment plan in 2015 [13]. The SREP was established to scale up the deployment of renewable energy solutions and expand renewables markets in the world's poorest countries [20]. The National Rooftop Solar Programme, a Capital Subsidy Scheme, was introduced in 2016 by the Energy commission of Ghana targeting residential, public, commercial and industrial sectors [21]. The objective of the programme was to install 200,000 solar PV systems on rooftops in the country to reduce peak load (lighting load) up to 200 MW in the medium term.

Nevertheless, there are still policies-oriented bottlenecks hampering the smooth take off of RE technologies in Ghana, key of which are unreliable off-taker, macroeconomic instabilities, regulatory uncertainty, pressures to keep prices low, insufficient but costly domestic financing [22] and inadequate information about RE technologies. Thus, suitable policies are essential to promote RE technology in Ghana. There is a need to introduce more RE into the energy portfolio of Ghana to reduce

Table 1

Current electricity tariffs for residential consumers in Ghana for the first and second quarters of 2021 [15].

Consumption (kWh/month)	Cost of electricity		Service charge	
	GHP/kWh	US cent/kWh*	GHP/month	US Cent/month*
0–50	32.61	5.66	213.00	36.98
51–300	65.42	11.35	745.69	129.46
301–600	84.90	14.74	745.69	129.46
601 and above	94.33	16.37	745.69	129.46
Average	69.32	12.03	612.51	106.33

* Exchange rate (2.7.2021): \$1 = GHe5.76 [18].

over-reliance on fossil fuel sources of energy [16]. Policy support may call for the introduction of tax incentives and regulations to promote and attract investment in renewable energy projects. For instance, tax holidays could serve as incentive for RE companies. The government could give incentives to the financial institutions to grant soft loans to both individuals or institutions to pre-finance RE setups. Also, the government could enter into a Public-Private Partnership agreements.

The PVT technology and experimental setup

Solar energy is collected as heat and electrical energy using thermal collectors and photovoltaics (PV), respectively. In the case of PVs, only a small fraction of the incidence irradiation is converted into electrical energy with the bigger portion dissipated as destructive heat energy leading to an increase in module's temperature and hence, reduction in its efficiency. A common way to improve the electrical efficiency of PVs is through cooling of the modules [8]. A hybrid photovoltaic-thermal (PVT) basically combines the functions of a solar thermal collector and those of PV in one unit and thus makes it possible for the excess heat to be extracted [23]. The PV cells generate electricity while the integrated thermal absorber collects useful heat energy from the cells, reducing the cells temperature and thus enhance their efficiency. The heat extraction is commonly done by circulating either water or air by artificial or natural means. Air circulation is relatively both simpler and cost effective, but it is less effective at low latitudes where the ambient air temperature is mostly over 20 °C in the year. Water heat extraction is more expensive than air heat extraction, but more effective even for regions with higher ambient temperatures [24].

The PVT generates more energy (thermal and electrical) per surface area than separate PV modules and thermal collectors installed side-by-side, therefore allowing smaller total area when requiring both outputs [23]. Furthermore, the advantage of the PVT system in generating electricity and useful heat energy simultaneously are suitable in many applications for residential [25], commercial (such as hotels and restaurants), and industrial uses (such as processing industries).

The setup for this study consists of a conventional solar PV and hybrid PVT installations. For purpose of comparison, the PV component of both modules are made of mono-crystalline Silicon (mc-Si) PV technology. Table 2 shows some selected technical specifications of the PV and PVT modules. The setup has been installed on the roof of solar energy applications laboratory at the Department of Mechanical Engineering (6.68° N, 1.57° W), Kwame Nkrumah University of Science and Technology (KNUST), Kumasi, Ghana. Fig. 1 shows a picture of the setup.

The setup also includes balance-of-system (BOS) components like water storage tank, circulation pump, copper pipes, battery chargers, and sealed lead acid AGM deep cycle battery. For the purpose of the study, an inverter is sized for the setup to complete its balance-of-system for a residential application. Cost of modules and peripherals were based on prices on the Ghanaian market.

Table 2

Main components in the basic setup.*

Parameter	Capacity	Remarks
Nominal electric power (PV)	270 W	Installed
Nominal electric power (PVT)	200 W	Installed
Nominal thermal power (PVT)	600 W	Installed
Water storage tank	100 L	Installed
Battery (each for PV & PVT)	12 V, 100 Ah	Installed
Battery charger	20 A	Installed
Mounting Rack	–	Installed
Water circulation pump	10 W	Installed
Water storage tank	100 L	Installed
Control station	Single unit	Assumed for study
Inverter/battery charger	Single unit	Assumed for study

* Source: Most data are from Ref. [26].



Fig. 1. PV (a) and PVT (b) installation on the rooftop of Solar Energy Applications Laboratory at Department of Mechanical Engineering, KNUST Ghana [26].

Techno-economic analysis

Techno-economic analysis (TEA) provides a structure for dealing with factors that lead to variability in cost estimates, such as equipment size, number of consumables and alternative feedstock. For alternative power generation technologies, TEA can be used to compare key measures of process feasibility among technology alternatives, including indicators of plant performance, cost and emissions. Furthermore, TEA results provide insights for making design choices and choosing the values of design variables [27]. The key input variables for TEA are categorized into technical, financial (economical), and geographical ones [28].

Energy and exergy generation model

Technical analysis provides the mass energy balance of a system and estimates plant performance, including power generation, efficiency and raw materials consumption [27]. Energy is a conserved quantity based on the first law of thermodynamics. On the contrary, exergy is not conserved and is based on the second law of thermodynamics. It is defined as the maximum amount of work which can be produced by a system or a flow of matter or energy when it is brought to a thermodynamic equilibrium state from a reference environment [29]. Use of exergy allows qualitative assessment by comparing electrical and thermal energy in PVT system based on the same standard.

For the energy generation model, only the impact from solar radiation, module degradation, subcomponents efficiencies and some selected effects of BOS components on the resultant exergy over the operating time are considered. The energy generated from a PVT module in year t is expressed by the following equations [28,30]:

$$E_{pvt,t} = E_{dc,t} + E_{th,t}, \quad (1)$$

$$E_{dc,t} = (D_t \times G_t \times \eta_{dc} \times A_{dc})(1 - dg)^{t-1}, \quad (2)$$

$$E_{th,t} = (D_t \times G_t \times \eta_{th} \times A_{th})(1 - dg)^{t-1}, \quad (3)$$

where t is the index of time in number of year, $E_{pvt,t}$ is the net energy from the PVT module (kWh/year) in year t , $E_{dc,t}$ is the direct current (DC) electrical energy (kWh/year) after the DC wiring losses, $E_{th,t}$ is the annual thermal energy (kWh/year), D_t is the number of days in year t , A_{dc} is the effective module surface area (m^2) for the PVT, A_{th} is the thermal absorber surface area (m^2), G_t is the yearly average daily solar energy in the year t (kWh/ m^2 /day), η_{dc} is the module electrical efficiency (%), η_{th} is the module thermal efficiency (%), and dg is module degradation (%/year) and is assumed to be the same for both systems.

From Fig. 2, it could be seen that not all the energy produced by a module, $E_{pvt,t}$, gets to the load. System losses are due to efficiency factors of the PV/PVT modules, the inverters, pumps, resistive losses in conductors and thermal losses in fluid system. BOS components like inverters, battery chargers and monitoring devices, may also use part of the energy to operate. Thus, for a PVT system, the resultant annual electrical energy available to the load ($E_{ac,t}$) could be expressed as:

$$E_{ac,t} = \eta_{cv,t} \times \beta_t \times E_{dc,t} + \eta_{inv,t}(1 - \beta_t)E_{dc,t} - E_{pmp,t}, \quad (4)$$

$$\eta_{cv,t} = \eta_{bat,t} \times \eta_{inv}, \quad (5)$$

$$\eta_{bat,t} = \eta_{bat,0} \times (1 - d_{bat})^{t-1}, \quad (6)$$

$$\eta_{inv,t} = \eta_{inv,0} \times (1 - d_{inv})^{t-1}, \quad (7)$$

$$E_{pmp,t} = E_{pmp,0} \times (1 + \rho)^{t-1} \quad (8)$$

where $\eta_{cv,t}$ is the energy conversion efficiency in year t , $\eta_{bat,t}$ and $\eta_{inv,t}$ are the respective efficiencies (%) for battery and inverter charging systems in year t , $\eta_{bat,0}$ and $\eta_{inv,0}$ are the initial efficiencies (%) for battery and inverter subsystems respectively, d_{bat} and d_{inv} are the annual derating factors of battery round-trip efficiency and inverter-charging system efficiency, β_t is the % of battery involvement in energy conversion, $E_{pmp,t}$ is the power consumption by pump in year t , $E_{pmp,0}$ is the initial power consumption at installation assumed to be same for $t = 1$ and ρ is the annual percentage increase in pump power consumption (%) due to tear and wear.

Eq. (4) presents three $E_{dc,t}$ ($E_{dc1,t}$ for PV) conversion to $E_{ac,t}$ ($E_{ac1,t}$ for PV) scenarios depicted as simplified block diagram in Fig. 3. The first scenario $E_{dc,t}$ is exclusively stored in battery bank ($\beta_t = 1$) before a later conversion into $E_{ac,t}$. In the second scenario, a proportion of $E_{dc,t}$ is converted directly $E_{ac,t}$ and the remaining stored in batteries ($0 < \beta_t < 1$) for later conversion. The final scenario is that $E_{dc,t}$ is converted directly into $E_{ac,t}$ without recourse to battery storage ($\beta_t = 0$).

The battery capacity, C_{bat} , is given as [31]

$$C_{bat} = \frac{E_{dc,t} \times D_{aut} \times DM}{D_t \times DOD}, \quad (9)$$

where D_{aut} is the days of autonomy, DM is battery design margin and DOD is the maximum depth of discharge (%). For this study, the battery is only used as storage for the DC power if production exceeds consumption. Thus, the days of autonomy is set to 1 in this analysis. The inverter capacity is also given as [31]

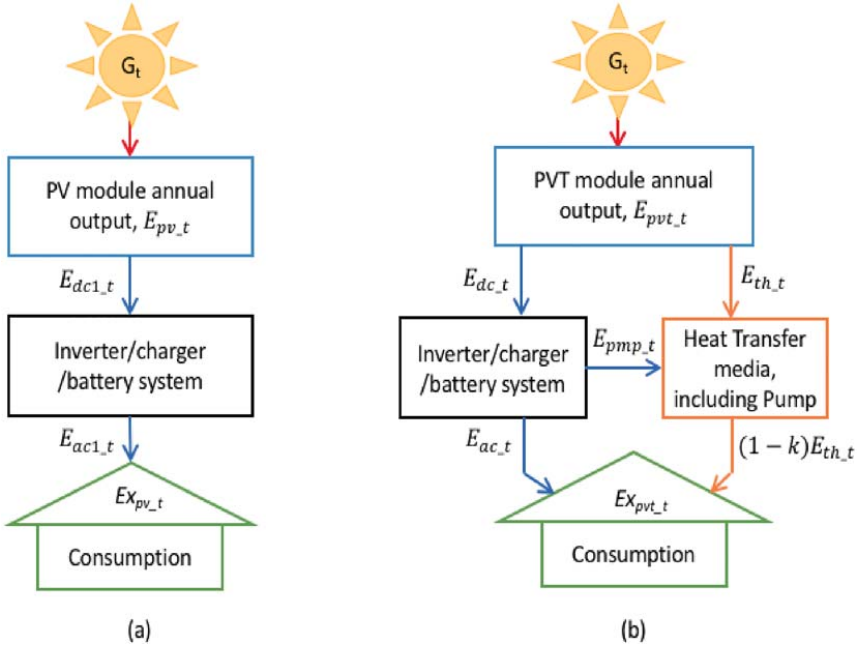


Fig. 2. The energy transfer schematics in this work showing (a) PV configuration and (b) PVT configuration; where $E_{dc,t}$ is the annual electrical energy from PV, $E_{ac,t}$ and $E_{pmp,t}$ are the annual net electrical energies to load, $E_{pmp,t}$ is the annual energy consumed by pump, k is the heat energy transfer losses factor (%) and $Ex_{pv,t}$ and $Ex_{pvt,t}$ are the net exergies to load from PV and PVT systems respectively, all in year t . (Schematic diagram drawn by the authors).

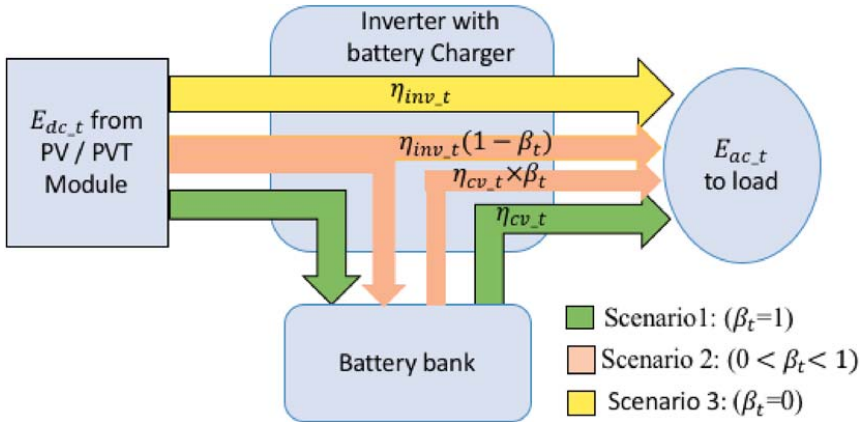


Fig. 3. A simplified block diagram of the three electrical energy conversion scenarios from direct current (DC) to alternating current (AC) presented in this work (See Eq. (3)).

$$C_{inv} = \frac{P_{pv-rated}}{1.25} \tag{10}$$

where $P_{pv-rated}$ is the module rated electrical capacity at STC in kW and 1.25 is the sizing ratio for installations with tilt angle less than 15.

From Fig. 2, the net annual electrical and thermal energies reaching the load can be expressed in exergetic terms in kWh/year as [32,33]:

$$Ex_{pv,t} = E_{ac,t} \tag{11}$$

$$Ex_{th,t} = E_{th,t} (1 - k) \left(1 - \frac{293}{293 + (T_o - T_a)} \right) \tag{12}$$

where k is the percentage transfer losses of heat energy through balance-of-system components, T_o and T_a are the yearly average daily ambient and water outlet temperatures in Kelvin, respectively and $Ex_{th,t}$ is the thermal exergy in kWh/year in year t . Thus, the net annual exergy from the PVT ($Ex_{pvt,t}$) system in year t can be expressed in kWh/year as

$$Ex_{pv,t} = E_{ac,t} + Ex_{th,t}, \tag{13}$$

$$Ex_{pv,t} = \eta_{cv,t} \times E_{dc,t} - E_{pmp,t} + E_{th}(1-k) \left(1 - \frac{293}{293 + (T_2 - T_a)} \right), \tag{14}$$

$$Ex_{pv,t} = (D_t \times G_t)(1-dg)^{t-1} \times \left[A_{dc} \times \eta_{dc} \times \eta_{bat,0}(1-d_{bat})^{t-1} \times \eta_{inv,0}(1-d_{inv})^{t-1} + A_{th} \times \eta_{th}(1-k) \left(1 - \frac{293}{293 + (T_o - T_a)} \right) \right] - E_{pmp,t} \times (1+\rho)^{t-1}, \tag{15}$$

while that from the PV system ($A_{th} = 0, E_{pmp,t} = 0$) in year t can be expressed in kWh/year as

$$Ex_{pv,t} = \eta_{cv,t} \times E_{dc,t}, \tag{16}$$

$$Ex_{pv,t} = \eta_{bat,0}(1-d_{bat})^{t-1} \times \eta_{inv,0}(1-d_{inv})^{t-1} \times (D_t \times G_t \times \eta_{dc1} \times A_{pv})(1-dg)^{t-1}, \tag{17}$$

where η_{dc1} is the efficiency of the PV module, $E_{dc1,t}$ is the annual net energy to load and A_{pv} is the effective PV module surface area.

A fundamental property of the analytical modules is the losses incurred in energy transition through the setup. Efficiency of energy systems are generally expressed as output over input energy. Thus, the overall electrical efficiency over a period t ($\eta_{el,t}$) can be expressed as:

$$\eta_{el,t} = \frac{E_{ac,t}}{A_{dc} \times G_t}, \tag{18}$$

Correspondingly, the thermal efficiency ($\eta_{th,t}$) could also be expressed as:

$$\eta_{th,t} = \frac{E_{th,t}}{A_{th} \times G_t}, \tag{19}$$

Eqs. (18) and (19) could be used to estimate the overall energy of the systems over the period of study. In the case of the PVT, the overall energy efficiency could be expressed as [34]:

$$\eta_{pvt,t} = \eta_{el,t} + \eta_{th,t}. \tag{20}$$

Economic performance indicators

The economic assessment is made up of costs and benefits of the system. There are many economic performance indicators used by investment professionals, such as leveled cost of energy (LCOE), net present value (NPV) and simple discounted payback period (PP) [28]. The LCOE is a regularly used metric for evaluating the financial and economic viability of energy technologies [13,41]. In the case of this study, LCOE is evaluated using NPV techniques. LCOE is the price at which energy must be generated from a specific source to break even over the lifetime of the project. In calculating LCOE, all cost factors such as financing, operation costs, maintenance cost, taxes, support, must be considered. The generalized expression for the LCOE over the life span of an energy system is given as [28,30]:

$$LCOE = \frac{Net\ Present\ value\ of\ cash\ flow}{Present\ value\ of\ energy}, \tag{21}$$

In exergetic terms, the leveled cost of exergy (LCOEx) is defined as

$$LCOEx = \frac{\sum_{t=0}^{n-1} PV_{CF}}{\sum_{t=0}^{n-1} PV_{Ex}}, \tag{22}$$

$$PV_{CF} = \frac{C_t}{(1+r)^t}, \tag{23}$$

$$PV_{Ex} = \frac{Ex_{pv,t}}{(1+r)^t}, \tag{24}$$

where PV_{CF} is the present value of the cash flow, PV_{Ex} is the present value of the exergy, n is the economic life of the system, r is the discount rate and C_t is the total cost in USD (\$) to the setup in year t . C_t could further be expressed as [30]

$$C_t = I_t + L_t + M_t + Tx_t - Sp_t, \tag{25}$$

where I_t is the total investment expenditure, L_t is the financial loan cost, M_t is total operation and maintenance cost, Tx_t is the total tax paid and Sp_t is the total support and incentives, all in the year t . For a self-financed project ($L_t = 0$) and Tx_t assumed to be negligible for such a small setup, Eq. (25) becomes

$$C_t = I_t + M_t - Sp_t, \tag{26}$$

Also, the cost of battery bank and inverter are expressed as

$$I_{bat,t} = C_{bat} \times U_{bat,t} \tag{27}$$

$$I_{inv,t} = C_{inv} \times U_{inv,t} \tag{28}$$

where $I_{bat,t}$ and $I_{inv,t}$ are the installed cost (\$) of battery and inverter respectively, and $U_{bat,t}$ and $U_{inv,t}$ are the respective unit cost of battery and inverter in \$/kWh.

PVT and PV energy output models

The analytical models for the PVT and PV performance are implemented in TRNSYS simulation software [42] and Microsoft excel, based on site measured data (meteorological and setup performance) in 0.25 h time steps and setup parameters. In the case of the PVT, component Type50b of TRNSYS is defined using setup parameters, measured weather data, collector inlet temperature, and mass flow rate as inputs. The simulated electrical and thermal gains from Type50b then served as inputs to the Equations feature in TRNSYS. For the system's electrical energy gain, the corresponding simulated final DC output ($E_{dc,t,sim}$) is defined in the Equation feature as $f(E_{dc,50b}, \eta_{dc,50b}, \eta_{dc,t})$ in the relation

$$E_{dc,t,sim} = \frac{\eta_{dc,t}}{\eta_{dc,50b}} \times E_{dc,50b,t}, \tag{29}$$

where $E_{dc,50b,t}$ and $\eta_{dc,50b,t}$ are respectively the electrical energy output and corresponding conversion efficiency from Type50b and $\eta_{dc,t}$ is measured electric efficiency of the experimental PVT module, all for the period t . For the annual simulations, $\eta_{dc,t}$ is based on yearly measured data (i.e $\eta_{dc} = \eta_{dc,t}$).

The $E_{dc,t,sim}$ is validated by comparing the experimental with simulated data. The model's accuracy is assessed by means of the relative mean error of the electrical power gains (ΔE_{dc}) for a period of t , which is defined as

$$\Delta E_{dc} = \frac{E_{dc,t,sim} - E_{dc,t}}{E_{dc,t}} = \frac{\int (E_{dc,t,sim} - E_{dc,t})dt}{\int E_{dc,t}dt}, \tag{30}$$

The simulated thermal gains ($E_{th,t,sim}$) and relative mean error (ΔE_{th}) are defined correspondingly. However, the simulated DC energy output from the PV module is modeled in the same order using Type94a as module.

As could be seen, Fig. 4 shows a comparison between simulated and experimented data for a clearer sky and a fluctuating sky conditions for the PVT module. Whereas the simulation model slightly underestimates the electrical yield with a mean error of -1.2% for the fluctuating weather condition, it over estimates it by 0.9% for the relatively clearer weather condition. The model however over estimates the thermal gains by 2.5% and 1.67% respectively for the fluctuating and clear weather conditions. However, in the case of annual cumulative mean errors, the model over estimated both thermal and electrical yields by 4.3% and 3.5% respectively.

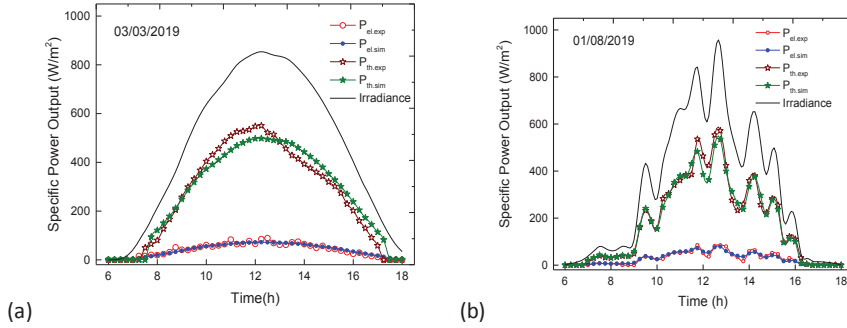


Fig. 4. Comparison of experimental and simulated PVT module's output data on (a) a clearer-sky weather and (b) a fluctuating weather.

Assumptions

This study is based on installations of mc-Si PV subsystem and water-based flat plate mc-Si hybrid PVT subsystem in Kumasi-Ghana (6.68° N 1.57° W) [26]. A year-long data in 2019 from the installations forms the basis for the research. Some assumptions made are as follows:

- The solar modules would last the entire 25-year period of study without breaking down. The end-of-life value of module subsystems and other balance of system components is assumed to be zero and will be disposed at zero cost to the project.
- Although degeneration will affect energy output from the solar modules with advancing years [36], the initial battery and inverter sizing based on DC outputs from the modules in the first year shall be used throughout the study.
- Both PV and PVT modules are assumed to exhibit the same percentage of yearly degradation (dg).
- System losses are mostly as a result of the efficiency factor of sub-components and soiling [43 44]. Unless where it is stated, energy transfer media are assumed lossless.
- The project is self-funded without any loan aspect. Taxes and other accessory costs are absorbed as part of maintenance cost.
- A unit cost of thermal exergy is the same as unit cost of electricity in Ghana [15].

Results and discussion

The analytical expressions in the previous section are applied to the basic installation involving the PV subsystem and PVT subsystem installed in the same location. This section discusses the energy and exergy performance of the setup and the economic implications for residential application. The use of exergy presents a better analysis for comparison of the two technologies, technically and economically.

Technical results

A reference scenario is that the electrical energy generated is exclusively stored in battery bank before use (Fig. 3: scenario 1) with primary inputs shown in Table 3. Whereas the life expectancy of the PV and PVT modules is assumed to be a 25-year period, that of the battery, the pump and the inverter are respectively 5, 8 and 10 years and will need replacement in due course. The measured annual average daily solar irradiation for the site is 4.65 kWh/m².

For the basic configuration, the estimated total electrical energy (or exergy) to load from the PV sub-system for the project period is 5.66 MWh (159.42 kWh/m²/annum), representing 79.95% of output from the module. In the case of the PVT system, the electrical and thermal exergies to load for the period of the study are respectively, 4.08 MWh

Table 3

Primary geographical and technical parameters for the energy and exergy model.

Parameters (technical)	Variable	Value	Reference (s)/ Remark
Life expectancy of PV/PVT modules	<i>n</i>	25 years	[8,2]
Number of Days in year <i>t</i>	<i>D_t</i>	365 days	Assumed
Annual average daily irradiation for <i>t</i> = 1	<i>G₀</i>	4.6 kWh/m ² /day	Measured (2019) [26]
Average daily peak sun hours	<i>S_h</i>	4.6 h	Measured [26 35]
Effective PV module surface area	<i>A_{pv}</i>	1.474 m ²	Technical information
Effective PVT module surface area	<i>A_{dc}</i>	1.326 m ²	Technical information
PVT thermal absorber surface area	<i>A_{th}</i>	1.194 m ²	Technical information
PV module average electric efficiency	<i>η_{dci}</i>	12.14%	Measured (2019) [26]
PVT module average electric efficiency	<i>η_{dc}</i>	10.80%	Measured (2019) [26]
PVT module average thermal efficiency	<i>η_{th}</i>	36.32%	Measured (2019) [26]
PV/PVT modules degradation factor	<i>dg</i>	0.5% per annum	[36,37]
PVT daily average water outlet temperature	<i>T_o</i>	35.71 °C	Measured (2019) [26]
Yearly average daily ambient temperature	<i>T_a</i>	27.13 °C	Measured (2019) [26]
Battery initial round trip efficiency (<i>t</i> = 0)	<i>η_{bat,0}</i>	90%	[14]
Battery life expectancy (<i>η_{bat}</i> < 80%)	<i>L_{bat}</i>	5 years	[38,39]
Battery degradation factor	<i>d_{bat}</i>	2.5% per annum	Computed
Battery depth of discharge (DOD)	DOD	50%	Manufacturer recommendation
Battery total capacity	<i>C_{bat}</i>	Calculated	Eq. (9)
Days of autonomy	<i>D_{aut}</i>	1	Assumed
Battery design margin	<i>DM</i>	1.1	Assumed
Inverter capacity	<i>C_{inv}</i>	Calculated	Eq. (10)
Initial inverter/charger efficiency	<i>η_{inv,0}</i>	97%	[40]
Inverter derating factor	<i>d_{inv}</i>	1%/year	Assumed
Inverter life expectancy	<i>L_{inv}</i>	10 years	[13]
Pump power rating	<i>P_w</i>	10 W	Installed [26]
Pump initial power consumption (<i>t</i> = 1)	<i>E_{pmp,0}</i>	14.8 kWh	Computed
Pump aging factor on power consumption	<i>ρ</i>	1.5%	Assumed
Pump life expectancy	<i>L_{pmp}</i>	8 years	Assumed
Heat energy transfer losses factor	<i>k</i>	10%	Assumed

and 6.81 MWh, making a total exergy of 10.89 MWh (330.15 kWh/m²/annum), representing 82.35% of total exergy from PVT module. Fig. 5 shows that final exergy outputs to load from the sub-systems decreases non-uniformly at average rates of 1% per annum and 0.7% per annum for the PV and PVT systems respectively, largely due to module degradation and balance of system (BOS) components losses. The undulating trend in net annual exergy outputs is influenced by efficiency and degradation changes in BOS components and their subsequent replacements when need be.

For the PV system, battery and inverter losses represent 13.27% and 6.77% respectively of total module output. In the case of the PVT system, BOS components account for 14.3% of losses to net output exergy, of which approximately 32.0% is attributed each to battery and thermal losses. Generally, the round-trip efficiency of the battery degenerates at a rate of 2.5% per annum from 90% in its first year ($t = 1$) of installation to 81% at the end of its life cycle ($t = 5$). In the case of the inverter, its efficiency degenerates from an initial efficiency of 97% at installation to 88.6% by the end of its life cycle.

Following the installed system losses, the overall average efficiency for the 25 year period of the PVT and PV systems are 42.5% ($\eta_{el,t} = 7.4$ and $\eta_{th,t} = 34.69\%$) and 9.6% respectively. Installing systems without batteries improve the average electrical energy efficiencies of both systems by approximately 17%.

Approximately 6.10% of energy is lost to degradation of modules over the period of study. Table 5 shows the effect of module degradation on the overall efficiency performance of the PV and PVT systems. It could be seen that for each percentage increase in module degradation the $\eta_{el,t}$ of the PV and PVT systems decrease respectively by 1.12% and 0.93% whereas the $\eta_{th,t}$ of the PVT decreases by 4.09%.

Economic analysis

The economic evaluation of the PV and PVT subsystems are based on a reference scenario with $\beta_t = 1$ and the default input parameters in Table 4 ($r = 0.05$, O&M = 5% of module cost and $Sp_t = 0$) for the project lifecycle of 25 years. The project is self-financed (see Eq. (26)) with no loan component or support. Fig. 6 shows that the net present value of cashflow, PV_{CF} (see Eq. (23)), per unit area for the PV and PVT systems are respectively \$ 1083/m² and \$ 1665/m². The observed $LCOEx$ for the PVT system (\$ 0.33/kWh), as calculated (see Eq. (22)), is observed to be lower than that of the PV system (\$ 0.45/kWh). However, the $LCOEx$ values are higher than what has been reported by the International Renewable Energy Agency (IRENA) for residential PV installations for 2019 (\$ 0.063–0.265/kWh) [45]. This could largely be attributed to the smaller size of installation [45], the inclusion of battery storage (with DOD = 0.5) and the absence of any support incentive for

Table 4
Economic parameters.

Item/Parameter	Size/Rating	Unit Value or cost (\$)	Unit value Reference
PV	270 W	\$ 254	Market cost
PVT	1.326 m ²	\$ 392.15/m ²	Market cost
Mounting rack	% of module cost	10%	[40]
Inverter Cost, $I_{inv,t}$	Eq. (10)	\$ 300/kW	Market survey
Battery bank Cost, $I_{bat,t}$	Eq. (9)	\$ 160/kWh	Local market price
Water circulation Pump, Control station	10 W	\$ 9/W	Market cost
O&M cost per year, M_t	Single unit	\$ 50	Assumed
	% of module cost	5%	Assumed
Storage tank with heat exchanger	100L	\$ 1.5/Liter	Market survey
Average Electricity tariff for residential users	Average	\$ 0.12/kWh	[15]
Discount rate, r	5%	5%	Assumed
Financial support package, Sp_t	% of module cost	0%	Assumed
Exchange rate (2.7.2021)	\$/GH	5.76	[18]

Table 5
Effect of modules degradation on energy efficiencies of PV and PVT systems.

%dg/annum	PV $\eta_{el,t}$	PVT $\eta_{el,t}$	PVT $\eta_{th,t}$
0.0	10.2	7.90	36.82
0.2	9.96	7.73	35.95
0.4	9.73	7.53	35.10
0.6	9.50	7.33	34.29
0.8	9.28	7.15	33.5
1.0	9.08	6.97	32.73

the scenario.

Fig. 7 details the contribution of components and activities to the present value of life cycle cost (LCC) of the PV/PVT systems. As shown in the Figure, the principal contributors to the PV_{CF} are almost the same for both systems. For the PV system, in descending order of quantum of contribution, they comprise battery (61%), PV module (16%) and O&M (12%), whereas in the case of the PVT system, they are battery (34%), PVT module (24%) and O&M (18%). Although the inverter is a major BOS component in processing the electrical energy to load, its contribution to LCC is only 4% for the PVT system and 8% for the PV system. BOS components (excluding inverter) contribution to cost of the PV and PVT systems are respectively 63% and 54%, which are lower than the

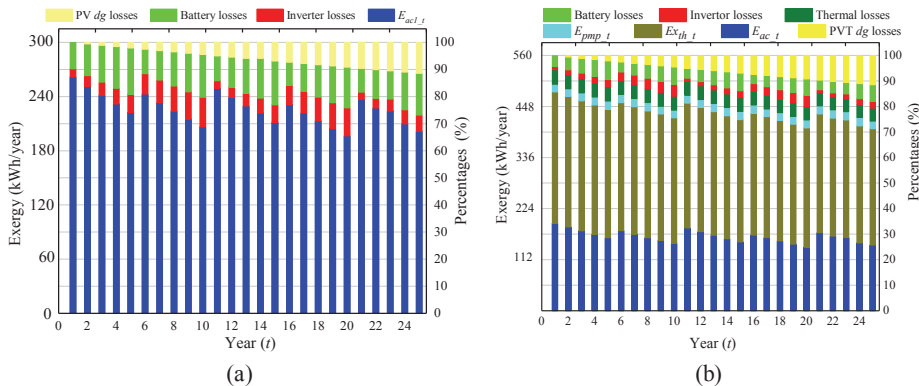


Fig. 5. Final exergy profiles of (a) PV and (b) PVT subsystems.

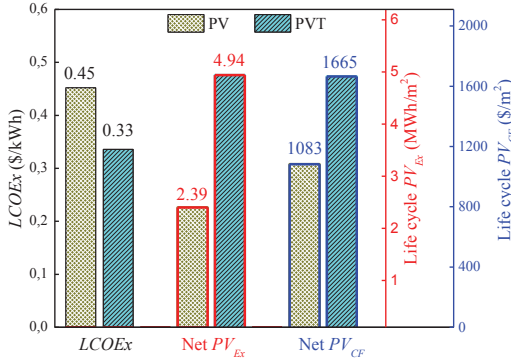


Fig. 6. Life cycle LCOEx, Net PV_{Ex} and Net PV_{CF} for the PV and PVT subsystems.

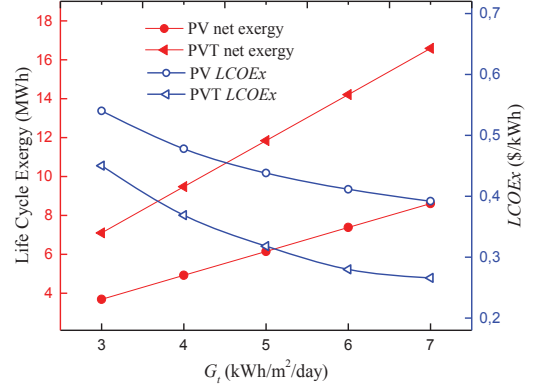


Fig. 8. Sensitivity of G_t to LCOEx and Exergy for PV and PVT systems.

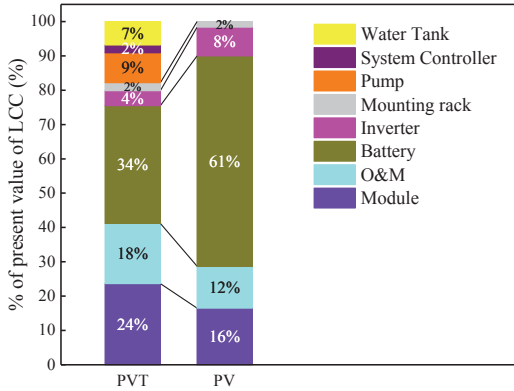


Fig. 7. Percentage contribution of components/activities to net present value of LCC of PV and PVT modules.

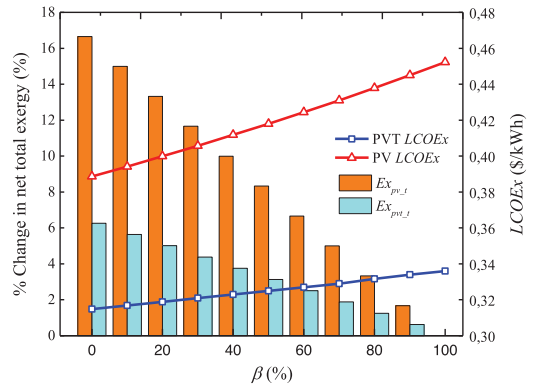


Fig. 9. The effect of percentage of stored DC energy in battery banks on net exergy outputs.

global average of about 64% for 2019 reported by IRENA [45].

Sensitivity analysis

The energy and economic outputs of the solar systems discussed so far could be affected by (i) geographical location of site (ambient conditions like G_t), (ii) technical parameters of system (like module area, efficiencies and β_t) and (ii) economic indicators and policies (like r, M_t and S_p).

Geographical effect: yearly average daily irradiation (G_t).

Ghana has abundant solar energy resources that varies from 3.1 kWh/m² in the country's coastal belt to 6.5 kWh/m² in its northmost regions. The effect of G_t (kWh/m²/day) on the energy systems is assessed and as could be seen from Fig. 8, varying G_t between 3.1 and 6.5 kWh/m²/day leads to a corresponding increase in net life cycle output exergies from 3.69 to 8.61 MWh/m² for the PV and 7.32–15.37 MWh/m² for the PVT. This also improves the LCOEx for the PV system and PVT system from \$ 0.54–0.40/kWh and \$ 0.45–0.27/kWh, respectively.

Technical parameters of system: impact of battery bank on outputs

The impact of percentage of DC energy stored in battery capacity (β_t) is analyzed. The three electrical energy transfer scenarios are summarized in Fig. 3. It could be seen from Eq. (4) and Fig. 9 that β_t has a direct

impact on net electrical energy transferred from the module to load. As β_t is varied from 100 – 0%, with all other parameters held constant, corresponding exergies increase. At β_t = 0% (i.e. batteries installed but storage capacity not involved in energy conversion process), the net electric energy outputs for both PV (E_{ac,t}) and PVT (E_{ac,t}) systems increase by 16.65%. This also translates into increase in the net exergy from the PVT system to load by 6.25%. The LCOEx for PV and PVT improve from \$ 0.38–0.45/kWh and \$ 0.31–0.34/kWh respectively.

Three scenarios of battery involvement (β_t) and cost to project (I_{bat,t}) are presented in Fig. 10(a). As seen in Scenario 1, if no battery bank is installed, it will impact on both cost buildup (I_{bat,t} = 0), and net exergy output (β_t = 0). This results in 15% lower LCOEx from the PV system (\$ 0.17/kWh) than recorded for the PVT system (\$ 0.2/kWh). In the case of Scenario 2 (Fig. 10), batteries are installed at no cost to project (i.e. S_p = 100% ∑ I_{bat,t}) and storage capacity fully utilized (β_t = 1). The LCOEx from the PV (\$ 0.17/kWh) remain better than that of PVT (\$ 0.23/kWh) by 26%. In Scenario 3, batteries are installed at full cost to project (i.e. S_p = 0% ∑ I_{bat,t}) but storage capacity not utilized at all (β_t = 0), as discussed in preceding paragraph. From the 3 scenarios, it could be observed that when the systems are installed without battery cost to the project, the PV becomes more economically viable than the PVT (see Fig. 10(a); Scenarios 1&2). Also, the LCOEx for both systems compare favorably with those reported for 2019 by IRENA (\$ 0.063–0.265/kWh) for residential setups [45]. As shown in Fig. 10(b), in the case of the

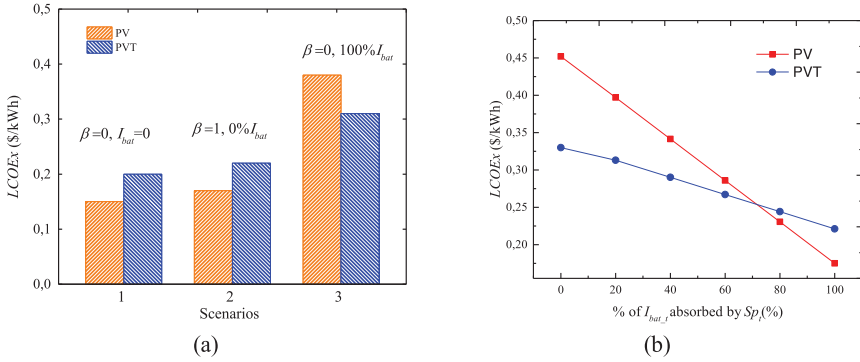


Fig. 10. Shows (a) sensitivity of battery cost (I_{bat}) and percentage of stored electrical energy (β_i) to LCOEx; (b) sensitivity of % of I_{bat} absorbed by support (Sp_i) on LCOEx for the reference scenario.

reference scenario, the PV becomes more economically viable than the PVT as support for battery cost (or reduction in cost) exceeds 67% of battery cost.

Economic indicators and policies: M_t , r and Sp_i

As seen earlier from Fig. 7, O&M cost (M_t) is a major contributor to both systems' life cycle cost. The M_t includes, but not limited to, replacement cost for failed minor peripherals (like breakers, valves and sensors), and quantified cost of routine maintenance (like cleaning of modules). Fig. 11 shows the sensitivity of varying M_t from 0 to 10% (of module cost) on LCOEx, with all other parameters held constant. Whereas the LCOEx for the PV increases from \$ 0.40–0.50/kWh, the corresponding increase in that of the PVT ranges from \$0.27–0.39/kWh.

One economic factor with direct impact on present value is the discount rate (r). Discounting of cash flows and exergies account for their time value over the project duration and associated risk (like inflation). Fig. 12 shows that when r is varied from 0 to 10%, with all other parameters kept constant, the LCOEx for the PV and PVT systems increase from \$ 0.40–0.51/kWh and \$ 0.27–0.40/kWh, respectively.

Financial subsidies and incentives are country or region specific and cannot be generalized. For this study, the assumed subsidy is set as a percentage of module cost. The reference scenario for the setup had no subsidy ($Sp_i = 0$). As expected, an introduction of Sp_i improves the LCOEx for net energy outputs from both systems. Fig. 13 shows the LCOEx for PV and PVT decline from \$ 0.45–0.37/kWh and \$ 0.33–0.26/kWh

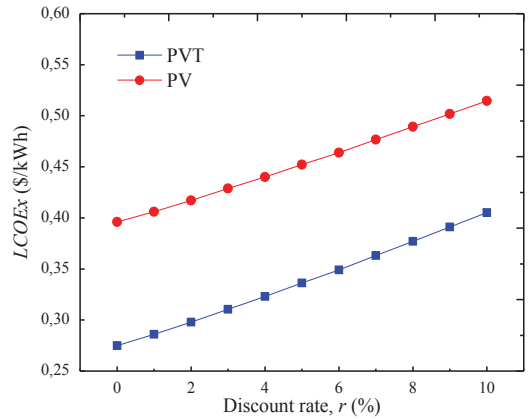


Fig. 12. Impact of discount rate variation on LCOEx.

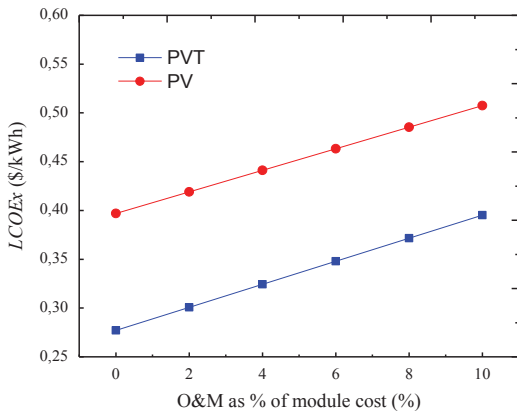


Fig. 11. Impact of O&M variation on LCOEx.

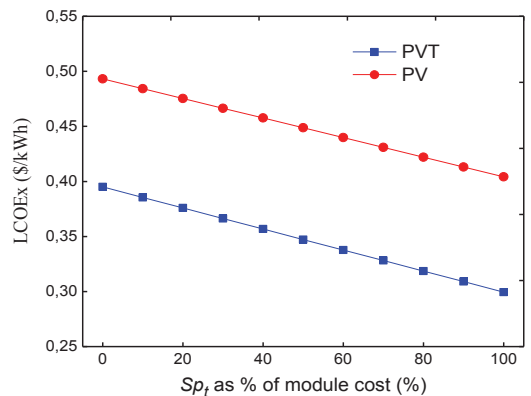


Fig. 13. Sensitivity of subsidy to LCOEx.

kWh, respectively as Sp_t is varied from a scenario of no support (0%) to full support (100%), with all other parameters held constant.

Grid tariff comparison

As shown so far, the $LCOEx$ could be affected by (1) geographically determined ambient conditions (G_t), (2) technical parameters of system (β_t) and (3) economic indicators and policies (r , M_t and Sp_t). However, the $LCOEx$ from the scenarios discussed so far are predominantly higher than buying energy from the grid for residential use in Ghana, which ranges from \$ 0.06/kWh for a life-line user to \$ 0.16/kWh for a high-end user (see Table 1). Thus, the simple payback period (SP) for both PV and PVT modules are not realizable within the 25-year study period.

An extreme scenario is proposed under the National Rooftop Solar Programme intervention in Ghana, where residential applicants are granted capital subsidy in the form of free solar modules ($Sp_t = 100\%$ of module cost). The PVT is assumed to benefit from that subsidy as well. Also, the systems are installed without batteries ($I_{bat} = 0$, $\beta_t = 0$) as discussed in Section "Technical parameters of system: Impact of battery bank on outputs" (Fig. 10(a): scenario 1). Table 6 shows the effect of that on $LCOEx$ in different regions in Ghana. Whereas the PV system achieves grid parity in all regions (\$ 0.13–0.06/kWh), the $LCOEx$ for PVT (\$ 0.20 – 0.09 kWh) compares favorably with grid tariff for regions with daily peak sun hours > 3.65 h. Thus, both systems become more economically favorable as installation site is moved northwards. This also confirms earlier observation (Section "Technical parameters of system: Impact of battery bank on outputs") that the PV performs better than the PVT when both systems are installed without batteries.

Conclusion

In this paper, the technical and economic performance of a PV system and a flat plate water-based PVT system are assessed as alternative energy sources in exergy terms for a 25-year period. The systems are installed in Kumasi, a region in Ghana with yearly average daily peak sun hours of 4.6 h. The following main findings were made from the assessment:

- The estimated average total electrical exergy to load from the PV and PVT sub-system were respectively 159.42 kWh/m²/annum and 330.15 kWh/m²/annum, representing 79.9% and 82.35% of gross module outputs.
- The overall energy efficiencies of the PV and PVT systems are respectively 9.6% and 42.5%. Approximately 6.1% of total energy is lost to degradation of both modules over the period of study.
- It requires about twice the initial cost for the PV-system/m² to setup the PVT-system/m². Battery cost makes 61% and 34% of LCC for PV and PVT systems respectively.
- Varying the average G_t from 3.1 to 6.5 kWh/m²/day improves the $LCOEx$ for the PV and PVT systems from \$ 0.53–0.40/kWh and \$ 0.44–0.27/kWh respectively.
- Varying discount rate, r and $O\&M$ upward respectively increase the $LCOEx$ for the PV and PVT systems by approximately 1 cent/kWh/% and 1.2 cent/kWh/%.
- The cost of exergy produced from the PVT system is generally cheaper than that from the PV system but more expensive than residential tariffs for grid power in Ghana (\$ 0.05–0.16/kWh). However, with support scenarios where modules are freely acquired ($Sp_t = 100\%$) and installed without batteries ($I_{bat} = 0$, $\beta_t = 0$), the PV system achieves grid parity in all regions (\$ 0.06–0.13/kWh), whereas the $LCOEx$ for PVT (\$ 0.06 – 0.20 kWh) compares favorably with tariffs in regions with daily peak sun hours > 3.65 h.

From the assessment, it could be concluded that although the flat plate water-based PVT system is more expensive to setup, it performs better than the conventional PV system when installed with batteries.

Table 6

$LCOEx$ for a scenario where batteries are not installed and module cost fully covered by subsidies.

G_t (kWh/m ² /day)	$LCOEx$ (\$/kWh) ^a	
	PV	PVT
3.10	0.128	0.196
4.6	0.086	0.132
5.00	0.079	0.120
6.00	0.066	0.101
6.50	0.061	0.094

^a $LCOEx$ (G_t , $I_{bat} = 0$, $Sp_t = 100\%$ of module cost).

Also, both systems become more economically viable as installation site is moved to the northernmost regions in the country. The PV system however performs better than the PVT system when installed without batteries in all regions in Ghana. Although the PVT system benefited from cooling, its electrical efficiency was generally lower than that of the conventional PV system. Different assembling techniques and materials could be used to improve the PVT electrical efficiency. Also, cheaper, and more efficient batteries with longer charge/discharge lifecycles could significantly improve both techno and economic performance of stand-alone PV/PVT systems. This observation is, however, based on mc-Si technology and specific commercial manufacturer's design, may not be generalized for all other PV/PVT technologies. Nonetheless, there is the need to investigate different PV/PVT modules and battery technologies in the study environment. The paper could not also cover carbon and cost savings made by installing PVT systems as an alternative energy to conventional sources (grid power, natural gas, and biomass) and the environmental impact of the technology and thus need to be investigated in the future. This information could be useful to stakeholders in Ghana in making informed decisions on energy systems.

CRedit authorship contribution statement

Saeed Abdul-Ganiyu: Conceptualization, Formal analysis, Investigation, Methodology, Writing – original draft. **David A. Quansah:** Supervision, Methodology, Writing – review & editing. **Emmanuel W. Rame:** Supervision, Methodology, Writing – review & editing. **Razak Seidu:** Resources, Supervision, Methodology, Writing – review & editing. **Muyiwa S. Adaramola:** Conceptualization, Resources, Supervision, Methodology, Writing – review & editing.

Declaration of Competing Interest

The authors declare that they have no known competing financial interests or personal relationships that could have appeared to influence the work reported in this paper.

Acknowledgment

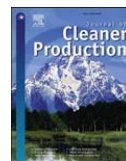
Saeed Abdul-Ganiyu acknowledges the PhD scholarship support through project titled 'Upgrading education and research capacity in Renewable energy technologies at Kwame Nkrumah University of Science and Technology (KNUST) Kumasi Ghana' collaborative project between KNUST and Norwegian University of Life Sciences, Ås Norway, which is funded by Norwegian Agency for Development Cooperation (Norad) through the EnPe programme.

References

- [1] IEA Africa Energy Outlook 2019, World Energy Outlook Special Report, [Online]. Available: <<https://www.iea.org/reports/africa-energy-outlook-2019>>. [accessed 22 April 2020].
- [2] De Boeck L, Van Asch S, De Bruecker P, Audenaert A. Comparison of support policies for residential photovoltaic systems in the major EU markets through investment profitability. *Renewable Energy* 2016;87:42–53.

- [3] IEA. Snapshot of Global PV Markets, PVPS, [Online]. Available: <https://iea-pvps.org/wp-content/uploads/2020/01/PVPS-report_-_A_Snapshot_of_Global_PV_-_1992-2014.pdf>; 2014. [accessed 29 05 2020].
- [4] PV/Battery Waste Management In The Context of Rural Electrification, Support on PV/Battery Waste Management For a Rural Electrification Program. [Online]. Available: <https://www.warefactor.com/docs/PV-Battery_Waste_Management.pdf>; 2016. [accessed 29 05 2020].
- [5] Ministry of Energy, [Online]. Available: <<https://www.energymin.gov.gh/sector-overview>>. [accessed 14 July 2020].
- [6] Volta River Authority, Power Generation: Facts & Figures, [Online]. Available: <<https://www.vra.com/resources/facts.php>>. [accessed 29 05 2020].
- [7] Tselepis S, Tripanagnostopoulos Y. Economic analysis of hybrid photovoltaic/thermal solar systems and comparison with standard PV modules. Proceedings of the International Conference On PV in Europe. 2001.
- [8] Herrando M, Markides CN. Hybrid PV and solar-thermal systems for domestic heat and power provision in the UK: techno-economic considerations. Appl Energy 2016;161:512–32.
- [9] Kalogirou S, Tripanagnostopoulos Y. Industrial application of PV/T solar energy systems. Appl Therm Eng 2007;27:1259–70.
- [10] Kalogirou SA. Use of TRNSYS for modelling and simulation of a hybrid pv–thermal solar system for Cyprus. Renewable Energy 2001;23(2):247–60.
- [11] Fuentes M, Vivar M, de la Casa J, Aguilera J. An experimental comparison between commercial hybrid PV-T and simple PV systems intended for BIPV. Renewable Sustainable Energy Rev 2018;93:110–20.
- [12] SHC TASK 60. Task 60. [Online]. Available: <<https://task60.iea-shc.org/highlights>>; February 2019. [accessed 20 September 2020].
- [13] Quansah DA, Adaramola MS, Edwin IA, Anto EK. An assessment of grid-charged inverter-battery systems for domestic applications in Ghana. J Solar Energy 2016;2016:1–11.
- [14] Denkyira S. Techno-Economic Analysis of Stand Alone PV Systems for Remote Base Stations in Ghana. (A Case Study of Abofrem Vodafone Cell Site). [Online]. Available: <<http://ir.knust.edu.gh/xmlui/bitstream/handle/123456789/7524/SAMUEL%20DENKYIRA.pdf?sequence=1>>; June 2015. [accessed 10 June 2020].
- [15] PURC. [Online]. Available: <<https://www.purc.com.gh/attachment/642643-20210225110236.pdf>>; 16 December 2021. [accessed 2 July 2021].
- [16] Appiah MO. Investigating the multivariate Granger causality between energy consumption, economic growth and CO2 emissions in Ghana. Energy Policy 2018; 112:198–208.
- [17] da Silva PP, Cerqueira PA, Ogbe W. Determinants of renewable energy growth in Sub-Saharan Africa: evidence from panel ARDL. Energy 2018;156:45–54.
- [18] BOG. [Online]. Available: <<https://www.bog.gov.gh/treasury-and-the-market/s/daily-interbank-fx-rates/>>; 2021 [accessed 2 July 2021].
- [19] Ghana Sustainable Energy For All Action Plan. [Online]. Available: <<http://www.energycom.gov.gh/renewables/se4all>>; June 2012. [accessed 10 June 2020].
- [20] Scaling up Renewable Energy Program (SREP). [Online]. Available: <<https://www.worldbank.org/en/country/armenia/brief/srep>>; 16 September 2014. [accessed 10 June 2020].
- [21] Appiah KF. The National Rooftop Solar Programme. [Online]. Available: <<http://energycom.gov.gh/files/ROOFTOP%20SOLAR%20PROG-Presentation%20%202nd%20Ghana%20Renewable%20Energy%20Fair1.pdf>>; 9 August 2016. [accessed 10 June 2020].
- [22] Pueyo A. What constrains renewable energy investment in Sub-Saharan Africa? A comparison of Kenya and Ghana. World Dev 2018;109:85–100.
- [23] Zondag HA, de Vries DW, van Helden WGJ, van Zolingen RJC, van Steenhoven AA. The yield of different combined PV–thermal collector designs. Sol Energy 2003;74(3):253–69.
- [24] Tripanagnostopoulos Y, Souliotis M, Battisti R, Corrado A. Energy, cost and LCA results of PV and hybrid PV/T solar systems. Prog Photovoltaics Res Appl 2005;13(3):235–50.
- [25] Zondag HA. Flat-plate PV-thermal collectors and systems: a review. Renewable Sustainable Energy Rev 2008;12(4):891–959.
- [26] Abdul-Ganiyu S, Quansah DA, Ramde EW, Seidu R, Adaramola MS. Investigation of solar photovoltaic-thermal (PVT) and solar photovoltaic (PV) performance: a case study in Ghana. Energies 2020;13(11):2701. <https://doi.org/10.3390/en13112701>.
- [27] Frey H, Zhu Y. Combined cycle systems for near-zero emission power generation. In: Woodhead Publishing Series in Energy; 2012. p. 306–28.
- [28] Gu Y, Zhang X, Are Myhren J, Han M, Chen X, Yuan Y. Techno-economic analysis of a solar photovoltaic/thermal (PV/T) concentrator for building application in Sweden using Monte Carlo method. Energy Convers Manage 2018;165:8–24.
- [29] Wu S-Y, Guo F-H, Xiao L. A review on the methodology for calculating heat and exergy losses of a conventional solar PV/T system. Int J Green Energy 2015;12(4): 379–97.
- [30] Riggs CB, Biedenharn R, Dougher C, Ji VY, Xu Q, Romanin V, et al. Techno-economic analysis of hybrid PV/T systems for process heat using electricity to subsidize the cost of heat. Appl Energy 2017;208:1370–8.
- [31] McEvoy A, Markvart LC. Practical Handbook of Photovoltaics: Fundamentals and Applications. Practical Handbook of Photovoltaics: Fundamentals and Applications. New York, NY: Elsevier; 2011.
- [32] Bosanac M, Sørensen B, Katic I, Sørensen H, Nielsen B, Badran J. Photovoltaic/Thermal Solar Collectors and Their Potential in Denmark. [Online]. Available: <<https://www.yumpu.com/en/document/read/4467325/photovoltaic-thermal-solar-collectors-and-their-potential-in-denmark>>; 21 May 2003. [accessed 8 June 2020].
- [33] Chow TT. A review on photovoltaic/thermal hybrid solar technology. Appl Energy 2010;87(2):365–79.
- [34] Radziemska E. performance analysis of a photovoltaic-thermal integrated system. Int J Photoenergy 2009;2009:1–6.
- [35] Aboagy B, Gyamfi S, Ofosu E, Djordjevic S. Status of renewable energy resources for electricity supply in Ghana. Sci Afr 2021;11.
- [36] Quansah DA, Adaramola MS, Takyi G. Degradation and longevity of solar photovoltaic modules—an analysis of recent field studies in Ghana. Energy Sci Eng 2020:1–13.
- [37] Mundada AS, Shah KK, Pearce JM. Levelized cost of electricity for solar photovoltaic, battery and cogen hybrid systems. Renewable Sustainable Energy Rev 2016;57:692–703.
- [38] Luo X, Wang J, Dooner M, Clarke J. Overview of current development in electrical energy storage technologies and the application potential in power system operation. Appl Energy 2015;137:511–36.
- [39] Crossland AF, Anuta OH, Wade NS. A socio-technical approach to increasing the battery lifetime of off-grid photovoltaic systems applied to a case study in Rwanda. Renewable Energy 2015;83:30–40.
- [40] Baumgartner F. Photovoltaic (PV) balance of system components: Basic, performance. In: The Performance of Photovoltaic (PV) Systems Modelling, Measurement and Assessment; 2017. p. 135–81.
- [41] Quansah DA, Adaramola MS. Economic assessment of a-Si and CIS thin film solar PV technologies in Ghana. Sustainable Energy Technol Assess 2016;18:164–74.
- [42] [Online]. Available: <<http://www.trnsys.com>>. [accessed 2 June 2021].
- [43] Pietruszko SM, Gradzki M. Performance of a grid connected small PV system in Poland. Appl Energy 2003;74(1-2):177–84.
- [44] Valdiserri P. Evaluation and control of thermal losses and solar fraction in a hot water solar system. Int J Low-Carbon Tech 2018;13(3):260–5.
- [45] IRENA. Renewable Power Generation Costs in 2019. [Online]. Available: <https://www.irena.org/-/media/Files/IRENA/Agency/Publication/2020/Jun/IRENA_Power_Generation_Costs_2019.pdf>; 2020. [accessed 20 July 2020].

Paper III



Study effect of flow rate on flat-plate water-based photovoltaic-thermal (PVT) system performance by analytical technique

Saeed Abdul-Ganiyu^a, David A. Quansah^{b,c}, Emmanuel W. Ramde^{b,c}, Razak Seidu^d, Muiyiwa S. Adaramola^{a,*}

^a Faculty of Environmental Sciences and Natural Resources Management, Norwegian University of Life Science, Ås, Norway

^b Department of Mechanical Engineering, Kwame Nkrumah University of Science and Technology (KNUST), Kumasi, Ghana

^c The Brew-Hammond Energy Centre, Kwame Nkrumah University of Science and Technology (KNUST), Kumasi, Ghana

^d Department of Ocean Operations and Civil Engineering, Norwegian University of Science and Technology, Ålesund, Norway

ARTICLE INFO

Handling Editor: Jiri Jaromir Klemes

Keywords:

Photovoltaic thermal system (PVT)

Tropical climatic condition

Exergy efficiency

Flow rate

Cooling effect

ABSTRACT

This paper assesses the effects of mass flow rate on the performance of a commercial Photovoltaic thermal (PVT) system in the dynamic tropical environment of Ghana. A water-based flat plate PVT and a conventional photovoltaic (PV) were installed side-by-side on a roof top in Kumasi, Ghana. The electrical, thermal and exergy performances of the PVT were studied for mass flow rates from 0.025 kg/s and 0.083 kg/s. For a specific solar irradiance, no significant change on module temperature occurs when flow rate is increased above 0.082 kg/s. The PVT exhibited a steady exergy efficiency of approximately 12.75% at manufacture's recommended mass flow rate of 0.033 kg/s irrespective of the irradiance. This was however lower than the exergy efficiency of the PV (13.0–12.75% for irradiance of 710–790 W/m²) for irradiances below 790 W/m² and vice versa. Also, although the PVT's energy-saving efficiency is generally above 50%, its thermal efficiency of 38.8–43.1% was below average compared to experimental (non-commercial) PVT systems. This could be attributed to poor thermal contact between the PV layer and the thermal absorber in the studied PVT module. In addition, from our experimental data, an expression between PVT module temperature and water-flow rate was derived and presented.

1. Introduction

Solar energy can be collected separately as thermal energy and as electrical energy using thermal collectors and photovoltaic (PV) modules, respectively. The combination of PV module and thermal collector into single module is referred to as solar photovoltaic thermal (PVT) collector. The PVT technologies make it possible to collect both useful thermal and electrical energy simultaneously using single module. The PVTs are designed as either flat plate or concentrating collectors and are classified according to the type of the working fluid (Reddy et al., 2015), with the most popular working fluids being water and air (Radziemiska, 2009). Water-based flat plate PVT collectors achieve higher overall efficiency than air-based systems, due to the relatively higher heat capacity of water (Reddy et al., 2015). Furthermore, the electrical energy efficiency is theoretically improved by the cooling effect of the PV cells in the PVT collector (Evans, 1981).

A number of PVT collectors are available as commercial products largely categorized as air and water collectors. However, the commercialization of PVT technology has generally not been successful (Fuentes et al., 2018) as the separate conventional PV and solar heaters. Nonetheless, the global market for commercial PVT collectors recorded an average growth of 9% in 2018 and 2019, with solar air system technologies having the largest PVT market share (TASK 60, 2020). In 2019 alone, a total of 606 MW and 208 MW of thermal energy and electrical energy respectively of commercial PVTs were installed globally (TASK 60, 2020). However, Sub-Saharan Africa recorded less than 1% (8767 m²) of the total installations for the period.

The PVT technologies have been studied since 1970s, including variation in designs, working fluids and other performance-influencing factors (Chow, 2010). The performance of PVT systems can be depicted by the combination of efficiency expression consisting of electrical and thermal efficiencies. For energy systems, improved efficiency means

* Corresponding author.

E-mail addresses: abdul-ganiyu.saeed@nmbu.no (S. Abdul-Ganiyu), daqansah.coe@knust.edu.gh (D.A. Quansah), eramde@gmail.com (E.W. Ramde), rased@ntnu.no (R. Seidu), muiyiwa.adaramola@nmbu.no (M.S. Adaramola).

<https://doi.org/10.1016/j.jclepro.2021.128985>

Received 17 December 2020; Received in revised form 3 September 2021; Accepted 8 September 2021

Available online 11 September 2021

0959-6526/© 2021 The Authors. Published by Elsevier Ltd. This is an open access article under the CC BY license (<http://creativecommons.org/licenses/by/4.0/>).

better energy conversion rate (Tiwari et al., 2009). However, from the principle of energy conservation, it is impossible to simultaneously obtain maximum electric and thermal efficiencies for a PVT system. Nonetheless, to generally improve the overall efficiency of the PVT module, the most important parameters are the flow rate and the fluid inlet temperature, since the cell temperature depends strongly on them (Radziemska, 2009), as well as ambient temperature.

For water-based PVT, increase in water flow rate increases heat transfer coefficient, and Charalambous et al. (2011) have shown that the PVT efficiency is a function of the flow rate. However, there are varying suggestions in literature about the optimum flow rate with the most commonly reported ranging from 0.001 to 0.008 kg/s m² (Tiwari et al., 2009) (Morita et al., 2000) (Kalogirou, 2001) (Chow, 2003) (Nual-boonrueng et al., 2012). Whereas, higher flow rates, such as 0.015 kg/s m² (Garg and Agarwal, 1995), have also been considered; even higher values between 0.025 and 0.04 kg/s m² have been recommended for building integrated PVT systems, given the module's potential to reach relatively high temperatures due to poor heat dissipation (Ji et al., 2006). Cells of PV modules (either in PV or PVT) in geographical locations with higher ambient temperatures, such as tropical regions, are expected to reach higher cell temperatures and would need innovative ways to further reduce their temperature.

Fuentes et al. (Fuentes et al., 2018) studied the performance of a commercial water-based PVT in climate conditions of Jaén in Spain. Although the study was based on real outdoor performance, the modules were intended for building integrated systems and also in a temperate weather condition, with direct effect on modules temperature. However, they showed that at mass flow rates of 0.1 kg/s (0.063 kg/s m²), the PVT system did not benefit from the active cooling in terms of performance in comparison with a conventional PV. They observed that the lower electrical output from the PVT system, in some cases, suggested higher module temperatures than the PV system. However, they reported that both thermal and exergy efficiencies were higher in their study when compared with other studies. Fudholi et al. (2014) also investigated the electrical and thermal performances of photovoltaic thermal (PVT) water collectors with alternative thermal absorbers under controlled conditions of solar irradiance levels of 500–800 W/m² at mass flow rates ranging from 0.011 kg/s to 0.041 kg/s (0.017–0.063 kg/s m²). Their study was not in a real weather condition. They found out that a spiral flow absorber performed better than web flow and direct flow absorbers at a solar irradiance of 800 W/m² and mass flow rate of 0.041 kg/s.

Two key factors, which are essential to assess PVT system performance and technical characterization are climatic conditions (Aste et al., 2014) (Rajoria et al., 2012) and operating temperature (Lämmle et al., 2017). However, studies about flow rates on PVT performance discussed in earlier section are all focused on regions other than sub-Saharan Africa (SSA). Considering the relatively high ambient temperature in SSA, reported optimum flow rates for other regions may not be applicable in SSA region. In an earlier study (Abdul-Ganiyu et al., 2020), cell temperatures of 70.6 °C and 60.5 °C were respectively recorded for PV module and PVT modules, configured at manufacturer's recommended constant flow rate of 0.033 kg/s, in the same environment. Therefore, varying the flowrate in the current study is expected to affect the performance of the PVT module in the same environment.

Fudholi et al. (2014) investigated higher flow rates configuration for a PVT above commonly reported optimal range in Malaysia. However, the study was focused on a steady-state collector performance under laboratory conditions. Under dynamic weather conditions, where factors such as irradiance and ambient temperature are uncontrolled, the performance of PVT in relation to fluid flow configuration may vary across different spatial locations with temporal variations. For example, Rajoria et al. (2012) have shown that PVT systems performance is directly related to climatic conditions. Therefore, the main objective of this paper is to determine the optimal mass flow rate configurations for a PVT in the dynamic tropical environment of Ghana. According to the IEA (Task 60), there is currently an information gap about the

possibilities and benefits of PVT technology (Task 60.iewa, 2020), indicating that this technology has been scarcely assessed. Hence, this paper contributes to bridging the knowledge gap on PVT technology in different climatic conditions in the world. Also, as of 2018, the electrification rate in sub-Saharan Africa was 45% with frequent electricity disruptions and economic losses (IEA Africa Energy Outlook, 2019). Therefore, adoption of PVT systems could provide good alternative for water heating and improve access to electricity in these locations.

The findings of this study would directly be beneficial to SDG 7, which is affordable and clean energy, and indirectly to other SDGs, such as SDG 3 (good health and well-being), SDG 11 (sustainable cities and communities), and SDG 13 (climate action). In addition, results from this study would be beneficial to stakeholders in the sub-region in decision making with regards to solar energy systems. Residential and hospitality industry could significantly benefit from reduced water heating and electricity bills using PVT systems. Furthermore, considering the economic challenges and environmental impact of large-scale power projects to supply clean and modern power to rural and remote communities in developing countries, with its dual benefits of electricity and heat generation, PVT system is an alternative and viable technology to meet the need of these communities.

2. Materials and methods

2.1. Experimental-setup and measurements

The installation for this study is on the roof of the solar energy applications laboratory at the Department of Mechanical Engineering (6.68° N, 1.57° W), Kwame Nkrumah University of Science and Technology (KNUST), Kumasi, Ghana. Fig. 1 shows a picture of the setup. The solar modules include a commercial hybrid PVT water system and a conventional PV installed side by side at a fixed angle of 8° southwards. The tilt angle is to ensure optimum capture of solar energy for the location and reduce soiling from dust settlement by natural cleaning of the modules during rainfalls. Table 1 shows some selected technical specifications of the module.

Fig. 2 shows a cross-sectional area of the commercial PVT module. It is made up of layer of 72 mc-Si PV cells with copper sheet and tube thermal absorber securely attached to its back. The adhesive compound for the attachment also acts as a shock absorber to further strengthen the PV module. The heat conducted by the copper strips from the PV module is transferred by water flowing through 14 evenly distributed parallel copper pipes thermally attached to the copper strips and connect from inlet to outlet copper manifolds. The thermal absorber is then covered with an insulator material and then finally sealed with an aluminum sheet in the back to complete its thermal insulation.

Fig. 3 shows a schematic diagram of the experimental setup. The main heat transfer medium (fluid) for the PVT in the setup was by force-circulated water in a closed-loop system. A 54 W (12 Vdc) rated pump, with regulated input power, circulated the water through the closed-



Fig. 1. PV (a) and PVT (b) setup on the rooftop of the Solar Energy Applications Laboratory at Department of Mechanical Engineering, KNUST Ghana (Abdul-Ganiyu et al., 2020).

Table 1
Selected technical specifications of the PVT and PV modules.

Parameter	PVT	PV
Nominal electrical power	200 W	270 W
Module electrical efficiency	0.1508	0.166
Nominal current	5.43 A	8.6 A
Nominal voltage	37.89 V	31.4 V
Temperature dependent coefficient of electrical efficiency	0.0045/ K	0.0045/ K
PV technology (material)	mc-Si*	mc-Si
Surface Area	1.326 m ²	1.474 m ²
Thermal absorber area	1.194 m ²	n.a**
Thermal power	630 W	n.a
Zero loss collector efficiency	0.48	n.a
Absorber type (material)	copper	n.a

*Mono-crystalline silicon; ** Not applicable.

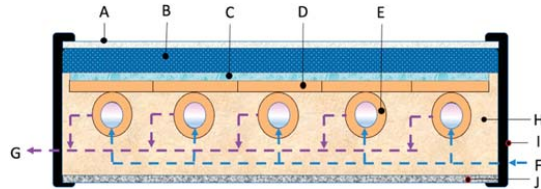


Fig. 2. PVT module made up of (A) non reflective protective glass, (B) PV module, (C) adhesive material, (D) strips copper sheet for thermal absorption, (E) heat exchange copper pipe, (F) water inlet manifold, (G) water outlet manifold, (H) thermal insulation, (I) aluminum frame and (J) aluminum back sheet.

loop system. The returning to the PVT's input is further cooled by a water to air radiator system fitted with two 40 W (12 Vdc) fans.

Table 2 shows a list of main characteristics of data instruments used in this study. A Campbell CR 300 data logger was used to record both meteorological and performance data at a temporal resolution of 15

min. The meteorological measurements included global solar irradiance at plane of array (POA), ambient temperature (°C), wind speed (m/s) and relative humidity (%). The performance data are voltage (V), current (A), PVT water inlet temperature (°C), PVT water outlet temperature (°C), module temperatures (°C) and temperature of water in storage tank (°C).

Flow rate is set by means of mechanical valves and monitored from a spring-loaded mechanical flow meter. One reason for the use of relatively lower flow rates for forced circulation in PVT setup is because higher flow rates may generate turbulence and unsettle the needed water stratification in the storage tank due to involuntary mixing. This may result in water returning to the PVT at higher temperatures than stratified condition and affect the collector instantaneous efficiency (Ji et al., 2006). This situation has been avoided by dissipating the heat from the circulating water to the water in the storage tank. This way, the

Table 2
Instrumentation (Abdul-Ganiyu et al., 2020).

Variable	Instrumentation	Measurement accuracy	Resolution
Temperature (°C)	109 Temperature Probe (PT100)	±0.2 °C (for 0 ⁰ -70 °C)	0.01
Solar irradiance (W/m ²)	Apogee SP-421 pyranometer	±1%	<0.001
Wind speed (m/s)	Decagon DL-2 wind sensor	3%	0.01
Air temperature (°C)	CS215 Temp/RH sensor	±0.4 °C (5 ⁰ -40 °C)	0.01
Relative humidity (%)	CS215 Temp/RH sensor	±4% (0%-100%) at 25 °C	0.03
Flow sensor/ Gauge	Mechanical spring flow meter	Not specified	0.2
Flow rate (litre/ min)	Mechanical valves set.	Not specified	0.2
Current (A)	Bim205 smart charger w/MPPT	Not specified	0.1
Voltage (V)	Bim205 smart charger w/MPPT	Not specified	0.1

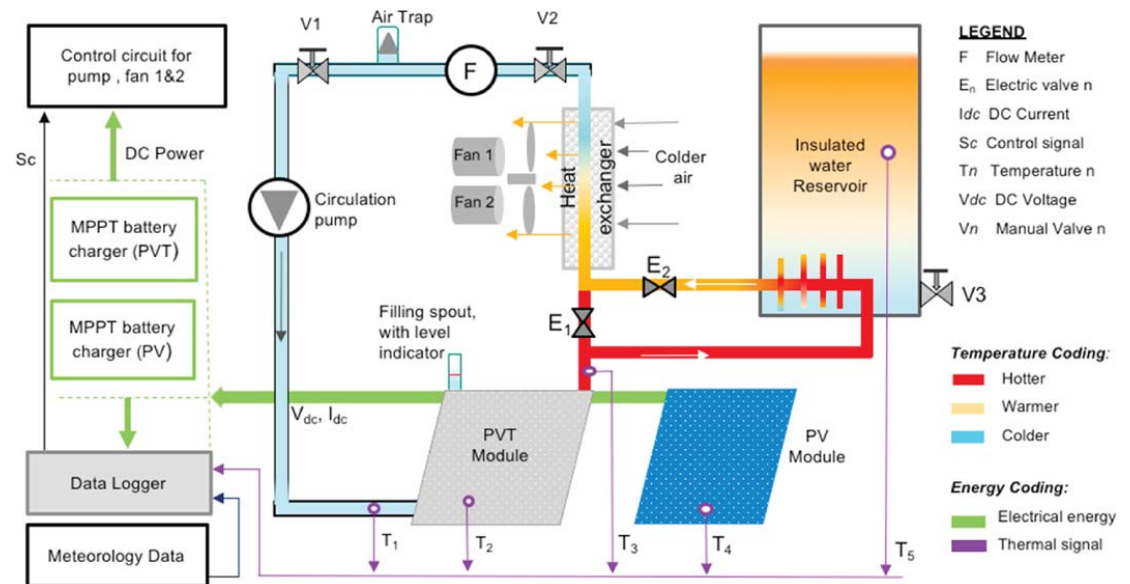


Fig. 3. The schematic shows the interconnection of components, data measurement points and energy flow of the experimental setup (Abdul-Ganiyu et al., 2020).

circulating water and the water in the storage tank do not mix at all. Secondly, the returning water from the heat exchanger in the tank is further cooled by a fan-cooled radiator system before it reaches the PVT inlet. The mass flow rates used in this study ranges from 0.025 kg/s to 0.083 kg/s.

2.2. Energetic efficiency analysis

The instantaneous electrical efficiency of a crystalline solar cell could be expressed as a function of its temperature (T_c) (Evans, 1981) as:

$$\eta_{el} = \eta_0 [1 - \beta(T_{cell} - 25)], \quad (1)$$

where η_0 is the efficiency at standard test condition (STC) (Irradiance = 1000 W/m² and $T_{cell} = 25$ °C), T_{cell} is the solar cell temperature and β is the temperature dependent coefficient of electrical efficiency. The value of β differs with different PV materials used (about 0.0045/K for crystalline silicon, 0.0035/K for CIS, 0.0025/K for CdTe and 0.002/K for a-Si). Efficiency of energy systems are generally expressed as output over input energy. The PV electrical efficiency (η_{el}) can therefore be given as:

$$\eta_{el} = \frac{E_{dc}}{A_m * G_p}, \quad (2)$$

where E_{dc} is the direct current (DC) power from the module in kW, A_m is the module total surface area (m²) and G_p is the in-plane irradiance (kW/m²). Depending on the available data and desired level of resolution, the efficiencies can be determined on instantaneous, hourly, daily, monthly and annually bases. In the same way, the thermal efficiency (η_{th}) could also be expressed as:

$$\eta_{th} = \frac{E_{th}}{A_m \times G_p} \quad (3)$$

where E_{th} is the useful thermal gains of the system and it is also given as:

$$E_{th} = m_w c_p (T_{out} - T_{in}), \quad (4)$$

where m_w is the water mass flow rate (kg/s), c_p is the specific heat capacity of water (kJ/kg °C) and T_{out} and T_{in} are the inlet and outlet water temperature respectively in °C. The total efficiency of the integrated PVT (η_{PVT}) is used to evaluate the overall performance of the system (Radziemska, 2009). It can be obtained by combining equations (2) and (3) as:

$$\eta_{PVT} = \eta_{th} + \eta_{el} = \frac{E_{dc} + E_{th}}{A_m \times G_p} \quad (5)$$

2.3. Energy-saving efficiency

Electrical energy is graded as higher form of energy gain than thermal energy (Fudholi et al., 2014). To correctly evaluate the thermal energy savings of the PVT system, a primary energy-saving efficiency (E_f) is defined as (Radziemska, 2009) (Fudholi et al., 2014) (Huang et al., 2001):

$$E_f = \frac{\eta_{el}}{\eta_p} + \eta_{th}, \quad (6)$$

where η_p is the electric-power generation efficiency of a conventional power plant which varies between 0.20 and 0.40. For this study η_p is 0.38 for good quality coal with low ash content (Huang et al., 2001). The primary energy-savings efficiency is another performance indicator of the energy-grade difference between electricity and thermal energy which considers the quality and quantity of the converted energy by the PVT system.

2.4. Exergy efficiency and analysis

The exergy analysis is based on the second law of thermodynamics. The overall output exergy (Ex_{out}) from the PVT system could be expressed as:

$$Ex_{out} = Ex_{th} + Ex_{el} \quad (7)$$

where Ex_{el} is the electrical exergy and Ex_{th} is the thermal exergy. Unlike thermal energy, electrical energy is perfectly convertible and its exergy content can be taken to be same as the energy content. Thus Ex_{el} and Ex_{th} can be expressed in energy terms in kWh as (Bosanac et al., 2003):

$$Ex_{el} = E_{dc} \quad (8)$$

$$Ex_{th} = E_{th} \left(1 - \frac{T_{ref} + 273}{T_{out} + 273} \right) \quad (9)$$

Equation (9) shows that the useful product of a PVT thermal collector is the heat extracted from the absorber plate to the fluid and made available at its outlet temperature, T_{out} . The Carnot Factor $[1 - (T_{ref} + 273)/(T_{out} + 273)]$ shows the reference temperature (T_{ref}) at which the exergy content of the thermal power is zero (Fuentes et al., 2018). T_{ref} is generally assumed to be equal to ambient temperature T_{amb} . This is adopted by numerous authors (Fuentes et al., 2018) (Pons, 2009). However, for an uncontrolled environment, T_{amb} frequently fluctuates periodically. Thermal exergy is affected by such fluctuations as it depends on the value of the reference temperature at the moment when heat is delivered (Pons, 2009). This therefore introduces thermodynamic contradictions because the reference temperature is supposed to be constant. Thus for this paper, the T_{ref} shall correspond to the monthly minimum ambient temperature $T_{amb,min}$ recorded in any given month (Pons, 2009). Therefore,

$$Ex_{th} = E_{th} \left(1 - \frac{T_{amb,min} + 273}{T_{out} + 273} \right) \quad (10)$$

Following the same minimum monthly ambient temperature reference point assumption, the overall exergy efficiency of the PVT could be expressed as (Tiwari and Sodha, 2006):

$$\eta_{ex} = \eta_{el} + \eta_{th} \left(1 - \frac{T_{amb,min} + 273}{T_{out} + 273} \right) \quad (11)$$

where η_{ex} is the overall exergy efficiency of the PVT water-heating system.

3. Results and discussion

The general performance of the PVT system is determined by its electrical and thermal characteristics. In this section, the efficiency of the PVT is analyzed based on its exposure to solar radiation, cell temperature and mass flow rate conditions by means of analytical techniques presented in the previous section. The analyses are divided into three sections, namely electrical efficiency, thermal efficiency, and exergetic efficiency.

3.1. Energy and exergy outputs

Fig. 4 shows one-year monthly performance profile of the commercial PVT with a forced circulation of water set at manufactures recommended flow rate of 0.033 kg/s (2 L/min). The outputs from the PVT module are 149.92 kWh/year, 601.57 kWh/year and 184.26 kWh/year for electrical energy (E_{dc}), thermal energy (E_{th}) and total exergy (Ex_{out}) respectively. These outputs are, however, not enough to evaluate the real performance of the module. The variations in monthly outputs could be influenced by many interactive factors that include ambient weather conditions, operational configurations, and the solar module's material composition and characteristics. Nonetheless, one better way of

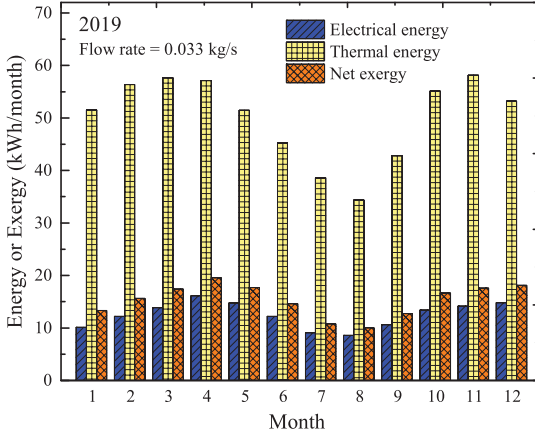


Fig. 4. An all year monthly energy and exergy output profile for the PVT system with water flow rate set at manufacturer’s recommended flow rate of 0.033 kg/s (i.e. 2 L/min).

assessing the real performance is by efficiency, as defined in the previous section. A previous study (Abdul-Ganiyu et al., 2020), showed that the electrical efficiency of the same experimental PVT module operating under the same environmental conditions varied from 9.9% to 11.5%, whereas its thermal efficiency varied from 29.44% to 44.84%. These efficiencies, however, need to be further analyzed in both energy and exergy terms to understand the true performance of the commercial PVT.

3.2. Effect of mass flow rate (m_w) on solar cell temperature (T_{cell})

The instantaneous efficiency of a solar cell is a function of its temperature, as shown in Equation (1). Fig. 5 shows that cell temperature (T_{cell}) significantly changes under various irradiance and mass flow rate variations. It could be seen that increasing in-plane irradiance (G_p) generally increases T_{cell} at constant mass flow rate (m_w), as well as T_{amb} . The Figure also shows that higher T_{cell} values are achieved at lower m_w (i.e. 0.025 kg/s in this case) with values ranging from 51.89 °C to 60.34 °C

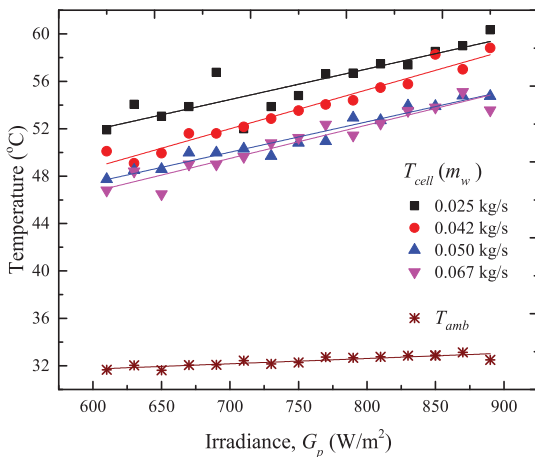


Fig. 5. Effect of varying irradiance on T_{amb} and T_{cell} of the PVT at different mass flow rates (m_w).

for respective G_p variation from 600 to 900 W/m². The G_p range of 600–900 W/m² is used because the level of irradiance fluctuations is noticed to be minimal in this range. On the other hand, T_{cell} is inversely proportional to the flow rate at constant G_p levels. The T_{cell} significantly reduces by almost 11.3% from 60.34 °C to 53.35 °C for m_w variation from 0.025 to 0.067 kg/s at an irradiance of 900 W/m².

It is further observed that there is non-linear relation between T_{cell} and m_w at individual irradiance. Fig. 6 shows that increasing m_w reduces T_{cell} non-linearly until such a flow rate that any further increase does not result in significant changes in T_{cell} for a specific irradiance. It could be seen from the fitted curve in Fig. 6 that the correlation expression between T_{cell} and m_w can be expressed as:

$$T_{cell}(m_w) = 62.73 - 256.57 m_w + 1519.53 m_w^2 \tag{12}$$

Equation (12) indicate that, for this specific PVT module, the maximum m_w beyond which no significant changes in T_{cell} would occur is, approximately, determined as 0.083 kg/s [i.e. $\frac{d}{dm_w}(T_{cell}) = 0$]. Although this observation (i.e 0.063 kg/s m²) compares favorably with what has been reported by Fuentes et al. in Spain (also 0.063 kg/s m²), it cannot be generalized for all PVT thermal designs and calls for further investigation.

3.3. Effect of mass flow rate (m_w) on electrical efficiency, η_{el}

Fig. 7 shows the relation between the electrical efficiency (η_{el}) of the PVT and changing in in-plane irradiance (G_p) at different m_w . It could be observed that for specific m_w , η_{el} decreases with increasing G_p , specifically due to increase in T_{cell} as discussed in the previous section. However, increasing the m_w through the thermal collector at constant G_p indirectly affects the cooling of the PV component resulting in relative reduction in T_{cell} . This results in significant increases in η_{el} . Higher η_{el} values are therefore realized at higher m_w for individual G_p . As could be seen from the curves in Fig. 7, at G_p of 800 W/m², the electrical efficiency increases from 10.1% to 10.83% as the m_w increases from 0.025 to 0.067 kg/s. However, at a constant m_w of 0.067 kg/s, the η_{el} slightly reduces from 10.92% to 10.72% respectively for G_p variation from 900 to 700 W/m².

Furthermore, Fig. 7 shows decreasing gradient of individual curves as m_w is increased from 0.025 to 0.067 kg/s. A plot of the gradients for the individual curves (i.e. $\Delta\eta_{el}/\Delta G_p$) against the respective flow rates shows a non-linear relation (see Fig. 8) given as:

$$\frac{\Delta\eta_{el}}{\Delta G_p} = -0.000062 + 0.00125m_w - 0.00759m_w^2. \tag{13}$$

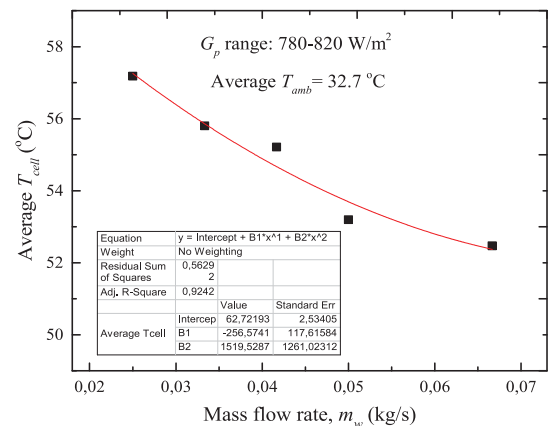


Fig. 6. Changes in average T_{cell} (for G_p range of 780–820 W/m²) to m_w .

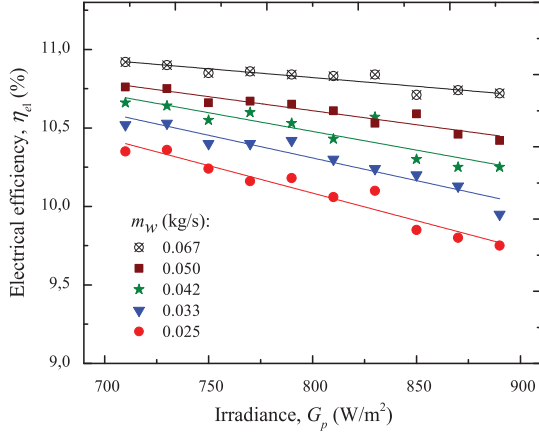


Fig. 7. Changes in PVT electrical efficiency with irradiance as mass flow rate is varied.

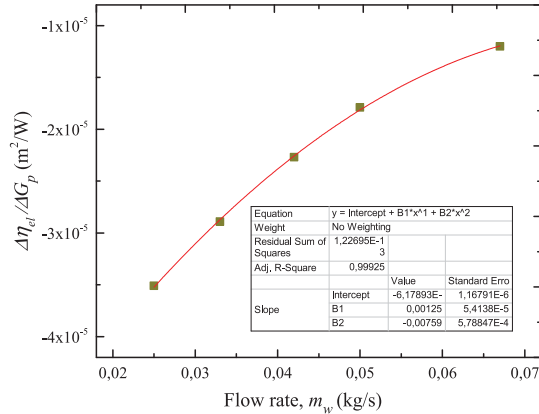


Fig. 8. Variation in electrical efficiency to irradiance slope with mass flow rate.

A first order differential of Equation (13) shows that its turning point occurs when flow rate is approximately 0.082 kg/s. This simply means that, for a specific G_p , the electrical efficiency of the PVT can be increased by increasing the flow rate appreciably till it reaches ~ 0.082 kg/s, beyond which no significant increase in efficiency can be realized for the PVT module. This observation confirms an earlier observation (in Section 3.2) which shows that the optimum flowrate for maximum electrical energy performance of a unit area of the PVT occurs at ~ 0.063 kg/s.

3.4. Effect of flow rate (m_w) on thermal efficiency, η_{th}

The thermal efficiency of a PVT module determines how much of input solar energy it can be converted into useful thermal gains. Fig. 9 shows the changes in thermal efficiency (η_{th}) of the PVT with G_p at different m_w of water through the PVT water channels. It could be seen from this Figure that, for a specific water flow rate, the η_{th} is relatively directly proportional to the G_p . This could be due to increase in T_{cell} with increasing G_p intensity as discussed in previous Section 3.2. Also, the η_{th} increases with increasing m_w and vice versa, at specific G_p . Thus, higher η_{th} were realized at relatively higher m_w and ranging from 42.46% to

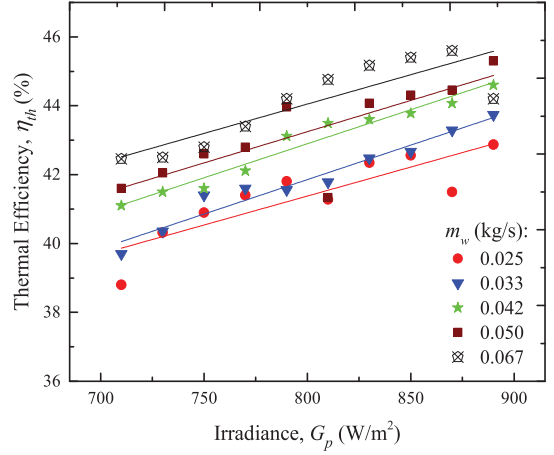


Fig. 9. Changes in PVT thermal efficiency with irradiance at different mass flow rates.

45.60% for G_p of 710–890 W/m².

As presented in Equation (4), the thermal energy gains is a function of temperature change (ΔT) between the output and input water temperatures ($T_{out}-T_{in}$). Fig. 10 shows that ΔT is affected by both G_p and m_w . As expected, for a specific m_w , increase in irradiance results in increase in ΔT . However, an increase in m_w for a specific input irradiance decreases ΔT until such a value that any further increase will not result in any significant changes in ΔT . This is similar to observations made in earlier sections. Also, lower ΔT means that, although higher flow rate results into higher efficiencies, the delivery temperature (T_{out}) is relatively lower (with respect to T_{in}). Thus, T_{out} is compromised and limits the thermal energy usability, which is greater at higher temperatures. On the other hand, higher ΔT increases thermal losses because the water reaches higher temperature. Thus, the losses are reduced at higher m_w .

3.5. Effect of mass flow rate (m_w) on overall energy efficiency, η_{PVT}

Many researchers have expressed the net energy efficiency of a PVT

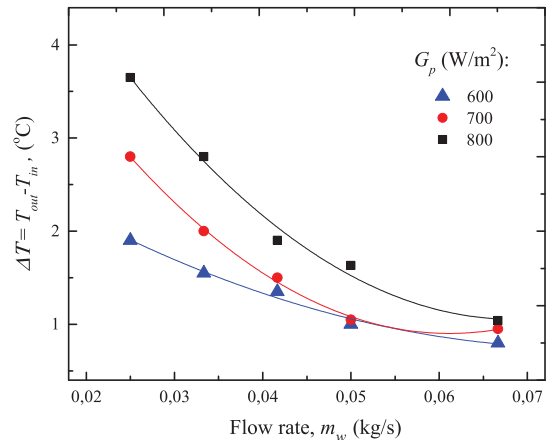


Fig. 10. Effect of mass flow rate and irradiance on temperature changes between outlet and inlet water flowing through the PVT thermal plate.

as the sum of its electrical and thermal efficiencies (Equation (5)). From the results discussed so far on the PVT module, both η_{el} and η_{th} increased with increase in m_w . It could therefore be said that the general configuration of the PVT could affect the net energetic efficiency (η_{PVT}). Fig. 11 shows the effects of m_w on the η_{PVT} of the flat-plate PVT system. As could be seen, the η_{PVT} increases with increase in either or both flow rate and irradiance. From the curves, the highest η_{PVT} of 56.34% was achieved at highest analyzed G_p (890 W/m²) and m_w (0.067 kg/s). Also, the lowest η_{PVT} of 49.15% occurred at lowest studied G_p (710 W/m²) and m_w (0.025 kg/s).

3.6. Effect of mass flow rate (m_w) on exergetic efficiency, η_{ex}

The exergy efficiency (η_{ex}) of the PVT module is based on the second law of thermodynamics as discussed in Section 2.2. Fig. 12 shows the variation of η_{ex} with m_w and G_p . The curves seem to suggest that lower m_w tend to influence the η_{ex} negatively at higher G_p . This could be attributed to the debilitating effect of increase in G_p on T_{cell} and hence η_{el} , which adversely affects η_{ex} . On the other hand, higher m_w relatively lower T_{cell} and increases η_{el} and, therefore increases, η_{ex} . Thus, higher η_{ex} is achieved at higher m_w and higher G_p .

From discussions so far, it could be seen that operational conditions like m_w are extremely important in maximising the total exergy from the PVT system. However, the curves in Fig. 13 tend to suggest that the effect of varying G_p on η_{ex} seems to be less at m_w of 0.033 kg/s. Fig. 13 shows the tradeoff between electrical and thermal energetic efficiencies at m_w of 0.033 kg/s. An increase in η_{el} relatively lowers η_{th} and vice versa and results in a relatively stable η_{ex} (approximately 12.75% in this case) at different G_p intensities.

3.7. Comparisons with conventional systems

3.7.1. Solar thermal systems

For a PVT system to compete with a separately installed solar hot water system, Huang et al. (2001) proposed that it's energy-saving efficiency (Equation (6)) should exceed 50%. Fig. 14 shows that the energy-savings efficiency for the tested commercial PVT is 66% for G_p of 710 W/m² at m_w of 0.025 kg/s. This increases to 73% for G_p of 890 W/m² at flow rate of 0.067 kg/s. These efficiencies are not only greater than 50%, but also significantly higher than the overall efficiency (η_{PVT}) defined in Equation (5). Table 3 shows that these efficiencies compare favorably with those reported in scientific literature.

However, in terms of thermal efficiency (η_{th}), Table 3 shows that the

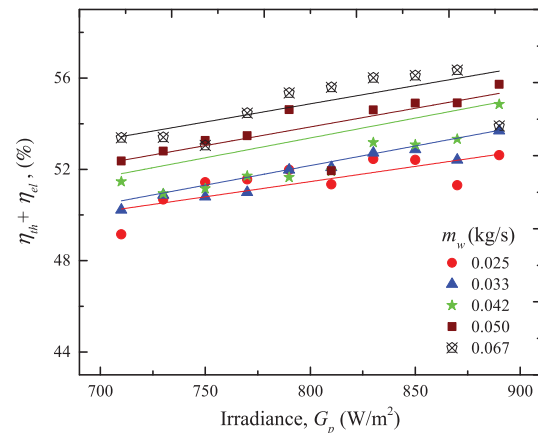


Fig. 11. Changes in PVT net efficiency with mass flow rate and irradiance.

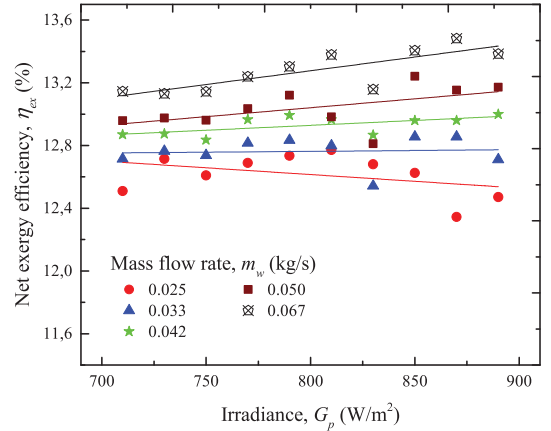


Fig. 12. The effect of mass flow rate and irradiance on net exergy efficiency of the PVT module.

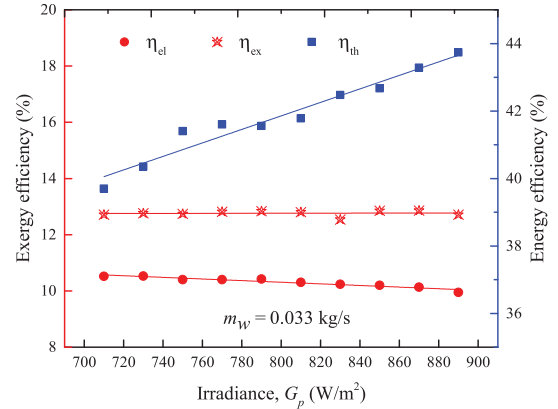


Fig. 13. A variation of thermal, electrical and net exergy efficiencies of the PVT with irradiance at flow rate of 0.033 kg/s (2 L/min).

commercial flat-plate water PVT has not performed better than those reported in literature even at a higher m_w of 0.067 kg/s. The effect of poor thermal contact problems on the commercial PVT system performance has been reported by (Guarracino et al., 2019) (Fuentes et al., 2018). The preferred method of encapsulating the thermal absorber under the PV layer to achieve a good thermal contact in the PVT module is to laminate the top cover, PV layer and absorber in a single assembly while electrically insulating the PV layer at the same time (Lalovic et al., 1986) (de Vries, 1998) (TASK60, 2020). A simpler and cheaper alternative commonly used in most commercial PVTs is the use of adhesives and thermally-conductive pastes to put together the PV layer and the thermal absorber (Lalovic et al., 1986) (de Vries, 1998) (TASK60, 2020). A deformation in the thermal absorber surface, non-uniform application of thermal paste and poor adhesion could result in poor thermal contacts.

3.7.2. Photovoltaic systems

Fig. 15 shows a comparison of cell temperatures (T_{cell}) between a conventional PV and the commercial PVT with water circulation at various m_w in a dynamic environment for G_p of 700–900 W/m². As could

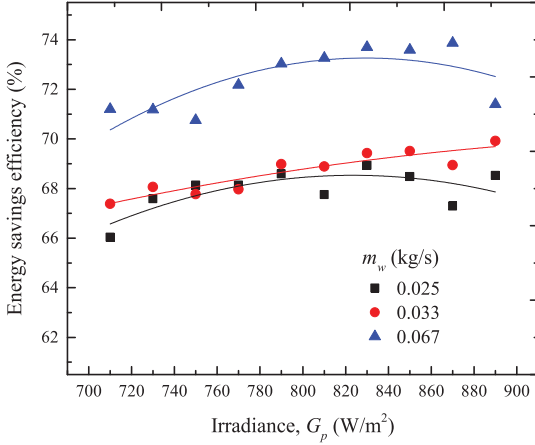


Fig. 14. Primary energy-saving efficiency at different flow rates.

Table 3
Comparison of present study with other water-based PVT systems showing thermal and energy-savings efficiency.

Reference	Performance	Remarks
Fuentes et al. (Fuentes et al., 2018)	$\eta_{th} = 50\text{--}70.4\%$	Commercial PVT, Array
Guarracino et al. (Guarracino et al., 2019)	$\eta_{th} = 37.0\%$	Commercial PVT
Abdul-Ganiyu et al. (Abdul-Ganiyu et al., 2020)	$\eta_{th} = 29\text{--}44.8\%$	Commercial PVT
Fudholi et al. (Fudholi et al., 2014)	$\eta_{th} = 46.4\text{--}54.1\%$ $E_f = 78.5\text{--}87.5\%$	Non-commercial, direct flow absorber
Fudholi et al. (Fudholi et al., 2014)	$\eta_{th} = 41.1\text{--}48\%$ $E_f = 72.4\text{--}80.6\%$	Non-commercial, web flow absorber
Fudholi et al. (Fudholi et al., 2014)	$\eta_{th} = 45.4\text{--}54.6\%$ $E_f = 79.2\text{--}90.0\%$	Non-commercial, Spiral flow absorber
Chow et al. (Chow et al., 2007)	$\eta_{th} = 51\%$ $E_f = 64.9\%$	Non-commercial, aluminum-alloy flat-box design
Current study	$\eta_{th} = 38.8\text{--}43.1\%$ $E_f = 66\text{--}73\%$	Commercial PVT, direct flow absorber

be seen, the PVT cells benefit from the primary water cooling by means of the thermal absorber and records lower average T_{cell} than the conventional PV. Whereas the PVT seems to show a relatively stable exergy efficiency with increase in G_p , the PV suffers a decrease in exergy efficiency due to the debilitating effect on T_{cell} in the absence of any active cooling. Also, an advantage of the cooling of the PVT is the useful thermal energy gains at its water outlet which is expected to increase its overall exergy conversion rate. Fig. 16 shows that this advantage plays in its favor only for G_p values above ~ 790 W/m² for this study.

One limitation of the PVT technology is that electricity production is enhanced at lower temperatures (Equation (1)), while the heat energy usability is greater with higher output temperatures (Fuentes et al., 2018). Thus, for the commercial PVT to compete well with the conventional systems, the cooling effect on the cells should translate into both electrical energy and thermal energy gains. This calls for alternative design and improvement of existing systems. The most common

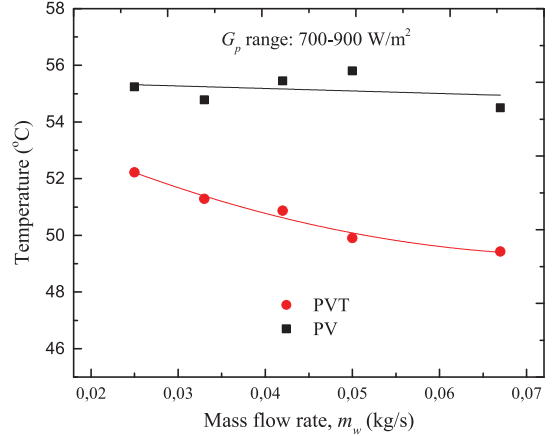


Fig. 15. Average T_{cell} comparison between a conventional PV and the commercial PVT for irradiance range of 700–900 W/m².

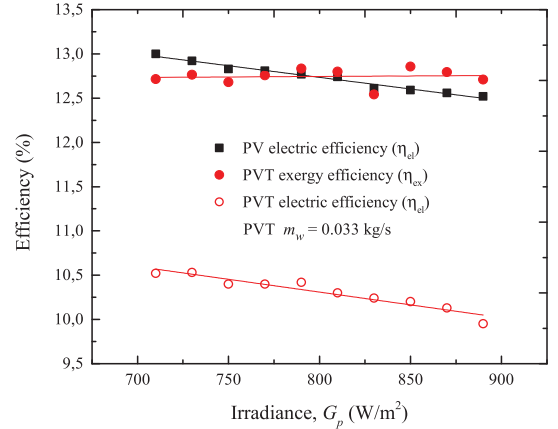


Fig. 16. Exergetic comparison between the conventional PV and the commercial PVT at mass flow rate of 0.033 kg/s.

thermal absorber in the commercial PVT is the tube and sheet design (Fuentes et al., 2018) (Abdul-Ganiyu et al., 2020) (Guarracino et al., 2019). However, some alternative absorber designs in literature with encouraging performance include spiral flow absorber (Fudholi et al., 2014), aluminum-alloy flat box with rectangular channel absorber (Chow et al., 2007), and serpentine channel absorber (Allan et al., 2015). The use of nanofluid technology for heat transfer has also been reported to improve both thermal and electrical energy performance of the PVT (Fayaz et al., 2018).

4. Conclusion

Water flow-rate analysis of a commercial flat-plate PVT system has been experimentally conducted in a dynamic environment. The study considered the effects of water flow rate and irradiance on both energetic and exergetic performance of the PVT. From this study.

- Higher mass flow rates result in lower cell temperatures and higher electrical efficiency, and vice versa. However, the lower cell

temperatures in the PVT did not translate absolutely into electrical energy gains as happens with the conventional PV system. Higher irradiance on the other hand resulted in lower electrical efficiency due to increase in cell temperature as expected.

- Higher mass flow rates at constant irradiance resulted into higher thermal gains but lower water output temperatures and vice versa. However, higher irradiance at constant flow rate increases both thermal efficiency and final output temperature
- The maximum water flow rate beyond which no significant improvement in active cooling could occur was determined to be approximately 0.082 kg/s (0.063 kg/s m²).
- The PVT exhibited a relatively stable exergy efficiency of approximately 12.75% at manufacture's recommended flow rate of 0.033 kg/s with changing irradiance. However, the PVT's exergy efficiency was lower than that of the conventional PV (13.0–12.75% respectively for irradiance of 710–790 W/m²) for irradiances below 790 W/m², but benefits from thermal gains at higher irradiance (>790 W/m²).
- Although the commercial PVT energy-saving efficiency is generally above 50%, suggesting its competitiveness with separately installed solar hot water system, its thermal efficiency was generally average compared to other experimental PVT systems. This was attributed to possible poor thermal contact between the PV layer and the thermal absorber in the PVT module, as has been widely reported in other studies.

With an average thermal energy yield of 602 kWh/yr by the PVT module (rated 200 W) used in this study, a 5 kW rooftop PVT (with similar module's configuration) could produce over 2300 L of warm water per day for users in remote locations. With assumption that an average water requirement of 50 L per day capita in Ghana, this type of installation can provide warm water for over 40 people. For this system, well water or ground water could serve as source of cold/cool water to operate this system in remote locations, while utility managed water source could be used in urban/semi-urban areas.

From the results presented, it could be concluded that the commercial PVT system did not perform as expected in exergy terms when compared with separately installed conventional PV and thermal systems. The use of exergy at various mass flow rates and irradiances showed that using only combined efficiency, which is widely used in literature, is not enough to assess its general performance. Thus, for the commercial PVT to be competitive, there is a need for innovative and design improvement research to further improve performance. Specifically, further research should be undertaken on electrical efficiency improvement with reduced cell temperatures at higher mass flow rates and alternative thermal contact techniques to further enhance their exergy performance. Also, further research for generalized correlation for the optimum mass flowrate for different modules should be undertaken.

Author statement

Saeed Abdul-Ganiyu: Conceptualization; Data curation, experimental set-up; Data collection and curation; Formal analysis; Investigation; Methodology; Writing – original draft. David A Quansah: Supervision; Methodology; Writing – review & editing. Emmanuel W Ramde: Supervision; Methodology; Writing – review & editing. Razak Seidu: Resources; Supervision; Methodology; Writing – review & editing. Muiyiva S Adaramola: Conceptualization; Resources; Supervision; Methodology; Writing – original draft, Writing – review & editing, Writing – drafting, review, and editing.

Declaration of competing interest

The authors declare that they have no known competing financial interests or personal relationships that could have appeared to influence

the work reported in this paper.

Acknowledgments

Authors acknowledge the PhD scholarship support by the UPERCRET Program with fund from the Energy and Petroleum (EnPe) Project of the Norwegian Agency for Development Cooperation (Norad).

References

- IEA Africa energy Outlook 2019. world energy Outlook special report [Online]. Available: <https://www.iea.org/reports/africa-energy-outlook-2019>. (Accessed 22 April 2020). Accessed.
- Abdul-Ganiyu, S., Quansah, A.D., Ramde, W.E., Seidu, R., Muiyiva, A.S., 2020. Investigation of Solar Photovoltaic-Thermal (PVT) and Solar Photovoltaic (PV) Performance: A Case Study in Ghana. *energies*.
- Allan, J., Dehouche, Z., Stankovic, S., Mauricette, L., 2015. Performance testing of thermal and photovoltaic thermal solar collectors. *Energy Sci. Eng.* 3 (4), 310–326.
- Aste, N., del Pero, C., Leonforte, F., 2014. Water flat plate PV-thermal collectors: a review. *Sol. Energy* 102, 98–115.
- Bosanaac, M., Sorensen, B., Katic, I., Sorensen, H., Nielsen, B., Badran, J., May 2003. Photovoltaic/thermal solar collectors and their potential in Denmark [Online]. Available: <https://www.yumpu.com/en/document/read/4467325/photovoltaic-thermal-solar-collectors-and-their-potential-in-denmark>. (Accessed 8 June 2020). Accessed:21.
- Charalambous, P., Kalogirou, S., Maidment, G., Yiakoumetti, K., 2011. Optimization of the photovoltaic thermal (PV/T) collector absorber. *Sol. Energy* 85 (5), 871–880.
- Chow, T., 2003. Performance analysis of photovoltaic-thermal collector by explicit dynamic model. *Sol. Energy* 75, 143–152.
- Chow, T., 2010. A review on photovoltaic/thermal hybrid solar technology. *Appl. Energy* 87, 365–379.
- Chow, T., Ji, J., He, W., 2007. Photovoltaic-thermal collector system for domestic application. *J. Sol. Energy Eng.* 129 (2), 205–209.
- de Vries, D., 1998. Design of a Photovoltaic/thermal Combi-Panel.
- Evans, D., 1981. Simplified method for predicting PV array output. *Sol. Energy* 27, 555–560.
- Fayaz, H., Nasrin, R., Rahim, N., Hasanuzzaman, M., 2018. Energy and exergy analysis of the PVT system: effect of nanofluid flow rate. *Sol. Energy* 169, 217–230.
- Fudholi, A., Kamaruzzaman, S., Yazdi, H.M., Ruslan, H.M., Ibrahim, A., Kazem, A.H., 2014. Performance analysis of photovoltaic thermal (PVT) water collectors. *Energy Convers. Manag.* 78, 641–651.
- Fuentes, M., Vivar, M., de la Casa, J., Aguilera, J., 2018. An Experimental Comparison between Commercial Hybrid PV-T and Simple PV Systems Intended for BIPV, vol. 93. *Renewable and Sustainable Energy Reviews*, pp. 110–120.
- Garg, H., Agarwal, R., 1995. Some aspects of a PV/T collector/forced circulation flat plate solar water heater with solar cells. *Energy Convers. Manag.* 36, 87–99.
- Guarracino, I., Freeman, J., Ramos, A., Kalogirou, A.S., Ekins-Daukes, J.N., Markides, N. C., 2019. Systematic testing of hybrid PV-thermal (PVT) solar collectors in steady-state and dynamic outdoor conditions. *Appl. Energy* 240, 1014–1030.
- Huang, B., Lin, T., Hung, W., Sun, F., 2001. Performance evaluation of solar photovoltaic/thermal system. *Sol. Energy* 70, 443–448.
- Ji, J., Han, J., Chow, T., Yi, H., Lu, J., He, W., Sun, W., 2006. Effect of fluid flow and packing factor on energy performance of a wall-mounted hybrid photovoltaic/water-heating collector system. *Energy Build.* 38, 1380–1387.
- Kalogirou, S., 2001. Use of TRNSYS for modelling and simulation of hybrid PV-Thermal solar system for Cyprus. *Renew. Energy* 23, 247–260.
- Lalovic, B., Kiss, Z., Weakliem, H., 1986. A hybrid amorphous silicon photovoltaic and thermal solar collector. *Sol. Cell.* 19 (2), 131–138.
- Lämmle, M., Olivia, A., Hermann, M., Kramer, K., Kramer, W., 2017. PVT collector technologies in solar thermal systems: A systematic assessment of electrical and thermal yields with the novel characteristic temperature approach. *Sol. Energy* 155, 867–879.
- Morita, Y., Fujisawa, T., Tani, T., 2000. Moment performance of photovoltaic/thermal hybrid panel (numerical analysis and exergetic evaluation). *Electr. Eng. Jpn.* 133, 43–51.
- Nualboonrueng, T., Tuenpusa, P., Ueda, Y., Akisawa, A., 2012. The Performance of PV-T Systems for Residential Application in Bangkok.
- Pons, M., 2009. On the reference state for exergy when ambient temperature fluctuates*. *Int. J. Therm.* 12 (3), 113–121.
- Radzimska, E., 2009. Performance analysis of a photovoltaic-thermal integrated system. *Int. J. Photoenergy* 2009.
- Rajoria, C., Agrawal, S., Tiwari, G., 2012. Overall thermal energy and exergy analysis of hybrid photovoltaic thermal array. *Sol. Energy* 86, 1531–1538.
- Reddy, R.S., Ebadian, A.M., Lin, C.-X., 2015. A review of PV-T systems: thermal management and efficiency with single phase cooling. *Int. J. Heat Mass Tran.* 91, 861–871.
- TASK 60, 2020 [Online]. Available: <https://task60.iea-shc.org>.
- Task 60iea [Online]. Available: <https://task60.iea-shc.org/highlights>. (Accessed 8 October 2020). Accessed.

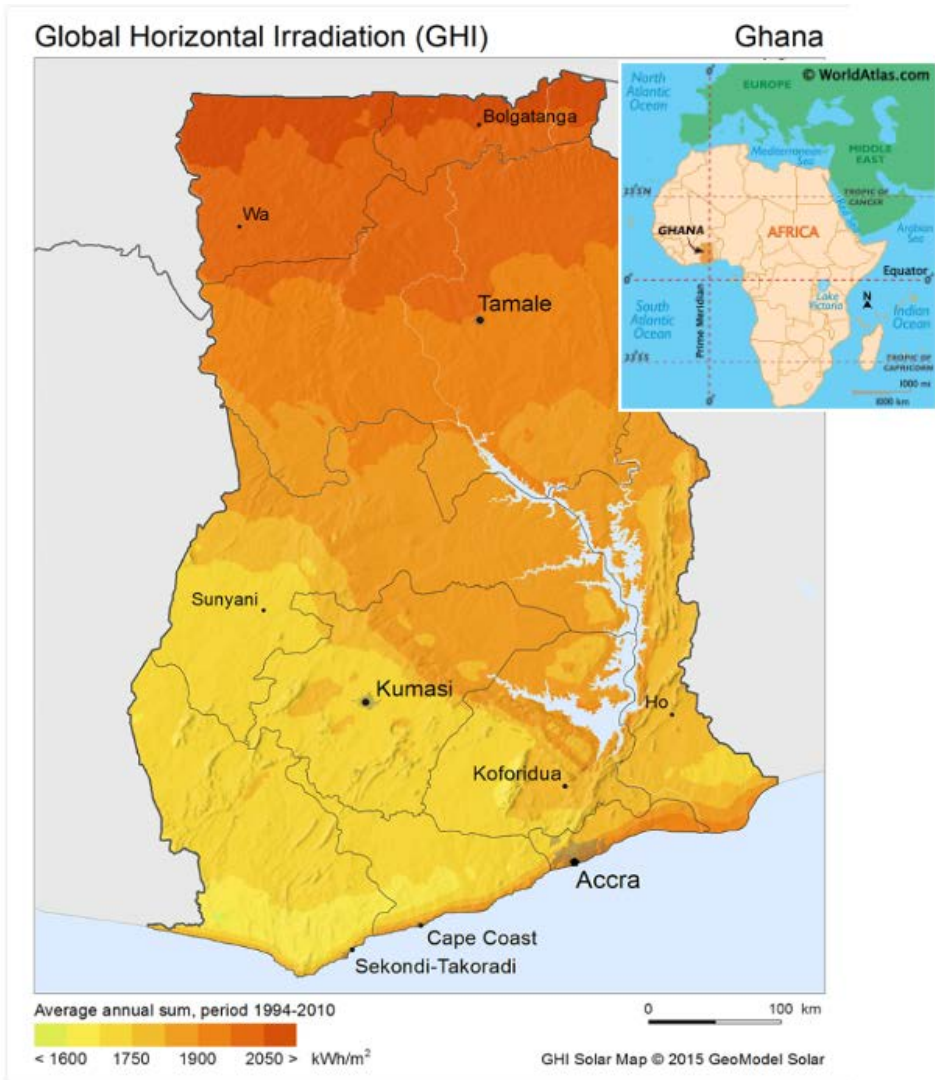
TASK60, I., July 2020. Design guidelines for PVT collectors [Online]. Available: <https://task60.iea-shc.org/Data/Sites/1/publications/IEA-SHC-Task60-B2-Design-Guidelines-for-PVT-Collectors.pdf>. (Accessed 5 October 2020). Accessed.

Tiwari, A., Sodha, M., 2006. Performance evaluation of solar PV/T system: an experimental validation. *Sol. Energy* 80 (7), 751–759.

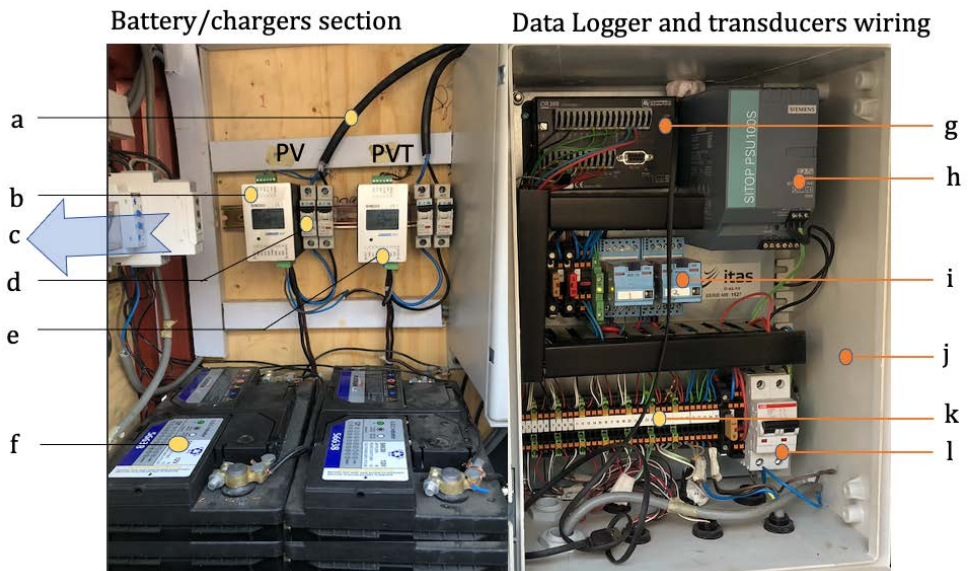
Tiwari, A., Dubey, S., Sandhu, C., Sodha, M.S., Anwar, S., 2009. Exergy analysis of integrated photovoltaic thermal solar water heater under constant flow rate and constant collection temperature modes. *Appl. Energy* 86, 2592–2597.

Appendices

Appendix A: Global Irradiance Map of Ghana



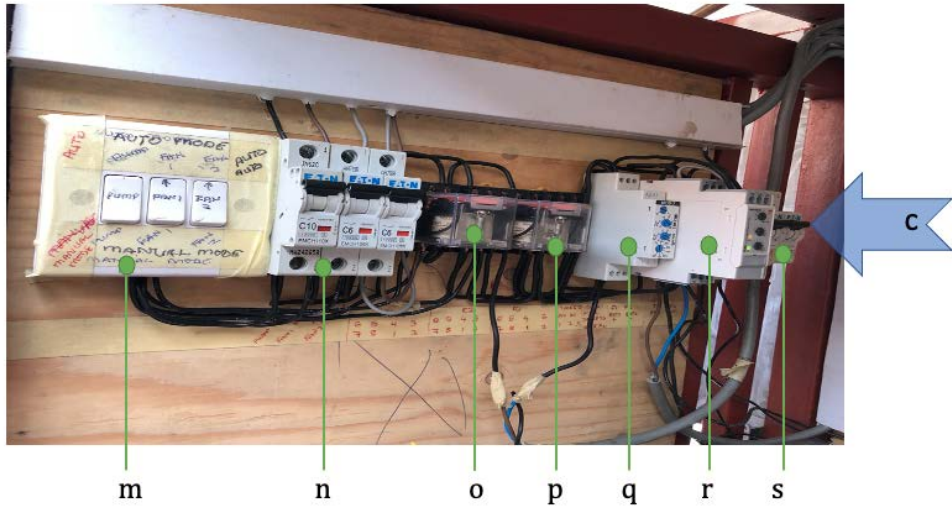
Appendix B: Electrical compartment showing data logger connections.



- a) Power output cable from PV module.
- b) Battery charger for PV
- c) Time delay relay and a section of control circuit (See Appendix C)
- d) Module output circuit breakers (See Figure 5.7: F1-F4)
- e) Battery charger for PVT
- f) Battery
- g) Data logger (Campbell Scientific CR300)
- h) Logger Power supply
- i) Data logger operated relay
- j) Cabinet for logger connections
- k) Cable connector module for transducer connections (see Appendix D)
- l) On/off circuit breaker

Appendix C

Wired components of the control circuit



c) Section continuation from Appendix B

m) Service/Manual switches for pump, Fan 1&2

n) Circuit breakers for pump, Fans 1&2 (See Figure 3.10: F5, F6 and F7)

o) Relay 1







p) Relay 2

q) Timer relay

r) Timer relay

s) Mode switch

Appendix D: Transducers

Variable (s)	Instrument	Description
Voltage, Current		BIM 205 intelligent charger V 1.0; Manufacturer: MicroStep-MIS https://www.microstep-mis.com/web/products?category=power_supplies_and_chargers&product=bim205_intelligent_charger
Irradiance		Apogee SP-421 digital output silicon-cell pyranometer Manufacturer: apogee instruments https://www.apogeeinstruments.com/content/SP-400-spec-sheet.pdf
Wind speed		Decagon DL-2 wind sensor Manufacturer: PESSL INSTRUMENTS GmbH Technical details: https://metos.at/es/portfolio/decagon-ultrasonic-wind-sensor/
Ambient temperature, Relative humidity		CS215 Temp/RH sensor. Manufacturer: Campbell Scientific Technical details: https://www.campbellsci.com/cs215-l
Temperature of surfaces and water		109 Temperature Probe (Pt100) Manufacturer: Campbell Scientific Technical details: https://www.campbellsci.com/109
Flow rate		Spring loaded flow meter with mechanical valves

Appendix E: PV/T MODULES

Manufacturer: Solimpeks, Turkey

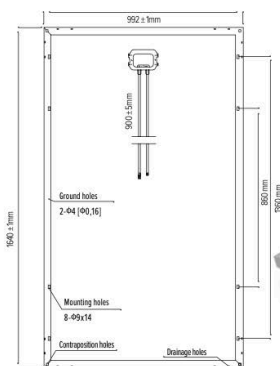
PV MODULES

PV SOL60S - 270W



Monocrystalline

Excellent performance in low light conditions
 Guarantee from 0 to +6W power tolerance,
 customers can obtain 5,8% more power than the rated output
 100% EL test before and after lamination, and finished products EL test, provid-
 ing higher quality assurance
 10 year %91 and 25 year %80 warranty



TECHNICAL SPECIFICATIONS

MECHANICAL CHARACTERISTICS

Cable Type Cross-sectional area and Length	φ = 4mm ² , L= 900± 5mm
Type of Connector	Compatible Type MC4
Dimension AxBxC	1640 x 992 x 45mm
Weight	18,3 kg (40.3 lb)
Number of Draining Holes in Frame	16
Glass	High Transmission, Low Iron Tempered 3,2mm
Encapsulation	EVA
Back Side	White Tedlar
Junction Box (protection degree)	IP 67
Frame	Clear Anodized Aluminum Alloy Type 6063T5 Frame

QUALIFICATION TEST PARAMETERS

Dielectric Insulation Voltage	6000V DC max
Operating Temperature	-40°C to +85 °C
Max Load	5400 Pa
Hailstone Impact	25mm at 23m/s

PACKAGING CONFIGURATION

Packaging Configuration	22 pcs/ box and 2 pcs/ box
Quantity of Big Box / Pallet	1 box / Pallet 1 box / Pallet
Quantity of Small Box / Pallet	- 10 boxes / Pallet
Loading Capacity	616 pcs / 40' HQ 240 pcs/ 20' GP

TYPICAL ELECTRICAL CHARACTERISTICS

Product Code	MA- 0603
Solar Cell	Mono-Crystalline 156X156mm 60pcs (6x10)3 bus bars
Max-Power	260Wp 265Wp 270Wp 275Wp 280Wp
Power Tolerance	0 + 6W
Voltage at Pmax (Vmp)	31,4V
Current at Pmax(Imp)	8,60A
Open- Circuit Voltage (Voc)	38,3V
Short- Circuit Current (Isc)	9,31A
Max- System Voltage (VDC)	1000V (IEC), 600V (UL)
Module Efficiency	16,6%
No. of Bypass Diodes (pcs)	3
Max. Series Fuse (A)	12A
Temperature Coefficient of Pmax	-0,45%/°C
Temperature Coefficient of Voc	-0,34%/°C
Temperature Coefficient of Isc	0,05%/°C
Nominal Operating Cell Temperature	45± 2 °C

* STC Conditions (1000W / m², 1,5 AM and 25 °C Cell Temperature)

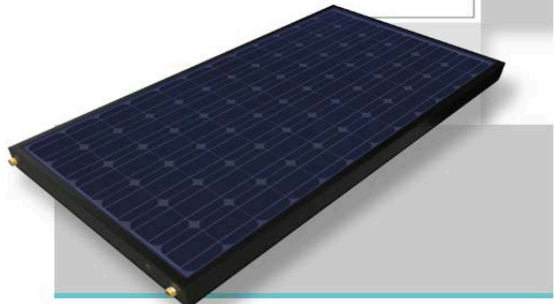
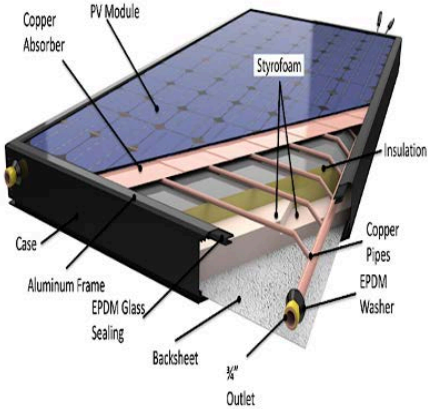
Manufacturer: Solimpeks, Turkey

PV-T PANELS



VOLTHER POWERVOLT

Electricity and usable thermal hot water at the same time from one panel
 Extra electricity production of up to 25% per year with cooled PV cells
 More electricity with PowerVolt



TECHNICAL SPECIFICATIONS

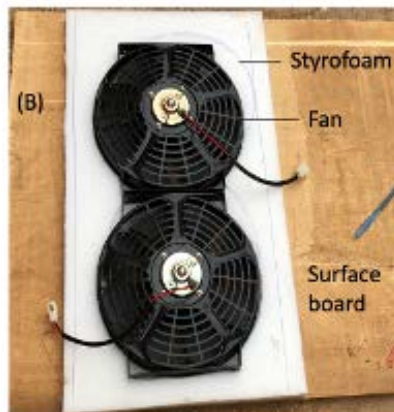
	PowerVolt
Product Code	MA- 0013
Dimensions (mm)	828x1601x90
Gross Area (m ²)	1,370
Aperture Area (m ²)	1,326
Absorber Area (m ²)	1,194
Weight (kg)	24,4
Liquid Content	1,21
Absorber Panel	Mono-Crystalline
Number of Cells	72
Cell Dimensions (mm)	125 x 125
WP (W) Nominal Power	200
Imp (A) Nominal Current	5,43 A
Isc (V) Short Circuit Current	5,67 A
Vmp (V) Nominal Current	36,8 V
Voc (V) Open Circuit Voltage	46,43 V
Heat Exchanger	Copper
Internal Piping	Copper
Test Pressure (bar)	13
Maximum Operating Pressure (bar)	6
Cover Glass	PV Glass
Sealing	EPDM & Silicone
Maximum Temperature	101°C
Base Sheeting	Embossed - Finished Aluminum
Rear Side	Aluminum
Product Warranty	10 Years
Production Guarantee	%90<10 years, %80<20 years

	PowerVolt
Product Code	MA- 0013
Temperature coefficient of Isc	0.06%/°C
Temperature coefficient of Voc	-0.34%/°C
Temperature coefficient of Pmax	-0.45%/°C
Power Tolerance	±3%
Module electrical efficiency	15.08%
η ₀ (Zero Loss Collector Efficiency)	0.475
a ₁ (first order heat loss)	8.37
a ₂ (second order heat loss)	0.586
MC4 connector (brand / model)	JMTHY / PV-JM601
WP (W) Thermal Power	630
Recommended flow rate (L/Hr)	65
Country of manufacture	Turkey
Manufacturer	Solimpeks Solar Energy Corp.

Appendix F: Radiator System

1. RADIATOR FAN

Manufacturer: Unknown
Source: China
Model: Universal
Power rating: 12 Vdc , 60 W



(A) Fans seat made from styrofoam to concentrate air flow through opening to Radiator. (B) Fans installed on styrofoam seat and surface board.

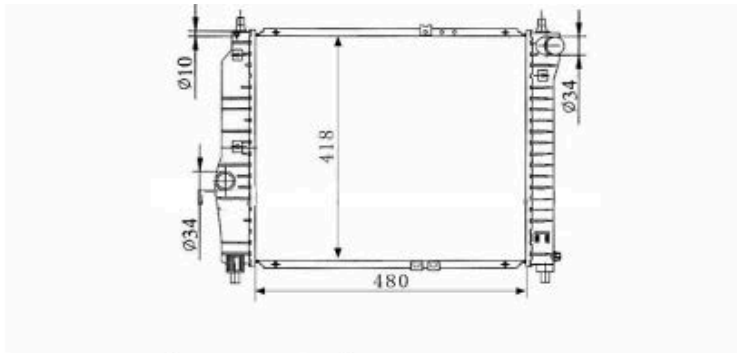
2. HEAT EXCHANGER

Manufacturer: HongDao Automotive Parts Company Limited

Origin: Guangzhou, China

Model: 96536523

Capacity: 1.2 L



CARTYPE : KALOS' 02-1.2-1.4 AVEO' 2003-06 MT DPI :

CORE SIZE:480*418*16

CARTON : 63.5*11*56.5

OEM: 96536523/96443475/p96536523

TANK SIZE : 438*45.5



Adapter
Header

Aluminium
Risers with
Finned air
spaces

Adapter

Appendix G: Water storage tank

1. THERMOS VESSEL

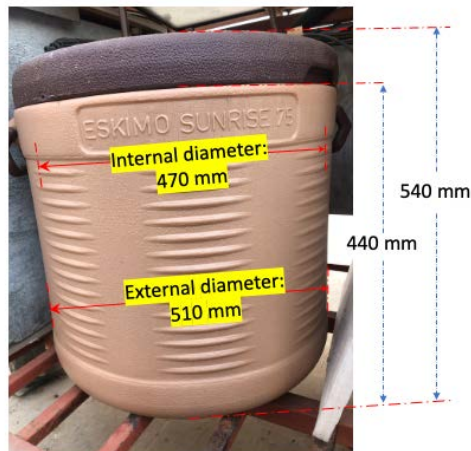
Manufacturer: Unknown

Brand: Eskimo

Model: Sunrise 75

Capacity: 75 Liters

Source: <https://shopfromsource.com/market/itemdetail.php?sku=0834f820-66b3-11e9-93ac-616263646566> (Date assessed: 2/01/2022)



2. ARMAFLEX

Type: Armaflex ACE plate 19 mm self-adhesive,

Market Source: <https://www.armaflex-shop.de/Armaflex-ACE-insulation-mat-self-adhesive-cut-to-size> (Date assessed: 2/01/2022)

Manufacturer: <https://www.armacell.com/products/insulation-solutions>
(Date assessed: 2/01/2022)



3. THERMAL RESISTIVE FOIL

Product name: Puma-folie
Type: hermetic
Manufacturer: W. Bosch+ Co.
Information: https://w-bosch.de/wpcontent/uploads/2018/10/w_bosch_puma-folien_181002.pdf. (Date assessed: 2/01/2022)



ISBN: 978-82-575-1862-2

ISSN: 1894-6402



Norwegian University
of Life Sciences

Postboks 5003
NO-1432 Ås, Norway
+47 67 23 00 00
www.nmbu.no